2

AFOSR-TR- 89-1756

Institute of Polymer Science

The University of Akron

FINAL TECHNICAL REPORT
June 30, 1989

CONTRACT F49620-86-C-0032
FUNDAMENTAL STUDIES OF TIME-DEPENDENT RESPONSE
AND FRACTURE OF CROSS-LINKED POLYMERS

Principal Investigator: Frank N. Kelley
Co-Principal Investigators: Maurice Morton
Ernst von Meerwall

Akron, Ohio, U.S.A.

Approved for public release;
distribution unlimited.

2

FINAL TECHNICAL REPORT
June 30, 1989

CONTRACT F49620-86-C-0032
FUNDAMENTAL STUDIES OF TIME-DEPENDENT RESPONSE
AND FRACTURE OF CROSS-LINKED POLYMERS

Principal Investigator: Frank N. Kelley
Co-Principal Investigators: Maurice Morton
Ernst von Meerwall

UNCLASSIFIED
SECURITY CLASSIFICATION OF THIS PAGE

REPORT DOCUMENTATION PAGE

Form Approved
OMB No. 0704-0188

1a. REPORT SECURITY CLASSIFICATION UNCLASSIFIED	1b. RESTRICTIVE MARKINGS
2a. SECURITY CLASSIFICATION AUTHORITY	3. DISTRIBUTION / AVAILABILITY OF REPORT Approved for public release; distribution unlimited.
2b. DECLASSIFICATION / DOWNGRADING SCHEDULE	
4. PERFORMING ORGANIZATION REPORT NUMBER(S)	5. MONITORING ORGANIZATION REPORT NUMBER(S) AFOSR TR. 89-1256
6a. NAME OF PERFORMING ORGANIZATION University of Akron 6b. OFFICE SYMBOL (If applicable)	7a. NAME OF MONITORING ORGANIZATION AFOSR/NC
6c. ADDRESS (City, State, and ZIP Code) Institute of Polymer Science Akron, OH 44325	7b. ADDRESS (City, State, and ZIP Code) Building 410 Bolling AFB, DC 20332-6448
8a. NAME OF FUNDING / SPONSORING ORGANIZATION AFOSR 8b. OFFICE SYMBOL (If applicable) NC	9. PROCUREMENT INSTRUMENT IDENTIFICATION NUMBER F49620-86-C-0032
8c. ADDRESS (City, State, and ZIP Code) Building 410 Bolling AFB, DC 20332-6448	10. SOURCE OF FUNDING NUMBERS PROGRAM ELEMENT NO. 61102F; PROJECT NO. 2303; TASK NO. A3; WORK UNIT ACCESSION NO.
11. TITLE (Include Security Classification) Fundamental Studies of Time-Dependent Response and Fracture of Cross-Linked Polymers	
12. PERSONAL AUTHOR(S) Frank N. Kelley, Maurice Morton, and Ernst von Meerwell	
13a. TYPE OF REPORT Final 13b. TIME COVERED FROM _____ TO _____ 14. DATE OF REPORT (Year, Month, Day) 15. PAGE COUNT 146	
16. SUPPLEMENTARY NOTATION	
17. COSATI CODES FIELD / GROUP / SUB-GROUP	18. SUBJECT TERMS (Continue on reverse if necessary and identify by block number)
19. ABSTRACT (Continue on reverse if necessary and identify by block number) See Back	
20. DISTRIBUTION / AVAILABILITY OF ABSTRACT ☐ UNCLASSIFIED/UNLIMITED ☐ SAME AS RPT. ☐ DTIC USERS	21. ABSTRACT SECURITY CLASSIFICATION UNCLASSIFIED
22a. NAME OF RESPONSIBLE INDIVIDUAL Dr Donald R. Ulrich	22b. TELEPHONE (Include Area Code) (202) 767-4963 22c. OFFICE SYMBOL AFOSR/NC

DD Form 1473, JUN 86 *Previous editions are obsolete.*

SECURITY CLASSIFICATION OF THIS PAGE
UNCLASSIFIED

19.

Epoxy resins based on diglycidyl ether of bisphenol A (DGEBA) and diamino diphenyl sulfone (DDS) resulted in networks characterized as a graded series with increasing network chain lengths and decreasing Tg. When studied during and after curing, the only a single reaction path was found during curing, but the reaction path was highly temperature sensitive. Physical aging is found to be an increase in density of amorphous materials that must occur below Tg and is reversible by heating the material above its Tg. The aging process was faster if it occurred during the curing reaction. Fracture energy measurements as a function of surface-constrained thin film thicknesses show that physical constraints on the plastically deformed crack tip may reduce strength. Creep measurements on Viton fluorohydrocarbon elastomers crosslinked to different degrees confirm that looser molecular networks have broader viscoelastic spectra with some mechanisms with longer characteristic times. A series of urethan crosslinked polybutadienes were found to exhibit an exceptionally low lying plateau in the creep compliance curve which had not previously been observed.

TABLE OF CONTENTS

FINAL TECHNICAL REPORT

"Fundamental Studies of Time Dependent Response and Fracture of Cross-Linked Polymers"

(a) Objectives:

i) To determine the relationships of polymer structure, network topology and other microstructural features to time-dependent, small deformation properties such as creep and volume relaxation in thermosetting resins.

ii) To determine the relationships between polymer network structure and the fracture energy of thermosetting resins.

(b) Status:

i) Epoxy resins based on diglycidyl ether of bisphenol A (DGEBA) and diamino diphenyl sulfone (DDS) have been prepared using an homologous series of 5 prepolymer molecular weights and a stoichiometric ratio of reactants. Resultant networks were characterized as a graded series having increasing network chain lengths and decreasing T_g.

ii) The series of Epoxy resins based on the diglycidyl ether of bisphenol A has been extensively investigated during and after curing. The degree of cure was monitored by four different methods: 1) density increase, 2) heat of reaction evolution, 3) glass temperature, T_g, increase, and 4) infrared absorption by the glycidyl ether group. The epoxy resins studied indicated that only a single reaction path was followed

during the curing but the kinetics were, of course, highly temperature sensitive. When curing temperatures were chosen that were lower than the glass temperature of the fully cured resins, the reaction slows down when the T_g increases to temperatures that are higher than the curing temperature, T_c, but the curing reaction continues more or less indefinitely. In about a month the T_g can become 50 degrees higher than the curing temperatures. When the curing is slowly progressing below T_g physical aging occurs concurrently. Physical aging is simply an increase in density of amorphous materials that must occur at temperatures below T_g. This drift toward equilibrium density is accompanied by a slowing down of all rate processes occurring in the material. Physical aging and all of its consequences are reversible; i.e., its effects can be erased by heating the material above its T_g.

It was determined that the same degree of aging was achievable after the curing was completed, but the process took less time if the aging was allowed to occur during the curing reaction.

The curing process was followed not only by determining the extent of reaction by means of volume shrinkage and by changes in infrared absorption, but by changes in the viscosity, gel fraction, fictive temperature and equilibrium compliance.

Reduced creep compliance J(t) curves of fully cured samples of a series of Epon epoxy resins, where the molecular weight per cross-linked unit M_x varied from 420 to 2870, were determined

and their retardation spectra were calculated. The results showed the systematic increase in the number of long-time mechanisms with the increase in M_x.

The kinetics of physical aging as monitored by the decrease in rates at several temperatures below T_g was determined for samples with four different crosslink densities. A reduction procedure was devised to enable comparison of the results obtained on the differing samples.

Different stages of the molecular network development were prepared and from the measured creep compliance curves the evolution of the viscoelastic retardation spectrum that occurs during the curing of an epoxy resin was determined. It was shown how the short-time behavior at T_g is independent of the material and the stage of network development; but the long-time behavior showed a dramatic increases in retardation mechanisms to an operationally infinite number at the point of incipient gelation, which was followed by an equally dramatic decrease in long-time mechanisms.

The specific volume was measured for one of the Epon epoxy resins at rates of cooling which varied over three orders of magnitude. The expected decrease in T_g with decrease in rate of cooling was observed. The ratios of these rates were compared with temperature shift factors obtained 1) from the kinetics of volume contraction following temperature jumps of 2.5^0C, 2) from torsional creep measurements, and 3) elongational creep

measurements. All values from the four different kinetic processes fell on the same curve.

iii) Well-characterized epoxy networks have been studied as constrained thin films in mode I fracture measurements. Fracture energy measurements as a function of surface-constrained thin film thicknesses have shown that physical constraints on the plastically deformed crack tip may well reduce strength. Also thin films (< 0.5 mm) may be expected to show the effects of adherend surfaces as reductions in the state of cure (cross-link density) and results of fracture testing must be corrected for such effects.

iv) Creep measurements on three Viton fluorohydrocarbon elastomers crosslinked to different degrees have confirmed that looser molecular networks have broader viscoelastic spectra with some mechanisms with longer characteristic times.

A corresponding greater spread in the tear energies that was expected was not significant. Tear energy data as a function rate were reducible with the temperature shift factors obtained from creep compliance measurements.

However, the tear results do appear to substantiate the $M_x^{1/2}$ proportionality as predicted by the theory of Thomas and Lake. M_x is the molecular weight per crosslinked unit.

v) A series of urethane crosslinked polybutadienes were found to exhibit an exceptionally low lying plateau in the creep compliance curve which had not previously been observed. Since the presence of this plateau gives rise to an exceptionally

broad viscoelastic retardation spectrum higher average energy dissipation is seen as a function of frequency. Correspondingly broader tear energy curves are also observed. Sustained high losses are often desirable and an increasing number of means to create such losses are needed. A unique strong temperature dependence was also found to be exhibited by these unusual elastomers.

The creep and tear measurements obtained on the widely varied elastomers constitutes a unique data base that has enabled us to correlate the linear viscoelastic behavior with the kinetics of failure. An equation enabling the calculation of the rate dependence and the magnitude of the tear energy from the viscoelastic retardation function has been found. The latter is obtained from the creep compliance curves. Creep measurements are more precise, quicker, and more convenient to measure than the tear energy curves. In addition, the understanding of the molecular basis for creep behavior will therefore be transferable to rationalize elastomeric failure.

vi) The integration of knowledge gained from these studies provides strong insights into the origins of strength and creep properties of thermosetting resins. Also the cure path, which is dependent on thermal history for full property development, may be optimized.

(c) Cumulative List of Publications from This Contract

F. N. Kelley, B. J. Swetlin and D. Trainor, "Structure-Property Relationships in Composite Matrix Resins," IUPAC Macromolecules, H. Benoit and P. Rempp, editors, Pergamon Press, Oxford and New York, 1982.

F. N. Kelley and L.-J. Su, "Time-Dependent Fracture of Elastomeric Network Polymers," Proceedings IUPAC MACRO 82, Amherst, MA, July, 1982.

F. N. Kelley and D. Trainor, "Model Inhomogeneous Glassy Network Polymers," Polymer Bulletin, 7, 369 (1982).

D. J.Plazek, In-Chul Choy, E. von Meerwall, Long-Ji Su and F. N. Kelley, "Viscoelasticity and Tearing Energy of Fluorinated Hydrocarbon Elastomers, Rubber Chem. Technol., 56, 866 (1983).

J. LeMay, B. Swetlin and F. N. Kelley, "Characterization and Properties of Some Epoxy-Amine Networks," Proceedings of the Division of Organic Coatings and Plastics Chemistry, ACS, Seattle Meeting, March, 1983. Published in ACS Symposium Series No. 243 (1984).

E. von Meerwall, D. Shook, K. J. Min, and F. N. Kelley, "Self-Diffusion of C_6F_6 in Filled Rubber Polymers," J. Appl. Phys. 56, 9 (1984).

J. LeMay and F. N. Kelley, "Structure and Ultimate Properties of Epoxy Resins," book chapter, Advances in Polymer Science 78, K. Dusek, editor, Springer-Verlag, Heidelberg, Berlin, 1986.

R. G. Stacer, L. Yanyo and F. N. Kelley, "Observations on the Tearing of Elastomers," Rubber Chem. Technol., 59, May/June, 1985.

R. G. Stacer, E. D. von Meerwall and F. N. Kelley, "Time-Dependent Tearing of Carbon Black-Filled and Strain-Crystallizing Vulcanizates," Rubber Chem. Technol., 58, No. 5, p. 913, November-December 1985.

R. G. Stacer and F. N. Kelley, "Criteria for Unstable Tearing of Elastomers," Rubber Chem. Technol., 58, No. 5, p. 924, November-December 1985.

E. von Meerwall, D. Thompson, K.-J. Min, and F. N. Kelley, "Adaptive Modelling of Materials Test Results: Tear Energy in Filled Rubber Networks," J. Mat. Sci., 21, 1801 (1986).

J. D. LeMay and F. N. Kelley, "Structure and Ultimate Properties of Epoxy Resins," Advances in Polymer Science, 78, 115 (1986).

E. von Meerwall, R. D. Vargo, K.-J. Min and F. N. Kelley, "Molecular Motions during Curing in Simulated Solid Propellant," Bull. Am. Phys. Soc. OS/APS, 31, 1076 (1986).

E. von Meerwall, R. D. Vargo and K.-J. Min, and F. N. Kelley, "Molecular Kinetics during Polymer Network Formation," Bull. Am. Phys. Soc., 31, 307 (1986).

E. von Meerwall, P. Palunas and F. N. Kelley, "Diffusion in Entangled or Cross-linked Polydisperse Polymer Melts," Bull. Am. Phys. Soc., 32, 1290 (1987).

L. C. Yanyo and F. N. Kelley, "Effect of Chain Length Distribution on the Tearing Energy of Silicone Elastomers," Rubber Chem. Technol., 60, No. 1, March-April 1987.

L. C. Yanyo and F. N. Kelley, "Effect of Network Chain Length on the Tearing Energy of Master Curves of Poly(dimethyl diphenyl-siloxane)," Rubber Chem. Technol., 61, No. 1, March-April, 1988.

E. von Meerwall and F. N. Kelley, "Use of Parametric Models in Designing Polymeric Materials to Specifications," Internat. J. Fracture 39, Nos. 1-3, (1989). (Reprinted in Structural Integrity: Theory and Experiment, E. S. Folias, ed. (Festschrift in honor of M. L. Williams), Kluwer Acad. Publ., Dordrecht, 1989, pp. 79-92.)

Invited and Contributed Papers (abstracts in print)

M. Frank, E. von Meerwall and F. N. Kelley, "Finite-Element Numerical Simulation of Tearing, Cracking, and Fatigue in Polymers," Amer. Phys. Soc. (Ohio Section), May 2, 1987; Bull. Am. Phys. Soc. 32/10, 2162 (1988).

E. von Meerwall, "Materials Design through Analytic Adaptive Modeling of Test Results," invited lecture, AIME meeting, Symposium on Rational Design of Materials, in honor of M. L. Williams, Salt Lake City, Sept. 22, 1987; abstract published in conference abstracts volume, session 19.

I.-C. Choy and D. J. Plazek, "The Physical Properties of Bisphenol-A-Based Epoxy Resins During and After Curing," J. Polymer Sci., Part B: Polym. Phys. Ed. 24, 1303-1320 (1986).

D. J. Plazek, G.-F. Gu, R. G. Stacer., L.-J. Su, E. D. von Meerwall and F. N. Kelley, "Viscoelastic Dissipation and the Tear Energy of Urethane-Crosslinked Polybutadiene Elastomers," J. Materials Sci., 23, 1289-1300 (1988).

D. J. Plazek and I.-C. Choy, "The Physical Properties of Bisphenol-A-Based Epoxy Resins During and After Curing. II. Creep Behavior Above and Below the Glass Transition Temperature," J. Polymer Sci., Polym. Phys. Ed., 2, 307-324 (1988).

Papers Submitted for Publication

D. J. Plazek and Z. N. Frund, "Epoxy Resins (DGEBA), The Curing and Physical Aging Process," J. Polymer Sci., in press.

D. J. Plazek and In-Chul Choy, "The Evolution of the Viscoelastic Retardation Spectrum During the Development of an Epoxy Resin Network," J. Polymer Sci., submitted.

D. J. Plazek and M. Rosner, "The Calculation of the Tear Energy of Elastomers from Their Viscoelastic Behavior," J. Polymer Sci., to be submitted.

(d) Advanced Degrees Awarded

Theses/Dissertations, The University of Akron

Brian Swetlin (Ph. D., 1984), "Structure and Fracture of Glassy Thermosetting Polymers"

Long-ji Su (Ph. D., 1984), "Time-Dependent Tearing of Elastomer Networks"

Donna Trainor (Ph. D., 1984), "Model Inhomogeneous Glassy Network Polymers"

James LeMay (Ph. D., 1984), "Characterization and Properties of Densely Cross-linked Polymers"

Kenneth Ptak (Ph. D., 1987), "Model Rubber-Toughened Epoxies"

Lynn Yanyo (Ph. D., 1987), "Tearing of Silicone Elastomers: Effect of Network Architecture"

Kyung-ju Min (Ph. D., 1987), "Time-Dependent Properties of Highly-Filled Elastomers"

Ross Stacer (Ph. D., 1986), "Time-Dependent Tearing Phenomena in Filled and Unfilled Elastomers"

Robert Seiple (M. S., 1985), "Time-Dependent Tearing of Polyurethane Networks"

Jeffrey Patterson (M. S., 1987), "Fracture Toughness of Epoxy Networks Containing Pre-Reacted Epoxy Oligomers"

Scott Mudrich (Ph. D., expected 1990), "Fracture of Surface Constrained Epoxy Thin Films"

Ramesh Sundaram (Ph. D., expected 1990), "Correlation of Neat Resin and Unidirectional Composite Properties"

Michael R. Frank (B.S., Physics, Honors Thesis), "Finite Element Numerical Simulation of Tearing and Fatigue in Polymers"

<u>Thesis/Dissertation, University of Pittsburgh</u>

In-Chul Choy (Ph. D., 1987), "Physical Properties of Epoxy Resins During and After Curing"

Mark Rosner (M. S., 1988), "The Correlation between the Tear Energy of Elastomers and Linear Viscoelasticity"

(e) Interactions

Papers presented:

1. "Fracture of Surface-Constrained Epoxy Resins," Monash University, Melbourne, Australia, June, 1989
2. "Relationship between Neat Resin and Composite Properties," Keynote, Asian-Pacifica Composites Conference, Adelaide, Australia, June 1989
3. "Fracture of Surface Constrained Epoxy Resins," Society of Plastics Engineers Conference, Cleveland, Ohio, October 1989
4. "Use of Parametric Models in Designing Polymeric Materials to Specifications," Society of Engineering Science, Salt Lake City, Utah, September 1987
5. "Correlation of Composite and Bulk Matrix Resin Properties," Society of Plastics Engineers, Symposium on High Temperature Polymers

APPENDIX

I. EPOXY RESIN STUDIES OF FRACTURE IN THIN FILMS

A. Introduction

The fracture properties of epoxy networks have been successfully determined in the bulk[1-4], as adhesives[5-10], and in fiber-reinforced composites[11-13] using the concepts of linear elastic fracture mechanics. However, comparison of the data from the various types of test specimens indicates that the bulk network properties do not translate to the adhesive/composite properties. In order to better understand why this is so, a logical starting point is the realization that there is a major difference in the surface to volume ratio between the bulk and the adhesive/composite type specimens. When cast as adhesives or as the binding matrix in highly-filled, fiber-reinforced composites, the epoxy networks can be envisioned as highly surface-constrained thin films which have very high surface to volume ratios. Since the surface layer is often different from the bulk, thin film properties may be different as well.

As the epoxy networks move from the bulk configuration to very thin films the following factors may become increasingly important:

1) Residual stresses arising from the geometry of the layer and bonding between the adherends/fibers may increase so that the resin layer is *significantly preloaded.*

2) The presence of the adherends/fibers may chemically or physically affect the interfacial (interphase) layer. Large chemical interactions may cause deviations in network morphology which may extend well into the resin layer.

3) The high modulus adherends/fibers may constrain the plastically deformed region ahead of the propagating crack causing a change in the amount of energy dissipation occurring during fracture.

In this work the fracture properties of the epoxy networks cast as surface-constrained thin films were determined and compared to the bulk network fracture properties. Network morphology (average chain molecular weight between crosslinks, M_c) was determined for epoxy networks cast as both constrained (bonded) and unconstrained (non-bonded) thin films.

The importance of knowing M_c becomes obvious based on previous work by LeMay[14] which showed a relationship between M_c and the arrest fracture energy, $G_{Ic}{}^a$, for epoxy networks below T_g (see Fig. 1). Interestingly, it was found that the arrest fracture energy was proportional to the 1/2 power of the

molecular weight between crosslinks. This relationship is similar to that proposed by Lake and Thomas[15] which predicts that the threshold tearing energy should be proportional to the 1/2 power of the molecular weight between crosslinks for an endlinked network. The theory requires that the polymer chains crossing the fracture plane have enough mobility so that each bond along the backbone of the molecule can be stressed to near its breaking stress before chain breakage occurs. Althougth the epoxy networks are well below Tg, the occurrence of plastic deformation at the crack tip suggests that there may be sufficient chain mobility occurring for the theory to hold. Thus, variations in M_c caused by the presence of adherends or reinforcing fibers in thin epoxy layers could be responsible for discrepancies in fracture energies between bulk and adhesive/composite configurations.

Although there are numerous suggestions of a 'plastic zone' at the advancing crack front in highly crosslinked epoxy networks[1-3,7-9,11-13,16,17], experimental determination of the size and shape of the zone is extremely difficult, if not impossible. Yamini and Young[18] measured the length of highly deformed regions of material on the fracture surfaces of double torsion fracture specimens at positions of crack initiation/arrest in an epoxy resin and found that the length correlates with the size of the plastic zone predicted by the classical Dugdale model[19]. LeMay[14] used the blunt crack analysis model[10,20] to calculate the critical length for an homologous series of epoxy resins which differed primarily in M_c and found that the critical length was equal to the plastic zone radius predicted by the classical Irwin model[21]. The results also showed that the log of the critical length varied as the 1/2 power of the log of M_c (see Fig. 2). It seems reasonable to assume that the plastic zone size may be dependent upon M_c, becoming larger as M_c increases.

The experimentally determined fracture energy for epoxy networks is found to be much greater than the energy predicted by theoretical calculations based soley on bond cleavage[22]. This excess energy must be due to dissipative processes occurring in the material. For an elastic, glassy polymer, which fractures at small strains, it seems logical to assume that any viscoelastic and plastic energy dissipative processes occur in a very small region (plastic zone) local to the crack tip. If the development of this zone is inhibited in any way during crack growth then the fracture energy may be different. When epoxy resins are used as adhesives or as the matrix for a highly-filled fiber-reinforced composite the layer thickness may be less than the size of the plastic zone (see

Fig. 3). If the plastic zone size (and its overall volume) is diminished by the constraints, the fracture energy should decrease.

An experimental attempt was made to physically constrain the plastic zone and measure the resulting fracture energy by using a modified version of the *'Outwater' double torsion test*[23-25]. The constrained testpiece is similar in design to one suggested by Gent[26] and consist of a thin layer of epoxy sandwiched between two aluminum adherends (see Fig. 4). Six different epoxy networks which varied in M_c and presumably in plastic zone size were used in this work. The thickness of the epoxy layer was systematically decreased from approximately 2.0 to 0.1 mm and the resulting fracture energies were determined. The fracture energies of bulk double torsion testpieces were also measured for comparison.

The average molecular weight between crosslinks was measured as a function of film thickness for both constrained and unconstrained epoxy films. *Constrained (bonded) films were cast between* phosphoric acid anodized aluminum sheets which were subsequently etched away completely in hydrochloric acid after the network had cured. Unconstrained (nonbonded) films were cast between silicone rubber plattens which had extremely smooth 'glasslike' surfaces. The film thicknesses ranged from 0.1 to 2.0 mm for the unconstrained films and 0.3 to 0.8 mm for the constrained films.

B. Experimental

1. Materials

Stoichiometric endlinking of difunctional epoxy resins of different initial *molecular weights with a tetrafunctional*, aromatic amine allowed accurate control of M_c. An homologous series of commercial DGEBA type resins (Shell Chemical Company) having average molecular weights ranging from 370 to 4200 g/mol was used in this work. The curing agent used was 4,4'-aminodiphenyl sulfone (Aldrich Chemical Company). The resulting networks are identified, in order of increasing M_c, by the trade name of the resin from which they were made: 828, 1001F, 1002F, 1004F, 1007F, and 1009F. The higher molecular weight resins were synthesized by fusion of the 828 oligomer and thus have the 'F' designation. The adherends for the constrained testpieces were the aluminum *alloy 6061-T6 (Alcoa).*

2. Fracture energy measurements

All of the double torsion testpieces were fractured at 25°C on an Instron Universal Testing machine at a crosshead speed of 0.5 mm/min. The compliance of the double torsion testpiece varies linearly with crack length. Thus, the stress

intensity factor, K_{Ic}, is proportional to the applied load and is given by the following relationship (for plane strain)

$$K_{Ic} = Pw_m[3/wt_nt^3(1-v)]^{1/2} \qquad \text{(for } w/2 > 6\text{)}$$

where P is the load at fracture, w_m is the torsional moment arm, w is the width of the testpiece, t_n is the fracture plane thickness, and v is Poisson's ratio (assumed to be 0.35). Details of the mathematical analysis of the double torsion testpiece can be found in a paper by Williams and Evans[25]. The fracture energies of the epoxy networks were calculated from the stress intensity factors using the well-known relationship

$$G_{Ic} = K_{Ic}^2/E$$

where E is Young's modulus of the testpiece. Young's modulus was determined from static three-point bend measurements based on simple elastic beam theory.

In brittle epoxy networks, cracks often propagate intermittently in a 'stick/slip' manner over a fairly broad range of test temperatures and loading rates. This type of crack growth yields a load vs. time (or displacement) curve which is sawtooth shaped (see Fig. 5). In this work, all the epoxy networks fractured in a stick/slip manner. Therefore, two values of fracture energy were calculated for each network. Initiation fracture energies, G_{Ic}^i, were calculated from the average value of the crack initiation peak loads and, likewise, arrest fracture energies, G_{Ic}^a, were calculated from the average crack arrest values.

3. M_c measurements

The average molecular weight between crosslinks for each network was determined from near equilibrium rubbery tensile modulus measurements made on an Instron Universal Testing machine equiped with an environmental chamber (see Table 1). The moduli were determined for dogbone-shaped epoxy films ranging in thickness from 0.1 to 2.0 mm. The stress-strain measurements were made at 40°C above the epoxy glass transition temperatures. Previous work[14] has shown that these epoxies behave sufficiently like an elastic rubbery material at these temperatures and reasonable results were obtained when the kinetic theory of rubber elasticity was applied. M_c was calculated for each testpiece using the following relationship

$$M_C = 3\phi pRT/E$$

where ø is the front factor, p is the density, R is the universal gas constant, T is the absolute temperature, and E is the equilibrium rubbery tensile modulus.

C. Summary of results

1. M_C vs. epoxy film thickness

The dependence of M_C on film thickness for the epoxy networks is shown in Fig. 6. Data was not obtained for the 828 or 1009F networks (the 828 testpieces were too brittle to handle and the 1009F resin was too viscous to be cast as a thin film). No variation in M_C with film thickness was observed for the 1001F network. However, M_C increases as the epoxy film thickness decreases for the 1002F, 1004F, and the 1007F networks. The deviation in M_C becomes greater as the initial resin molecular weight is increased.

The variation of M_C may be the result of a non-stoichiometric reactant ratio caused by a loss of curing agent to surface contaminants (e.g. moisture). Since the surface to volume ratio is extremely large for very thin films as compared to bulk castings, it is conceivable that a significant percentage of curing agent may be lost. Small quantities of resin (approx. 100 g) were used to cast the thin films. A loss of as little as 330 mg in the 1007F networks would result in a 10% deviation from a stoichiometric reactant ratio (epoxy excess).

Since the more tightly crosslinked networks require larger quantities of curative for a stoichiometric reactant ratio for the same amount of resin, smaller deviations (approx. 3% for the 1001F network) would be expected if the same amount of curing agent is lost. Previous work[14] has shown that M_C is a sensitive function of the amine/epoxy reactant ratio for the epoxy networks used in this investigation. It was shown that deviations of 20% from stoichiometry (epoxy excess) resulted in a twofold increase in M_C for 1002F epoxy networks.

Thin films were cast between anodized aluminum sheets (6061-T6) for the 1002F networks. No difference was observed in M_C as compared to thin films cast between silicone rubber. This result suggests that the observed variation in M_C with film thickness is not due to residual stresses caused by bonding and subsequent thermal shrinkage.

2. $G_{Ic}{}^{a}$ vs. epoxy layer thickness

The dependence of the arrest fracture energies on epoxy layer thickness (gap thickness) obtained from the constrained double torsion testpieces for the epoxy networks is shown in Fig. 7. The initiation fracture energies are not shown. The

initiation values mimic the behavior of the arrest values but are greater in magnitude. Data was not obtained for the 828 and 1009F networks (the 828 testpieces contained numerous cracks caused by thermal shrinkage upon cooling after cure and the 1009F resin was too viscous to be cast between the aluminum adherends). No variation in $G_{Ic}{}^{a}$ was observed for the 1001F, 1002F, and 1004F networks. However, a significant decrease in $G_{Ic}{}^{a}$ was observed when the epoxy layer thickness was reduced to less than 0.5 mm for the 1007F network. It is suggested that this decrease in fracture energy may be due to physical constrainment of the plastic zone at the crack tip by the aluminum adherends. This decrease in $G_{Ic}{}^{a}$ is not observed in the more tightly crosslinked networks because their plastic zones may be smaller than the constraining dimensions of the testpiece.

Although 0.5 mm is much greater than the plastic zone dimensions predicted for the bulk networks using the classical plastic zone models, it should be noted that the stress field at the crack tip may be significantly different in the constrained configuration than in the bulk. Strong bonding to the aluminum adherends will create residual stresses in the epoxy layer which may increase the size of the plastic zone. In the bulk double torsion testpieces residual stresses were relieved by annealing. The constrained double torsion testpieces exhibited significant residual stresses when viewed through polarizers set at extinction even after annealing.

The data in Fig. 7 have been corrected for the change in arrest fracture energy caused by an increase in M_c with decreasing film thickness. The data in Fig. 6 were fit to a second degree polynomial for epoxy film thicknesses less than 1 mm. (There is no known significance for this type of fit but it did provide the best fit.) This equation was used to calculate M_c for the appropriate epoxy layer thicknesses obtained in the constrained testpieces. The arrest fracture energies were corrected using the half-power relationship found by LeMay[14] (see Fig. 1). Although, correcting for M_c lowers the arrest fracture energy, the change is about 40 - 50 J/m^2 for the network with the largest M_c variation (1007F). Thus, it is still assumed that the decrease in arrest fracture energy for epoxy layer thicknesses less than 0.5 mm in the 1007F network is due primarily to constrainment of the plastic zone.

3. Bulk vs. constrained testpiece fracture energies

The initiation and arrest fracture energies obtained from the bulk double torsion testpieces are listed in Table 1. The values are the averages of no less than

22 testpieces with the exception of 1009F (6 testpieces averaged). The initiation and arrest fracture energies obtained from the constrained double torsion testpiece are also listed in the table. These values were obtained by averaging the fracture energies obtained from testpieces in which the epoxy layer thickness varied from 1.0 to 2.0 mm. The initiation fracture energies are significantly higher for the bulk testpieces as compared to the fracure energies obtained from the constrained testpieces. Good agreement, however, is found between the arrest fracture energies from the two types of testpieces. This suggests that the constraints may influence the crack initiation process but do not affect crack arrest.

4. Unstable fracture

The difference between the the initiation and arrest fracture energies (G_{Ic}^{i} - G_{Ic}^{a}) increases as M_c increases for both types of testpieces. In other words, the magnitude of the 'stick-slip' behavior increases as the epoxy networks become tougher. The ratio of G_{Ic}^{i} to G_{Ic}^{a} is shown in Table 1. The ratio increases as M_c increases for the bulk double torsion testpiece but remains fairly constant for the constrained testpiece. Thus, the amount of 'stick-slip' behavior is found to increase dramatically in the bulk testpieces as M_c increases whereas it remains constant in proportion to molecular weight between crosslinks in the constrained testpiece.

References

1. R. Griffiths and D.G. Holloway, J. Mater. Sci., 5, 302 (1970)
2. S. Yamini and R.J. Young, Polymer, 18, 1075 (1977)
3. D.C. Phillips, J.M. Scott, and M. Jones, J. Mater. Sci., 13, 311 (1978)
4. S. Yamini and R.J. Young, J. Mater. Sci., 14, 1609, (1979)
5. S. Mostovoy and E.J. Ripling, J. Appl. Polym. Sci., 10, 1351 (1966)
6. *Idem*, J. Adhesion, 3, 125 (1971)
7. R.A. Gledhill and A.J. Kinloch, J. Mater. Sci. Lett., 10, 1261 (1975)
8. *Idem*, Polymer, 17, 727, (1976)
9. *Idem*, Polym. Eng. Sci., 19, 82, (1979)
10. R.A. Gledhill et al., Polymer, 19, 574 (1978)
11. S.M. Lee, J. Comp. Mater., 20, 185 (1985)
12. H. Chai, Eng. Fract. Mech., 24, 413 (1986)
13. A.C. Garg and Y.W. Mai, Compos. Sci. Tech., 31, 225 (1988)
14. J.D. LeMay, Ph.D. Dissertation, Univ. of Akron (1985)
15. G.J. Lake and A.G. Thomas, Proc. Roy. Soc., Ser. A, 300, 108 (1967)
16. W.D. Bascom et al., Composites, 11, 9 (1980)
17. W.D. Bascom and R.L. Cottington, J. Adhesion, 7, 333 (1976)
18. S. Yamini and R.J. Young. J. Mater. Sci., 15, 1823 (1980)
19. D.S. Dugdale, J. Mech. Phys. Solids, 8, 100 (1960)
20. A.J. Kinloch and J.G. Williams, J. Mater. Sci., 15, 987 (1980)
21. G.R. Irwin, Appl. Mechs. Res., 3, 65 (1965)
22. J.P. Berry, J. Polym. Sci., 59, 197 (1961)
23. J.D. Outwater and D.J. Gerry, J. Adhesion, 1, 290 (1969)
24. J.A. Kies and A.B.J. Clark, "Fracture 1969," (Proc. of the 2nd Int. Conf. on Fract., Brighton, 1969), ed. by P.L. Pratt (Chapman and Hall, London, 1969) p. 483.
25. D.P. Williams and A.G. Evans, J. Test. Eval., 1, 264 (1973)
26. K. Cho and A.N. Gent, Int. J. Fract., 28, 239 (1985)

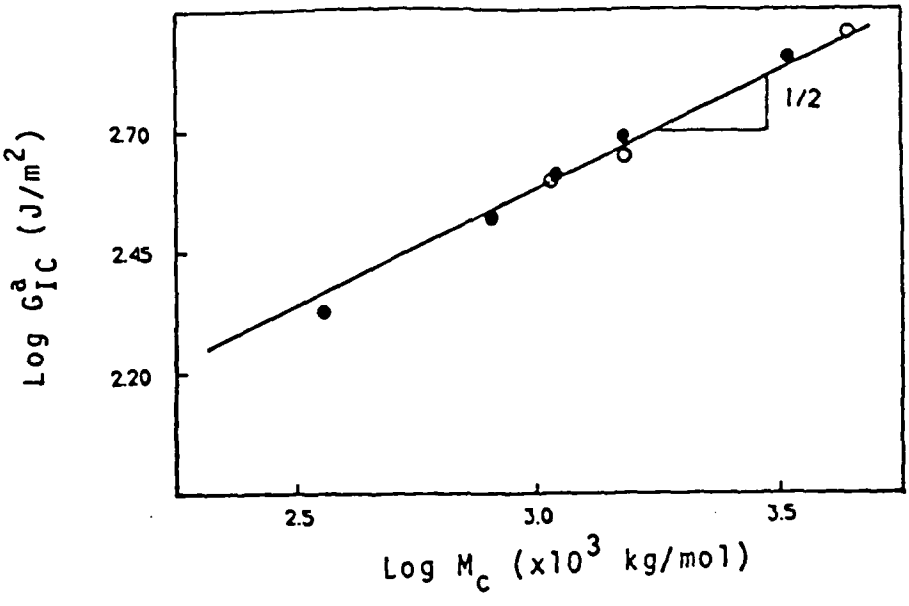

Figure 1. Log-log plot of G_{IC}^a vs. M_c for the 828, 1001F, 1002F, 1004F, and 1007F epoxy networks. Closed circles are data obtained by LeMay[14]; open circles were obtained in this work.

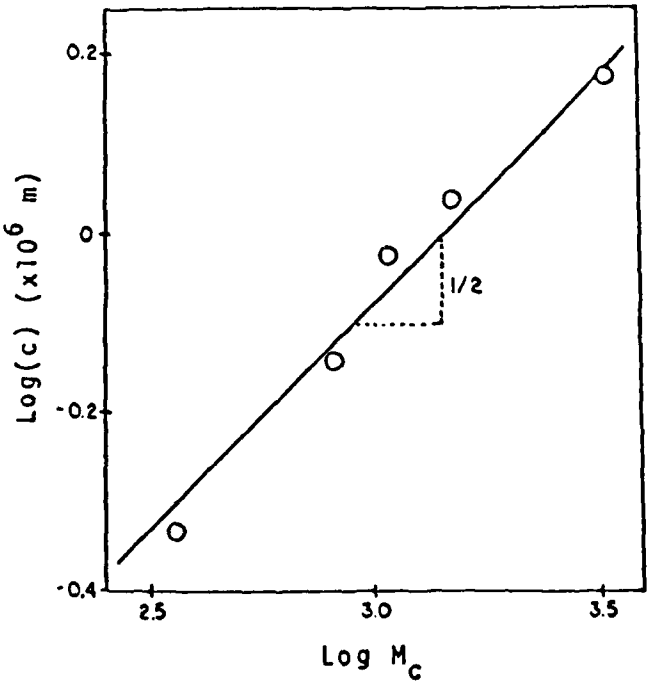

Figure 2. Log-log plot of critical distance vs. M_c (After LeMay[14]).

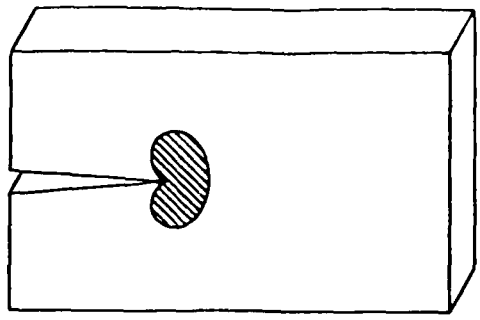

(a)

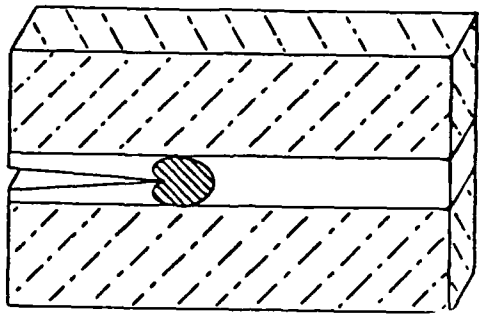

(b)

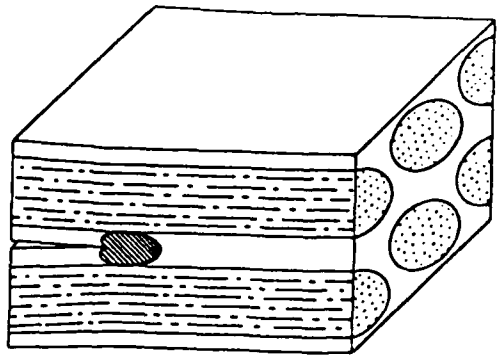

(c)

Figure 3. Crack tip plastic zones. (a) unconstrained in the bulk (b) constrained by rigid adherends (c) constrained by high modulus fibers in a composite.

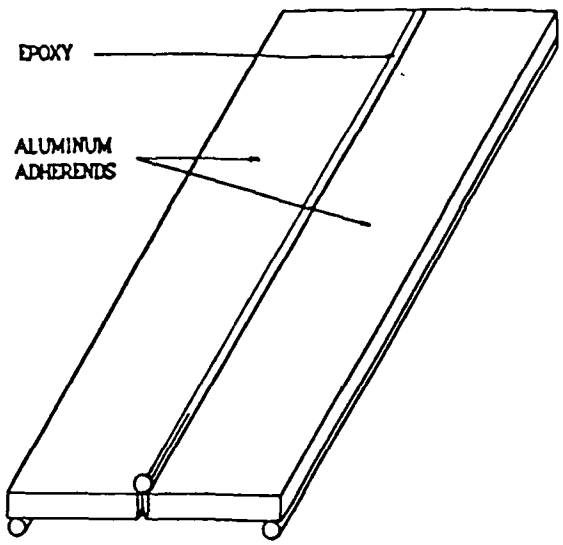

Figure 4. Modified version of the 'Outwater' double torsion testpiece.

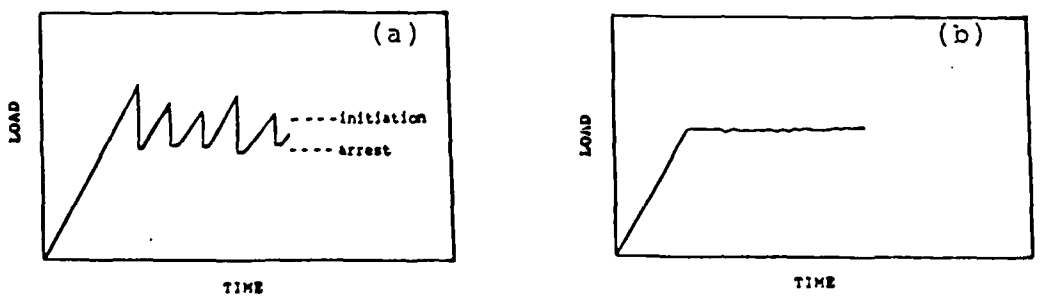

Figure 5. Typical load vs. time chart traces obtained from the double torsion testpiece for epoxy fracture. (a) unstable crack propagation (b) stable crack propagation.

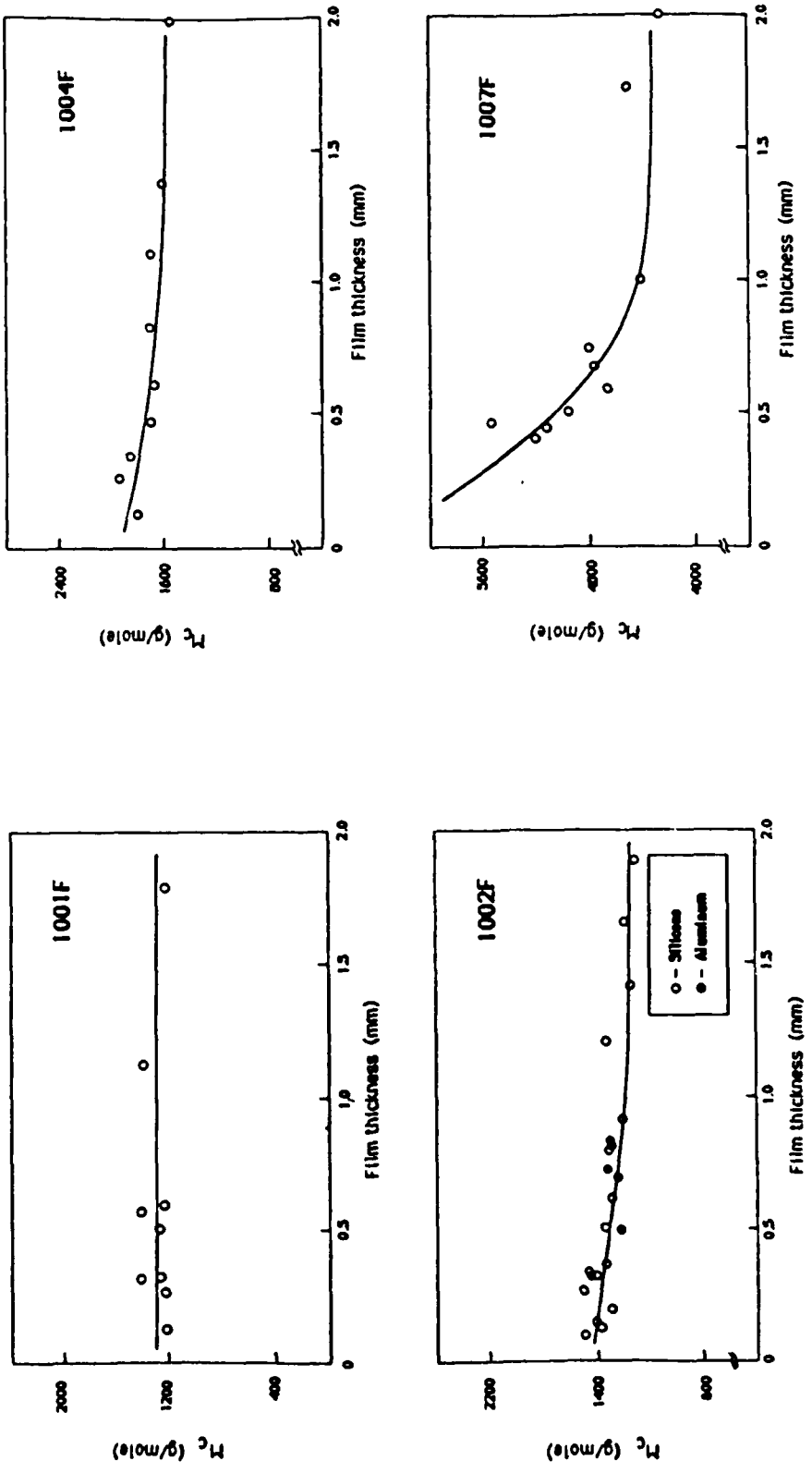

Figure 6. Plot of M_C vs. epoxy network film thickness for the 1001F, 1002F, 1004F, 1007F networks.

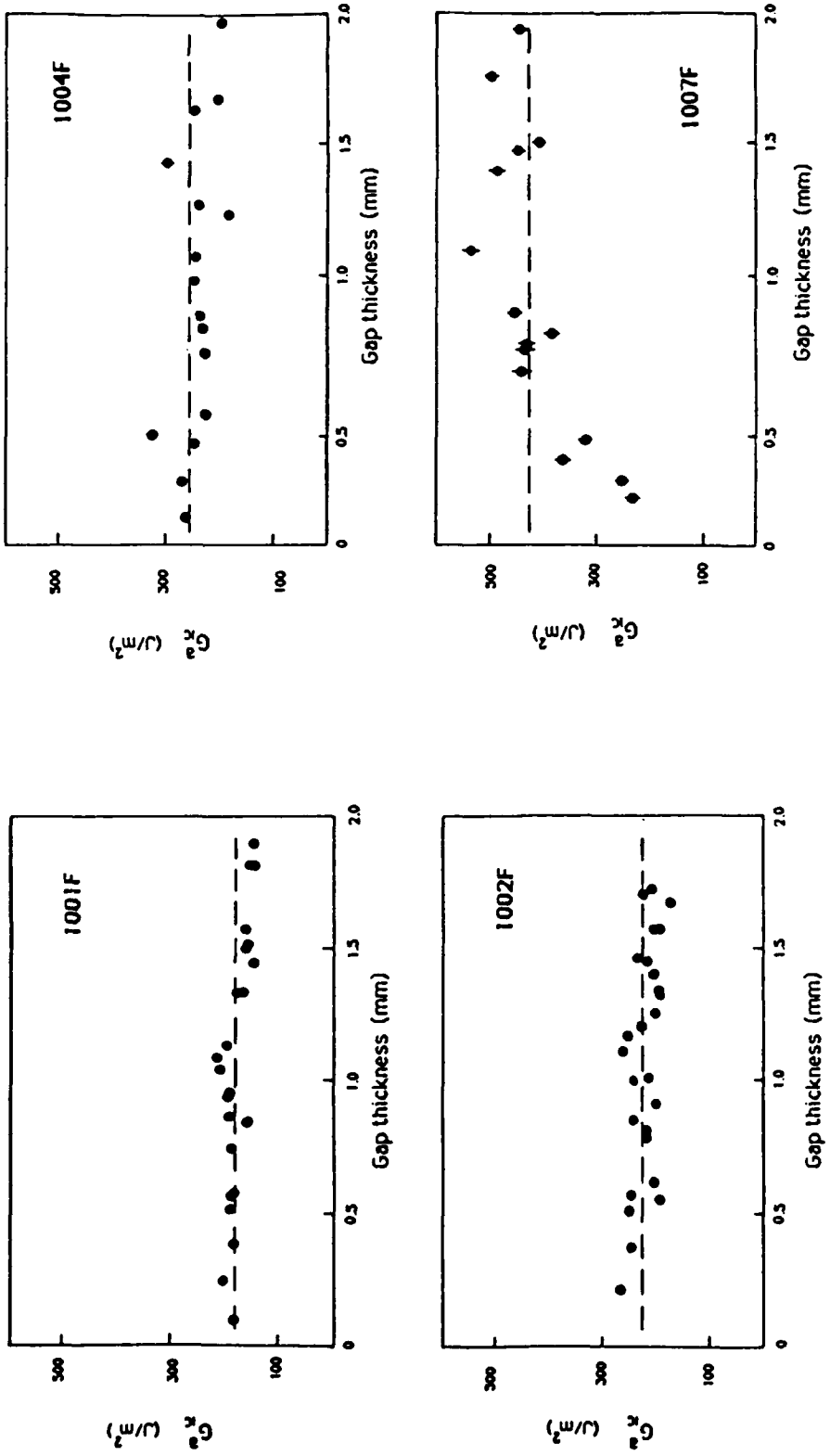

Figure 7. Plot of arrest fracture energies, G_{Ic}^a, vs. epoxy layer thickness obtained from the constrained double torsion testpieces for the 1001F, 1002F, 1004F, and 1007F networks. Dotted lines are the average fracture energies obtained from the bulk double torsion testpieces.

Table 1

Network	Initial resin molecular weight (g/mol)	M_c (g/mol)	Fracture energies G_{Ici} (J/m^2) bulk	G_{Ici} (J/m^2) constrained	G_{Ic}^a (J/m^2) bulk	G_{Ic}^a (J/m^2) constrained	G_{Ici}/G_{Ic}^a (J/m^2) bulk	G_{Ici}/G_{Ic}^a (J/m^2) constrained
828	370	----	161	----	132	---	1.22	----
1001F	1050	1200	223	183	184	164	1.21	1.12
1002F	1250	1200	323	235	226	213	1.43	1.10
1004F	1560	1600	368	260	262	230	1.40	1.13
1007F	2950	4200	667	510	427	468	1.56	1.09
1009F	4250	----	951	----	518	---	1.84	----

II. THE EVOLUTION OF THE VISCOELASTIC RETARDATION SPECTRUM DURING THE DEVELOPMENT OF AN EPOXY RESIN NETWORK

by

Donald J. Plazek

and

In-Chul Chay*

Materials Science and Engineering Department

848 Benedum Hall

University of Pittsburgh

Pittsburgh, PA 15261

* Formerly In-Chul Choy

II. THE EVOLUTION OF THE VISCOELASTIC RETARDATION SPECTRUM DURING THE DEVELOPMENT OF AN EPOXY RESIN NETWORK

INTRODUCTION

Many epoxy resin systems are formed from the reaction of a difunctional epoxy resin with a tetrafunctional amine. The rate of reaction, hence the curing, depends on the kind of diamine used. Aromatic amines such as 4,4/-methylene dianiline MDA and 4,4/-diamino diphenyl sulfone DDS react more slowly with diepoxides than aliphatic diamines and yield higher glass temperatures. It is well known that three reactions are usually involved in the curing of such epoxy resin systems.[1]

I Reaction of the primary amine hydrogens

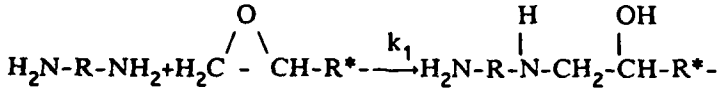

II Reaction of the secondary amine hydrogens

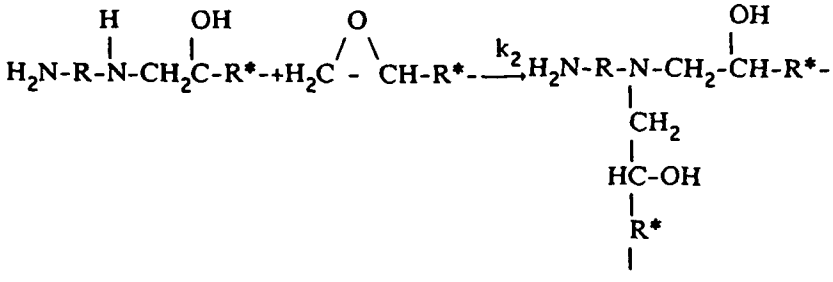

III Etherification

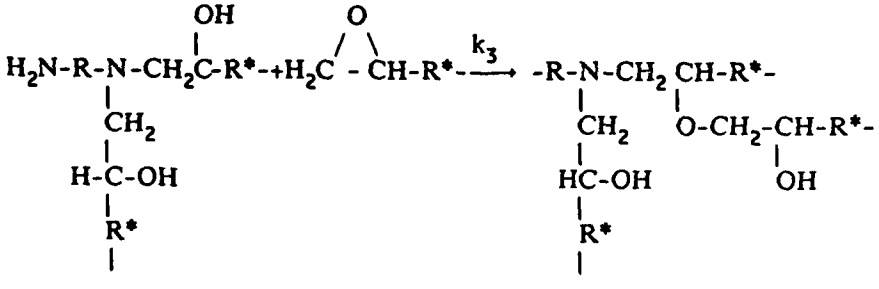

If the rate constants k_1 and k_2 differ, the intermediates formed on the way to a full cure will vary. This variation is called the substitutional effect. With $k_1 > k_2$, the usual case, linear chain growth will tend to precede branching with subsequent network formation. Nevertheless with exact

stoichiometric concentrations of reactants the same network is obtained when the reaction is complete. The etherification reaction is usually negligible unless an excess of epoxide group is present or the curing is carried out at exceptionally high temperatures. We don't believe we have encountered any noticeable etherification at curing temperature up to 210°C with DDS and the diglycidyl ether of bisphenol A.[2,3]

During the curing of an epoxy resin the viscoelastic behavior of the reactant mixture is expected to change as the molecular architecture varies during the reaction. It was desired to follow the evolution of the retardation spectrum L as the reaction proceeded from the mixture of reactants to the fully completed molecular network.

The retardation spectrum can be determined from the dynamic shear compliance function $J'(\omega)$ and $J''(\omega)$, the storage and loss components of the complex dynamic compliance $J^*(\omega) = J'(\omega) - iJ''(\omega)$ or from the creep and the recoverable creep compliances $J(t)$ and $J_r(t)$. All of the compliances have the units cm^2/dyne or Pa^{-1}. The pertinent relations are[4]:

$$J'(\omega) = J_g + \int_{-\infty}^{\infty} \frac{L}{1+\omega^2\tau^2} \, d \ln \tau \tag{1}$$

$$J''(\omega) = \frac{1}{\omega\eta} + \int_{-\infty}^{\infty} \frac{L\omega\tau}{1+\omega^2\tau^2} \, d \ln \tau \tag{2}$$

$$J(t) = J_r(t) + t/\eta = J_g + \int_{-\infty}^{\infty} L(1-e^{-t/\tau}) \, d \ln \tau + t/\eta \tag{3}$$

where J_g is the time independent glassy compliance which in principle is the strain per unit stress contributed to the deformation by the stretching and bending of bonds. In practice it usually includes the deformation that arises from very local molecular motions such as side group vibration and rotations;

t is the time, sec.;

ω is the circular frequency, radians $sec.^{-1}$;

η is the viscosity, poise or Pa sec.;

and τ is the retardation time.

It is crucial to note that $J''(\omega)$ is dominated by $1/\omega\eta$ at low frequencies and J(t) by t/η at long times in the terminal zone of response. Because of this domination, values for the retardation spectrum at long times cannot be obtained from these functions. The viscous dissipation of energy in a creep measurement involves the mutual displacement of molecules past one another resulting in a permanent deformation; whereas the time-dependent recoverable deformations which are characterized by L reflect the orientation imparted to the molecules during the approach to steady state creep. True steady-state creep is achieved when the orientation occurring reaches a maximum limiting value under constant stress conditions and not by an experimentally perceived constant rate of creep, as is sometimes inferred. The time dependent motion occurring without the presence of stress during recovery is thus traceable to the thermal diffusion of the viscoelastic material back to a state of maximum entropy with isotropic properties and randomly disposed molecules.

It was not possible to stop the reaction at various stages by reducing the temperature since the viscoelastic characterization of the material has to be made over a range of temperatures where the molecules are mobile (above T_g) and hence usually reactive. Therefore it was decided to complete the reaction of all epoxide groups at various stages of the molecular network development. Subsequent viscoelastic characterization by means of creep and creep recovery measurements would then be made. The different stages of development were obtained by first reacting a fraction of the epoxide groups with the monofunctional amine, methyl aniline. The remaining oxirane rings were then reacted with a stoichiometric amount of DDS in the frictionless creep apparatus with which the creep measurements were made.

In this manner our structures and results are not affected by any substitutional effect, since the secondary amine methyl aniline reacts with oxirane rings randomly and all the amine hydrogens on the tetrafunctional crosslinking amine DDS are reacted before the creep and creep recovery measurements are made. Eight different concentrations of DDS were used in preparing samples with various stages of network development. The fractions of the equivalent ratios of DDS employed were 0.25, 0.35, 0.40, 0.45, 0.50, 0.60, 0.70 and 1.0.

EXPERIMENTAL

Materials

The epoxy resin used in this study was an Epon 1001F produced by the Shell Corp. It was characterized by our collaborators LeMay, Swetlin, and Kelley[5] at the Polymer Institute of the University of Akron. Its structure is given by:

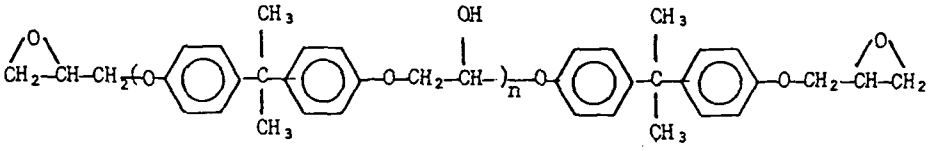

Some of the characterization parameters are:

M_n = 996 g/mole; n = 2.31; and it fictive temperature T_f = 31 C.

The tetrafunctional crosslinking diamine used was 4,4/ diamino diphenyl sulfone, DDS, (MW = 248.3 g/mole)

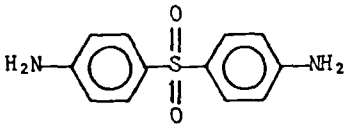

with a melting point mp range of 175° - 178°C. and a density ρ(23°C) = 1.38 g/cm^3 and the monofunctional chain stopping amine used was methyl aniline MA (MW = 107.2 g/mole) with a mp = -57°C and a boiling point range bp = 194 - 196°C. The reagent grade methyl aniline was redistilled in our laboratory. To produce a series of partially - developed epoxy systems representing different stages of the curing process which reflects different stages of molecular network development, we used, as curing agents, various combinations of the mono- and tetra- functional amines, while maintaining the stoichiometry between the oxirane ring concentration and the amine hydrogens.

Sample preparation

As an example, the procedure of preparing the Epon 1001F/0.50 MA/0.50 DDS sample is given below:

1) A sealed flask containing the mixture of 8g of Epon 1001F and 0.50 equivalent ratio of methylaniline, was heated in an oil bath on a magnetic stirrer to the reaction temperature of 143°C. The mixture was reacted for 45 minutes while being constantly stirred. A Fourier Transformer IR (FTIR) spectrum showed that the reaction between Epon 1001F and methylaniline was completed in less than 45 minutes.

2) The reaction product was transferred onto a Teflon sheet, cooled to the room temperature, and was ground into powder with a porcelain mortar and pestle.

3) 0.50 equivalent ratio of DDS powder was added to a measured amount of the reaction product Epon 1001 F/0.50 MA. The well - mixed powders were then heated to 160°C. When the DDS completely dissolved, the mixture was transferred into a vacuum oven at 110°C and was degassed until it became a bubble-free, transparent solution.

4) Portions of the solution were transferred into DSC sample pans which were placed into the sample chamber of the creep apparatus. These samples therefore experienced the same thermal history as the material whose creep behavior was determined. The reaction was completed in the creep apparatus. An unchanging equilibrium compliance J_e measured well above T_g indicates a completed reaction as well or better than other indicators.

Instrumentation

Fictive temperatures which approximate the glass temperature $T_{f,g}$[2,3,6,7] were measured with a Perkin - Elmer Differential Scanning Calorimeter DSC II (Main Ave -M.S.12, Norwalk, CT 06856). Thermograms were obtained with a heating rate of 10°/min immediately following cooling from above T_g at a rate of 10°/min.

Creep and recovery measurements which yield viscosities and recoverable compliance curves were carried out with a frictionless magnetic bearing torsional creep apparatus (Time - Temperature Instruments, P.O. Box 40156, Pittsburgh, PA 15201)[8]. Measurements were made in a nitrogen atmosphere after drying and degassing the sample in vacuum in situ.

RESULTS

Recoverable Compliance and Viscosity of the Neat 1001F Resin.

The recoverable shear compliance $J_r(t)$, (cm^2/dyne or Pa^{-1}) and the shear viscosity coefficient η,(poise, dyne sec/cm^2 or Pa sec) have been determined for the neat (unreacted) Epon 1001F resin in the temperature range 30° to 77°C. $J_r(t)$ curves were obtained at 9 temperatures from 30.2° to 53.5°C; see Fig. 1. A dramatic 10 fold decrease of the steady state recoverable compliance J_e° is seen to occur with a 20°C decrease in temperature. This strong temperature dependence is shown in Fig.2.

Consequently the log $J_r(t)$ curves cannot be reduced to a common curve. In Fig. 3 the log $J_r(t)$ curves are shifted along the logarithmic time scale to a reference temperature T_o chosen to be 30.2°C by using the logarithm of the viscosity ratio $\eta(T_o)/\eta(T)$. $\eta(T_o)$ and $\eta(T)$ are the viscosities at the reference temperature and at the other temperature of measurement, respectively. This plot attempts to compensate for the difference molecular mobilities at the different temperature and clearly depicts how the curves fan out. This thermorheological complexity persists even if the data are reduced to a common J_e°. Reduced recoverable compliances $J_r^R(t)$ were calculated with the expression

$$J_r^R(t) = M(J_r(t) - J_g) + J_g \tag{4}$$

where J_g = the glassy compliance = 8.0×10^{-11} cm^2/dyne

$$M = \frac{J_e^\circ(T_o) - J_g(T_o)}{J_e^\circ(T) - J_g(T)} \tag{5}$$

T_o = the chosen reference temperature

T = the temperature of measurement.

The glassy compliance must be left out of the reduction because it results from mechanisms found at shorter times that have a much smaller temperature sensitivity. J_g was assumed to be temperature independent over the 23°C involved. The process was carried out with the result shown in Fig. 4 that the resulting curves were not superposable because the higher temperature logarithmic curves rise more abruptly toward log J_e°.

Sixteen viscosities were measured between 30.2° and 76.5 where η fell from 1.32×10^{12} poise down to 5.28×10^3 poise. The data which varied over the eight orders of magnitude are well described by the Vogel,[9] Fulcher,[10] Tamman and Hesse,[11] VFTH, equation

$$\eta = Ae^{\frac{C}{T-T_\infty}} \qquad (6)$$

$$\text{or } \log \eta = \log A + \frac{C/2.303}{T - T_\infty} = -2.36 + \frac{470}{T-0°C}$$

where A, C, and T_∞ are characterizing parameters. The latter two are usually interpreted in terms of a free volume model.[4]

Curing Simulation

In the early stages of curing the average molecular weight increases and branching appears. In the case of an epoxy resin displaying an extreme substitution effect linear molecules would grow to appreciable lengths and hence high molecular weights before branch points would appear. In this study branching should occur simultaneously with molecular weight increase, since oxirane rings are randomly reacted first with the secondary amine MA and all of the DDS hydrogens are reacted before our measurements begin. When only 25% of the oxirane rings are reacted with DDS crosslinking molecules it can be seen in Fig. 5 that J_e° has increased by about 30 fold reflecting the increase in molecular weight. Short of the point of incipient gelation the curing system is a viscoelastic liquid whose retardation spectrum in the terminal zone is determined by the molecular weight; more so by its distribution, and by long chain branching.

It should be noted that in Fig. 5 for the system with 25% crosslinking DDS, and for all higher concentrations, the thermorheological complexity exhibited by the neat resin has disappeared; i.e. all of the cured systems yielded $J_r(t)$ curves that were reducible to a common curve within the experimental scatter of the data. Although we have encountered a number of viscoelastic liquids which show deviations from the time-temperature equivalence principle[4], no polymer sample with a molecular network has been observed by us to show such deviations. The reducibility of all of the data beyond that of the neat resin makes our presentation simpler and clearer.

At 35% DDS a modest intermediate plateau is present in the reduced recoverable compliance curve as seen in Fig. 6. This is strongly suggestive of an entanglement plateau. If a bifunctional analogue of DDS were synthesized this conjecture could be tested.

It was expected that the terminal value for $J_r(t)$ would increase to infinity at the point of incipient gelation where an effectively infinite molecular weight was reached. Indeed, when an equivalent ratio of 0.45 DDS was used in the curing, the reduced creep compliance $J_p(t) = J(t)[T\rho/T_o\rho_o]$ increases nine orders of magnitude from the glassy level before indicating a tendency to level off as seen in Fig. 7. Which clearly shows it is just beyond the gel point. The reduced compliance $J_p(t)$ is used for temperature shifting of crosslinked systems only. It has been shown to be inappropriate for uncrosslinked polymers.[12]

The complete effect of the curing of this epoxy resin is depicted in Fig. 8 where the time dependent recoverable compliance, $J(t) - J_{g,o}$, is shown for all of the materials cured with different reaction ratios of amines as a function of the reduced time.* $J_{g,o}$ is the glassy compliance obtained by extrapolating the short time data to zero time with an Andrade plot.

$$J(t) = J_{g,o} + \beta t^{1/3} + t/\eta \tag{7}$$

where J(t) plotted as a function of the cube root of time, yields the glassy compliance from the zero time intercept. This functional form is normally found at compliances below 10^{-9}cm^2/dyne. The time-dependent recoverable creep compliance that is common to all of the systems studied is most clearly seen when the glassy compliance is not included in the comparison. In general the J_g values should be analyzed separately. At the lower degrees of crosslinking (0.25 through 0.40 DDS) the molecular network is not developed and hence the fully reacted materials are still viscoelastic liquids. The dashed lines shown in Fig. 8 represent the recoverable compliance $J_r(t)$; whereas at the greater degrees of branching the molecular network is intact and the solid lines represent the creep compliance J(t). Of course, for a crosslinked material $J(t) = J_r(t)$. The reference temperatures T_o used in the preparation of Fig. 8 were chosen to superpose the short time portions of the $J(t) - J_g$ curves. It can be seen in Table I that the T_os required are on the average two degrees higher than the measured $T_{f,g}$ temperatures. We consider this difference to be within the uncertainty of our knowledge of corresponding glass temperatures. The evolution of the recoverable compliance appears

---

* $J_p(t)-J_{g,o}$ is shown for the viscoelastic solids with molecular networks (solid lines in Fig. 8) and $J_r(t) - J_{g,o}$ is shown for the viscoelastic liquids (dashed lines); i.e. specimens with no gel fraction.

to be reasonable and straightforward. J_e^o increases with molecular weight (0.25 DDS). A rubberlike plateau appears with further increase in molecular weight and branching (0.35 DDS). With further branching and a presumed broadening of the molecular weight distribution, the response broadens on the time scale and the entanglement plateau disappears. At the point of incipient gelation the macroscopic tenuous molecular network is infinitely compliant (0.45 DDS). As the network further develops and becomes tighter the enormously long-time mechanisms disappear due to the intervention of the branchpoints (0.50 DDS). This process of eliminating long-time mechanisms which involves cooperative motions over long distances with the concomitant decrease of the equilibrium compliance (0.60, 0.70, and 1.0 DDS) will be clearly depicted below by the narrowing of the retardation spectrum. In spite of enormous changes observed in the long time deformations with the development of the tight molecular network the short time deformation appears to be unchanged. Of course, the position of the compliance curves on the time scale is dictated by the local free volume which decreases with the elimination of dangling chain ends and the increase of the concentration of tetrafunctional branch points. This decrease in free volume with further network development is the reason for the ascending $T_{f,g}$. The coincidence in form of all of the recoverable response at short times reflects the fact that locally the polymer chain segments are the same and the short time contributions to the deformation arise only from the local segmental chain motions. This coincidence at very short times, may in addition, just reflect contributions to the deformation which are universal for all glassy materials.

The retardation spectrum obtained[13,14] for the earliest stage of pre-gel network-development from the data shown in Fig. 5 (0.25 DDS) is presented in Fig. 9. A short time Andrade region with a log-log slope of 1/3 is followed by a slightly skewed peak. This $L(\tau)$ is typical for a linear polymer with a molecular weight which is less than M_e, the molecular weight per entangled unit[15,16].

The plateau seen in Fig. 6, which is presumed to reflect the presence of an entanglement network, gives rise to the development of the usual two peaks in $L(\tau)^4$, as seen in Fig. 10. In this case the first peak appears as a strong shoulder preceding the rather high long time terminal peak. This shoulder is largely filled-in as the molecular weight distribution is presumed to broaden with increased branching; (0.40 DDS). This can be seen in the comparison plot of all of the retardation

spectra obtained; shown in Fig. 11. The divergence of $L(\tau)$ toward infinity at long times, near the gel point, is clearly seen for the material cured with 45% DDS. $L(\tau)$ increases ten orders of magnitude from the glassy level of response up to the value at long times where the material is enormously compliant (ca 0.1 cm^2/dyne).

Both comparison plots of J(t) and $L(\tau)$, Figs. 8 and 11, clearly indicate from the regions of common response that the curves for reduced times less than 10^9 seconds show characteristic curvature. Only at longer times does there appear to be exponential behavior which is indicated by the straight line segments extending for approximately 5 measured decades. The long-time straight-line slopes are 0.75 for d log $J_r(t)$/d log (t/a_t) and 0.88 for d log $L(\tau)$/d log τ_r.

Temperature Dependence

The temperature dependence of the shift factors a_T used in obtaining all of the reduced creep and compliance curves presented in Fig. 8 are shown in Fig. 12 where the data are linearized according to variation of the VFTH equation

$$a_T = A' e^{\frac{C}{T-T_\infty}} \tag{8}$$

where the constants A and C are 1.231×10^{-16}, 1850, respectively and $T_\infty = T_{f,g} - 50.5°C$. This equation is equivalent to the Williams, Landel and Ferry equation[17] and therefore is an expression of the free volume determination of rate phenomena. The fit of the data was accomplished in the manner used to represent the a_T dependence for polystyrenes of widely varying molecular weights. The resin cured with 0.35 equivalent ratio of DDS was chosen as the reference material. Its optimum T_∞ was 50.5°C below its measured $T_{f,g}$, the best estimate of the glass temperature obtained from heating experiments with a differential scanning calorimeter DDS[2,3,18,19]. The heating at 20°C/min immediately followed cooling from above T_g at the same rate*. Its $T_{f,g}$ was chosen as the reference Temperature T_o where $a_T = 1.00$. Corresponding T_∞s were chosen for all of the other materials so that the same constant C was obtained. It was then assumed that the corresponding "$T_{f,g}$"s were all 50.5°C above the obtained T_∞s. With these "$T_{f,g}$"s chosen to be $T_{o,a}$s

---

* Therefore little physical aging took place while the material was below its T_g.

the value for A = 1.231 X 10^{-16} obtains. The values of the various characterizing temperatures used in this and the compliance analysis presented above are shown for comparison with the DSC $T_{f,g}$ values in Table I.

The viscosities of the viscoelastic liquids 0.25, 0.35, and 0.40 DDS) at the reference temperature $T_{o,J}$ for the reduction of the compliance curves are given in Table II. The temperature dependence of the viscosities of these liquids were found to be the close to that of the recoverable compliance curves over the following temperature ranges: for 0.25 DDS, 65° to 96°C; for 0.35 DDS, 70 to 122°C; and for 0.40 DDS, 79° to 158°C. Viscosities can be calculated with Eq. (6) where the VFTH parameters are given in Table II. All of the values for C are the same as that from the recoverable compliance; see Fig. 12. For 0.25 DDS the T_∞ of 15.8°C is the same as that for $T_r(t)$. For 0.35 and 0.40 DDS the T_∞ = 10°C are a few degrees lower than that used for $J_r(t)$ indicating a slightly smaller sensitivity to temperature for η.

It is of interest to note that the viscosities determined on the neat 1001°F resin were best fitted to a VFTH plot with T_∞ = 0°C so that $\Delta = (T_{f,g} - T_\infty) \approx 31$°C and C = 1080. These values for C and Δ differ substantially from the values of 1850 and 50.5° determined from the fitting of all of the data for Fig. 12. However, since all of the cured systems showed no measurable change in J_e or J_e° with temperature as did the neat resin, it was conjectured that the temperature dependence of the characteristic time constant $\tau_c = \eta J_e^\circ$, which is a pure rate parameter with seconds for units (not dyne sec/cm^2, which are the units of the viscosity coefficient). A plot of log ηJ_e° versus $(T-T_\infty)^{-1}$ with T_∞ = -20°C yielded a good fit to all but the lowest temperature points. From this τ_c fit C = 1890 and Δ = 51°C. These values are certainly within experimental error of the values obtained from the shift factors in Fig. 12. The more fundamental nature of τ_c as a rate parameter, rather than η, has been noted previously under similar circumstances where J_e° of a low molecular weight polystyrene was found to be strongly dependent on temperature[20].

Real Time Curing Beyond the Gel Point

With the stoichiometric amount of crosslinker DDS = 1.0 used in the curing of Epon 1001F it was possible to periodically obtain J(t) curves from about one second out to several hundred seconds. In all of the eight measurements shown in Fig. 13 the compliance obtained at creep times

greater than one hundred seconds were close to the equilibrium values. The approach toward zero slope is the evidence for this claim. The measured J(t) curves are indicated by the solid line curves. The long-dashed lines were deduced in the following manner. The $T_{f,g}$ values shown in Fig. 13 were obtained from the relationship established previously; see Fig. 9 in reference 2. The common short-time compliance curve at $T_{f,g}$ was obtained from Fig. 8 and a glassy compliance of 1.0×10^{-10} cm^2/dyne. Temperature shift factors for the J(t) curves at each stage of cure were then obtained from the common temperature dependence shown in Fig. 10. With these log a_T values each curve was shifted from its $T_{f,g}$ to the temperature of cure, 142.8°C. Where the deduced curves were close to the short time measured points (at 22.4 and 120.6 hrs. of curing) slight addition empirical shifts were allowed to obtain reasonable extrapolations to short times. These are represented by the short-dashed lines.

To make possible a comparison between the results obtained on the fully reacted but partially developed networks and the reacting and developing network, the four extrapolated curves from Fig. 13 were reduced as shown in Fig. 14. The curve corresponding to 22.4 hours of curing was chosen as the reference curve at the temperature of the curing. The curve with the $T_{f,g}$ of 96.8°C represents a degree of cure of 62%; $T_{f,g}$ of 107.2°C - 72%; 125.0° - 88%; and 135.1° - 98%. Examination of Figs. 8 and 14 together shows that the extent of the time dependence and the approach toward equilibrium compliances are comparable. This indicates that beyond the gel point the networks formed are similar. The reduced curves in Fig. 14 are shifted to shorten times relative to those in Fig. 8 by about four decades of time. This is consistent with the fact that the reference temperature in Fig. 14 is approximately 68° above the T_∞ of the reference material; see Fig. 12, $(T-T_\infty)^{-1} \simeq 14.7 \times 10^{-3}$.

DISCUSSION

There has been considerable interest recently in the viscoelastic behavior of the nascent molecular network that forms at the point of incipient gelation. The behavior at high compliance (beyond rubbery levels) and long times has been exclusively examined. Hopes for a universal behavior have been pursued[21] and percolation theory[22-24] suggests material independent exponential behaviors of the viscoelastic functions. Since most investigators show a proclivity to only examine and consider modulus functions, the readily interpretable compliance curves and retardation spectra, that have been obtained in this investigation, have been transformed to modulus curves and relaxation spectra[25]. For the transformations made here no approximation relations were used. Only iterative computer calculations were used for integral inversions, that minimized the discrepancies between the input curves with back calculated results, down to the level of the scatter of the reduced curves (Rheological Transforms Software RTS: Time-Temperature Instruments, P. O. Box 40156, Pittsburgh, PA 15201).

The real G' and imaginary G'' components of the complex dynamic shear modulus $G^* = G' + iG''$ for the nascent molecular network (Epon 1001F/0.55HA/0.45DDS) are presented in Fig. 15 along with a linear plot of the loss tangent, Tan $\delta = G''/G' = J''/J'$,. Except in the region of glassy response at high reduced frequencies, $\omega_r = \omega a_T$, the tenuous gel is very lossy with the loss tangent with values which exceed two. It is clear that exponential behavior is seen between reduced frequencies of 10^{-8} and 10^{-13} where the slopes of log G' and log G'' are both about 0.85. If true exponential behavior were displayed the loss tangent would be constant in the same frequency range. The low frequency peak is rather broad. The absence of constancy may be due to the fact that this sample is very slightly beyond the gel point.

To illustrate how the inclusion of the non-additive effects of the viscosity and the glassy compliance in the modulus destroys the systematic and readily interpretable changes seen in the compliance curves, most of the curves seen in Fig. 8 have been transformed to $G'(\omega)$ and $G''(\omega)$. The results are shown in Figs. 16 and 17 respectively. The low frequency limits of Log $G'(\omega)$ for 0.50, 0.70 and 1.0 DDS are the equilibrium moduli G_e of the increasingly tighter molecular networks. The limiting low frequency slopes of log $G'(\omega)$ and log $G''(\omega)$ for the nascent molecular network

sample 0.45 DDS are both 0.85. The low frequency slopes of log $G'(\omega)$ of the viscoelastic liquid samples 0.25, 0.35 and 0.40 DDS are 2.0, 1.4, and 1.7. The 0.25 DDS sample has reached the limiting value of 2.0 but the 0.35 and 0.40 DDS samples have not. Presumably when they do they will be in inverse order on the log ω scale according to their concentration of DDS; i.e. the 0.25 DDS curve will be found at the highest frequencies with the 0.35 and 0.40 DDS curves at correspondingly lower frequencies. At the lowest frequencies in Fig. 17 it can be seen that log $G''(\omega)$ curves for all of the materials with the exception of the 0.45 DDS sample have reached the limiting slope of one. For the viscoelastic liquids this represents complete domination by viscous flow since in this region $G''(\omega) = \omega\eta$, where η is the steady state shear viscosity coefficient. For the viscoelastic solids with microscopic molecules networks $\eta'(\omega)$ the real component of the dynamic viscosity has reached a constant low frequency limit. With both sets of modulus curves we find very little that is apparent or interpretable in terms of the changing molecular structure on the molecular network is developed. The $G''(\omega)$ are indeed the most unenlightening. Finally the corresponding relaxation spectra for the different stages in network development are shown in Fig. 18. We find them to be an unintelligible morass of crossing curves.

ACKNOWLEDGEMENT

This work was supported by the Air Force Office of Scientific Research under contract F49620-86-C-0032.

REFERENCES

1) J. J. King and J. P. Bell in "Epoxy Resin Chemistry", Ed. R. S. Bauer, ACS Symposium Ser. 114, American Chemical Society, Washington, DC 1979, p. 225.

2) I.-C. Choy and D. J. Plazek, J. Polymer Sci., Part B: Polym. Phys. Ed., 24, 1303 (1986).

3) D. J. Plazek and I.-C. Choy, J. Polymer Sci., Polym Phys. Ed., 27, 307 (1988).

4) J. D. Ferry, "Viscoelastic Properties of Polymers", 3rd Ed. Wiley, New York, 1980.

5) J. D. LeMay, B. J. Swetlin and F. N. Kelley in "Characterization of Highly Cross-linked Polymers, Am. Chem. Soc. Symp. Ser. 243, S. S. Labana and R. A. Dicke, Eds., American Chemical Society, Washington, DC, 1984, p. 165.

6) A. Q. Tool, J. Res. Nat. Bur. Stand., 37 73 (1946).

7) D. J. Plazek, M. J. Rosner and D. L. Plazek, J. Polymer Sci., Polym. Phys. Ed., 26, 473 (1988).

8) D. J. Plazek, J. Polymer Sci., A-2, 6, 621 (1968).

9) H. Vogel, Phys. Z., 22 645 (1921).

10) G. S. Fulcher, J. Am. Chem. Soc., 8, 339, 789 (1925).

11) G. Tamman and W. Hesse, Z. Amorg. Allg. Chem., 156, 245 (1926).

12) D. J. Plazek and A. J. Chelko, Jr., Polymer, 18, 15 (1977).

13) S. J. Orbon, Ph.D. Thesis, University of Pitsburgh, 1978.

14) E. Riande, H. Markovitz, D. J. Plazek, and N. Raghupathi, J. Polymer Sci. Symposium No. 50, 405 (1975).

15) G. C. Berry and D. J. Plazek, in "Glass, Science and Technology", Eds. D. R. Uhlmann and N. J. Kreidl, Academic Press, New York, 1986, Voume 3, p. 319.

16) D. J. Plazek, in Relaxations in Complex Systems", Eds. K. L. Ngai and G. B. Wright, U.S. GPO, Washington, DC, 1985.

17) M. L. Williams, R. F. Landel, and J. D. Ferry, J. Am. Chem. Soc., 77 3701 (1955).

18) D. J. Plazek and M. J. Rosner and D. L. Plazek, J. Polymer Sci., Polym. Phys. Ed., 26, 473 (1988).

19) Z. N. Frund and D. J. Plazek, J. Polymer Sci., Polym. Phys. Ed., 27, 000 (1989).

20) D. J. Plazek and V. M. O'Rourke, J. Polymer Sci., A-2, 9, 209 (1971).

21) F. Chambon and H. H. Winter, J. Rheology, 31, 683 (1987).

22) D. Stauffer, "Introduction to Percolation Theory," Taylor & Francis, London, (1985).

23) J. E. Martin, D. Adolf, and J. P. Wilcoxon, in Fractal Aspects of Materials: Disordered Systems, ed. by D. A. Weitz, L. M. Sander and B. B. Mandebrot, (Materials Research Society, 1989).

24) R. H. Colby, M. Rubinstein and J. R. Gillmor, Dynamic Scaling in Polymer Gelation, Presented at the 60th Annual Meeting Soc. of Rheology Feb. 12-16, 1989, Gainesville, Florida.

25) E. Riande, H. Markovitz, D. J. Plazek, and N. Raghupathi, J. Polym. Sci., Polym. Symp. 50, 405 (1975).

TABLE 1

CHARACTERIZING PARAMETERS

	$T_{f,g}$[a]	$T_{o,J}$[b]	$T_{o,s}$[c]	J_g x 10^{10}[d] cm^2/dyne	β x 10^{10}[d]	$\rho(25°C)$[e] g/cm^3	log J_e[f] cm^2/dyne	M_x[g]
0.25 DDS	63.0	64.1	66.3	1.13	1.46	-	-5.53	-
0.35 DDS	65.0	66.0	65.0	0.685	1.43	1.188	-4.10	-
0.40 DDS	70.6	69.9	66.4	0.65	1.95	-	-3.60	-
0.45 DDS	72.5	72.5	69.9	1.45	2.06	1.189	-	-
0.50 DDS	73.4	75.4	73.7	1.06	1.19	1.191	-5.00	2.95×10^5
0.60 DDS	80.0	84.9	82.0	1.15	2.63	1.194	-5.98	3.10×10^4
0.70 DDS	86.4	89.2	88.7	1.24	1.78	1.218	-6.43	1.12×10^4
1.0 DDS	132.0	135.6	135.5	1.36	1.95	1.205	-7.04	680

a. Measured using DSC; All heating rates were 10°C/min, following cooling at a rate of 10°C/min (20°C/min rate of cooling for 0.35 and 0.45 DDS; and 80°C/min for 1.0 DDS).
b. Reference temperatures which match the softening region on the creep compliance reduced time scale. Reference system was 0.45 DDS.
c. Reference temperature obtained from the temperature shift factor, a_T, analysis; see Fig. 12.
d. Andrade equation parameters for $T = T_{o,J}$.
e. Density of fully-cured samples was measured by flotation; followed by pycnometry.
f. For the viscoelastic liquids J_e is the steady state recoverable compliance and for the iscoelastic solids, beyond the gel point it is the equilibrium compliance.
g. Average molecular weight per cross-linked unit calculated from J_e: $M_x = \rho RTJ_e$.

TABLE II

Viscosities of Non-gelled Epons

$$\log \eta = \log A + C/[T-T_\infty)]$$

DDS Fraction	log A	C	T_∞ °C	log $\eta(T_{0,J})$ poise
0.25	-5.14	1850	15.8	11.49
0.35	-3.419	1850	10.0	10.93
0.40	-2.670	1850	10.0	10.74

LEGENDS

Fig. 1. Logarithmic presentation of the recoverable shear compliance $J_r(t)$ of Epon 1001F as a function of the logarithm of time t at 9 temperatures as indicated.

Fig. 2. Logarithmic plot of the steady state recoverable shear compliance J_e^o of the neat resin EPON 1001F as a function of temperature.

Fig. 3. Attempt to reduce the recoverable compliance curves to a common time-scale of response by using the viscosity ratio $\eta(T_o)/\eta(T)$ as the temperature shift factor. The chosen references temperature T_o = 30.2°C.

Fig. 4. Superposition failure for the Epon 1001F data from three temperatures shown by plotting the reduced recoverable compliance, $J_{r,p}$, as a function of the reduced time-scale.

Fig. 5. Logarithm of the recoverable compliance $J_r(t)$ of the EPON 1001F epoxy resin fully reacted with 0.25 equivalent ratio of DDS and 0.75 of MA plotted against the logarithm of the reduced time, t/a_T. Recoverable compliance curves from five temperatures were reduced to a reference temperature of 64.0°C. The dashed line represents the creep compliance curve, J(t).

Fig. 6. Reduced log $J_r(t)$ vs Log t/a_T plot for epoxy resin Epon 1001F reacted with 35% crosslinking amine, DDS. Five curves determined at the indicated temperatures were used to produce the curve reduced to 65°C as the reference temperature T_o.

Fig. 7. Reduced compliance $J_p(t)$ for epoxy cured with 45% DDS presented in similar fashion to the J(T) curves in Figs. 3 and 4. Six curves were shifted to 72.5°C. This material was exceedingly close to the incipient point of gelation.

Fig. 8. Comparison of all of the time dependent reduced compliance $[J_p(t) - J_g]$ dashed line curves as logarithmic functions of log t/a_T. Comparison temperatures are indicated above and in Table I.

Fig. 9. Double logarithmic plot of the retardation spectrum $L(\tau)$ as a function of the reduced retardation time obtained from the data of Fig. 3 for the epoxy cured with 0.25% DDS.

Fig. 10. Double logarithmic plot of $L(\tau)$ shown as a function of τ obtained from the data of Fig. 4 for an epoxy cured with 0.35% DDS.

Fig. 11. Double logarithmic comparison plot of all of the $L(\tau)$s obtained on the fully reacted Epon 1001F/DDS/MA mixtures. The dashed lines indicate the absence of a macroscopic network (gel). The solid lines indicate that a molecular network is present.

Fig. 12. VFTH plot of the time scale shift factors of a_T obtained from the reduction process to obtain the compliance curves of Fig. 6. See text for details.

Fig. 13.Logarithmic plot of the shear creep compliance measured during the curing of Epon 1001F with a stoichiometric amount of DDS at 142.8°C. All measurements were made after gelation occurred. Curing time T_c when creep measurements were made are indicated. Long-dashed extrapolation lines calculated as described in text. The short-dashed lines are empirically shifted to make reasonable extrapolations during the latter stages of cure.

Fig.14. Selected curves from Fig. 13 reduced to the curve with t_c = 22.4 hrs. of cure, after the subtractions of the glassy compliance J_g.

Fig. 15.The storage G' and loss G'' moduli of the incipient gel (Epon 1001/0.55 MA/0.45 DDS) plotted logarithmically as a function of the logarithm of the reduced frequency $\omega_r = \omega a_T$ (radius sec^{-1}). The loss tangent is also shown. The temperature of reduction is 72.5°C.

Fig. 16.The storage modulus G' plotted logarithmically as a function of the reduced frequency for the different stages of network development of the Epon 1001F/DDS system. A solid line indicates a viscoelastic solid. Long-dashed lines indicate viscoelastic liquids. Short-dashed lines are extrapolations beyond the reduced measurement range. The reference temperatures are the same as those indicated in Fig. 8.

Fig. 17.The loss modulus G'' for the various stages in network development plotted according to the description of Fig. 16.

Fig. 18.The relaxation spectra $H(\tau)$ for the different stages of network development presented as described in Fig. 16.

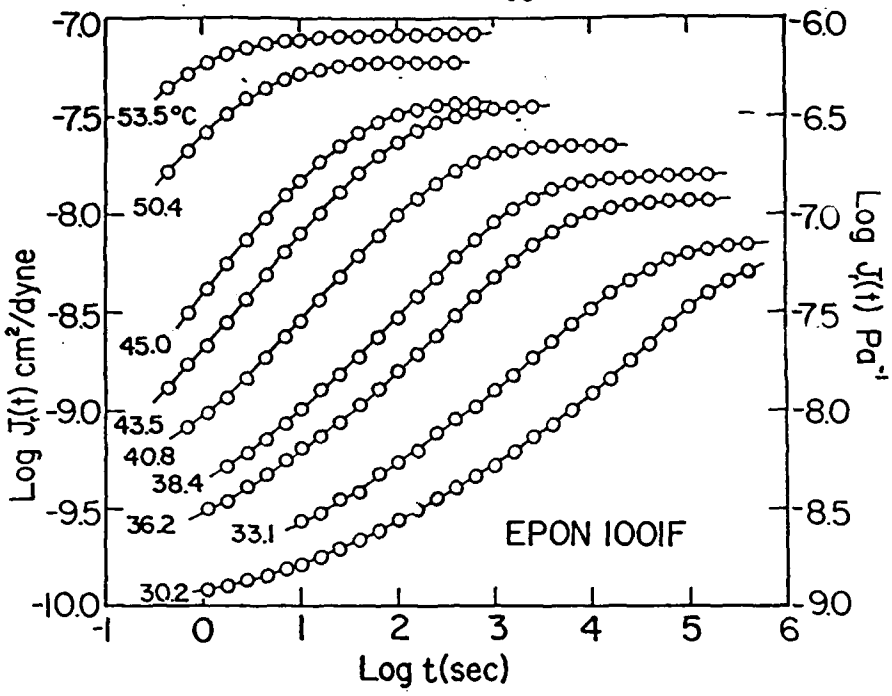

Figure 1

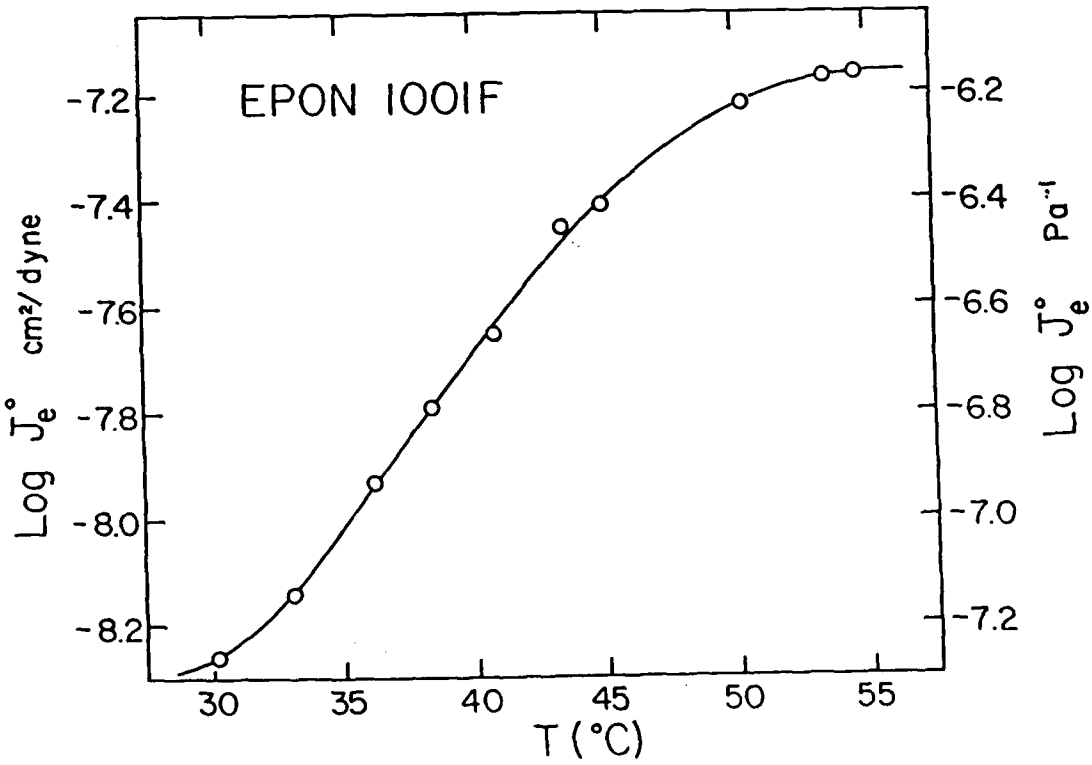

Figure 2

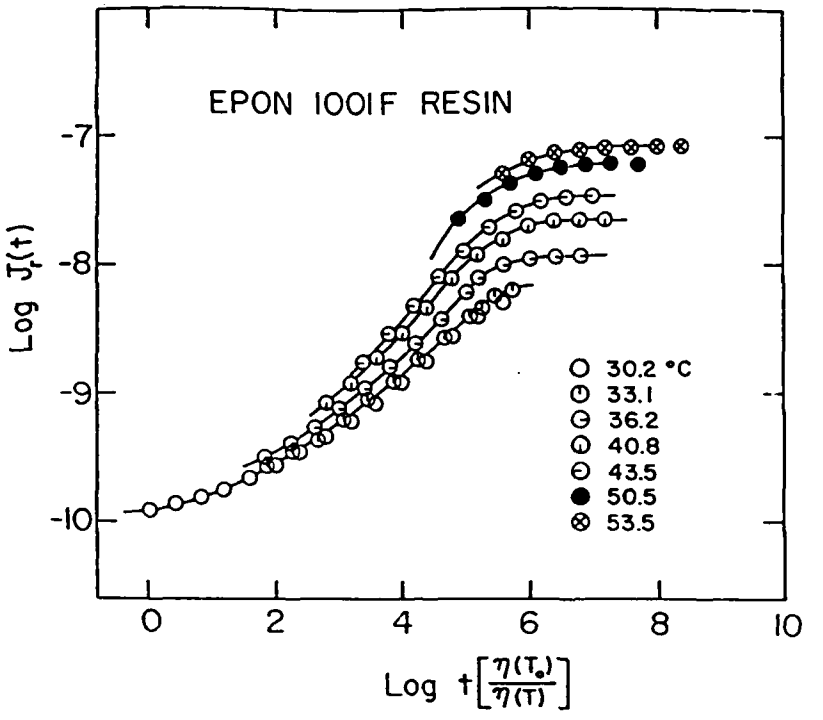

Figure 3

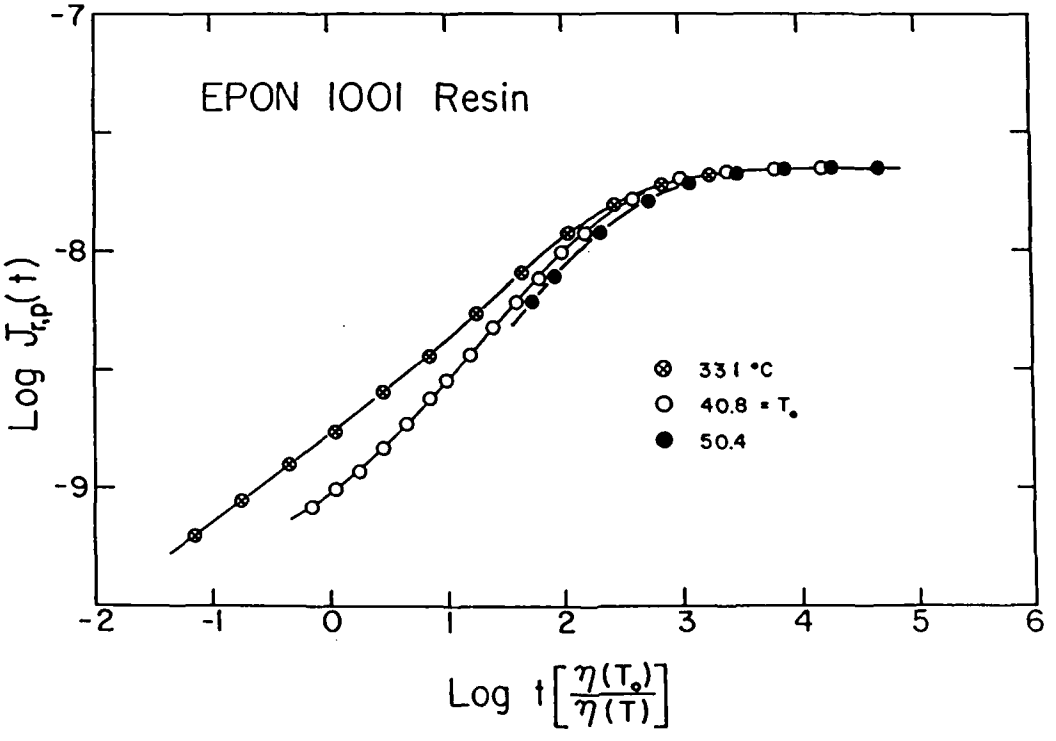

Figure 4

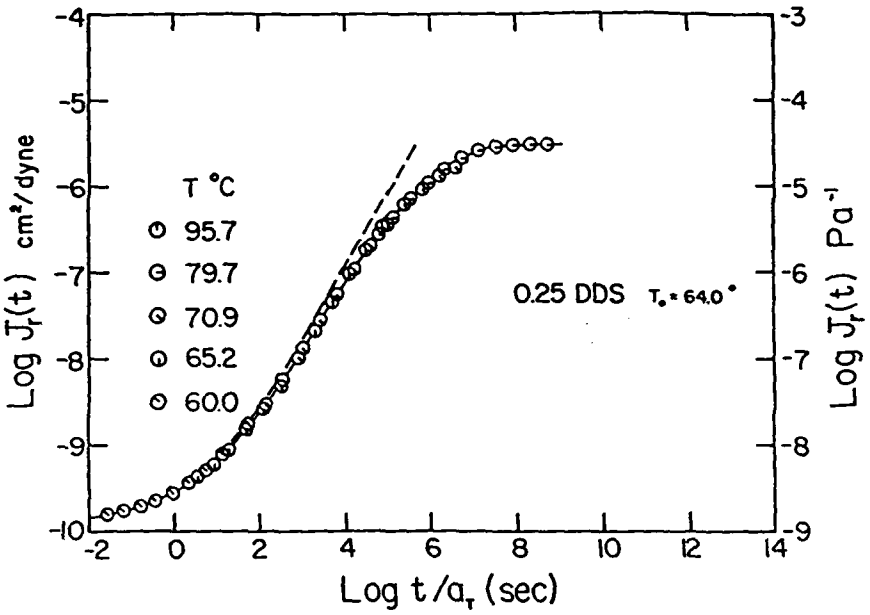

Figure 5

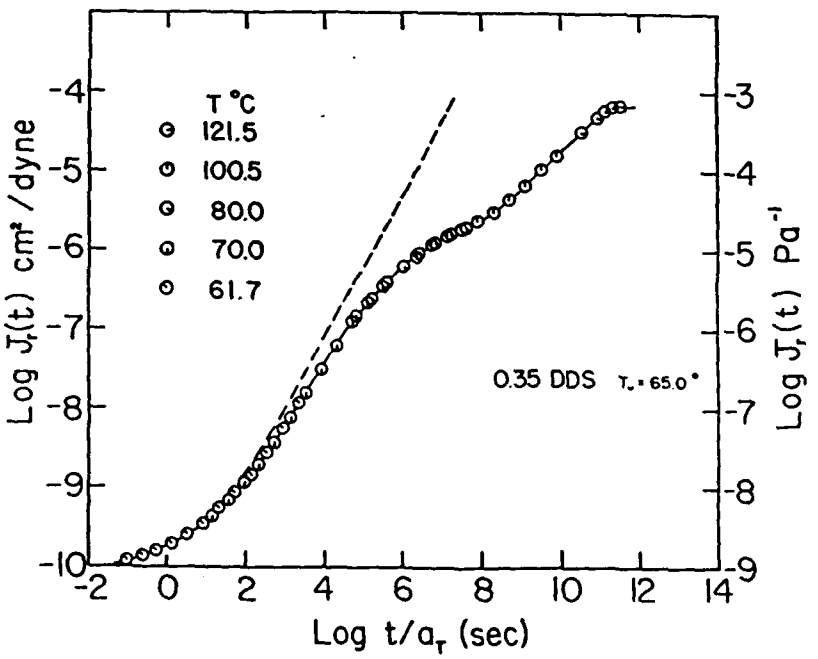

Figure 6

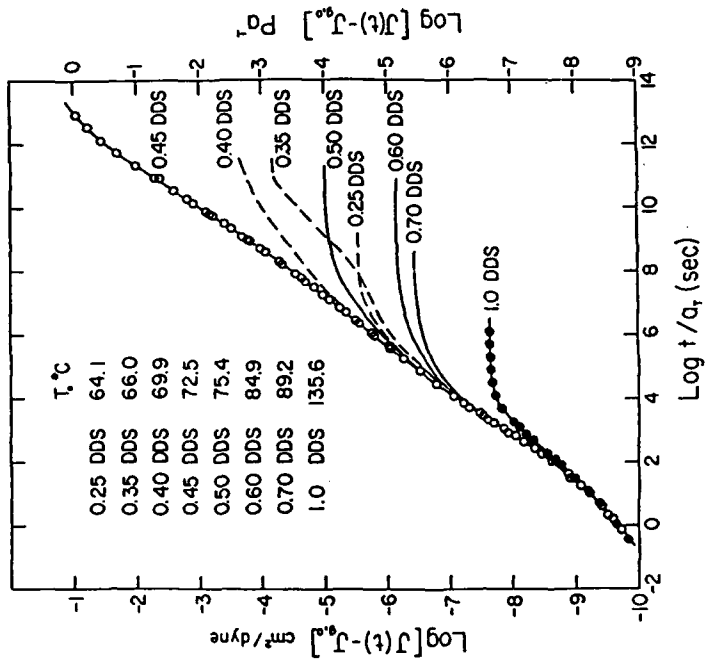

Figure 8

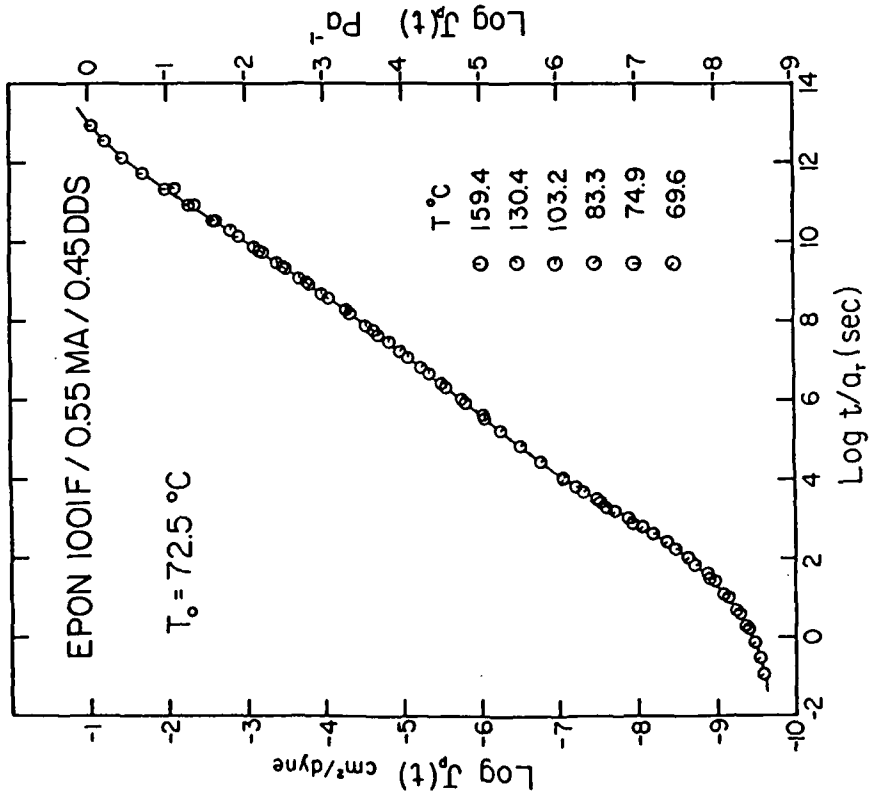

Figure 7

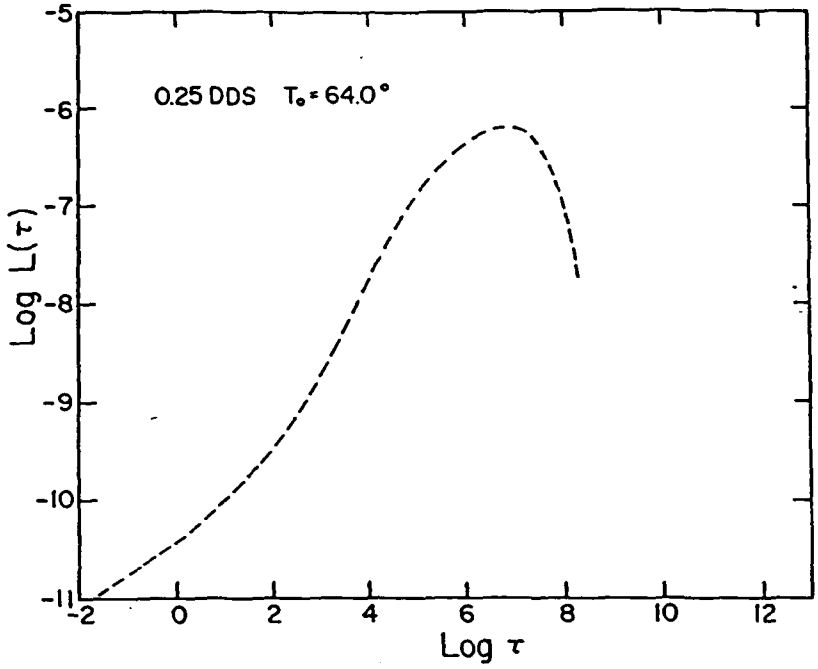

Figure 9

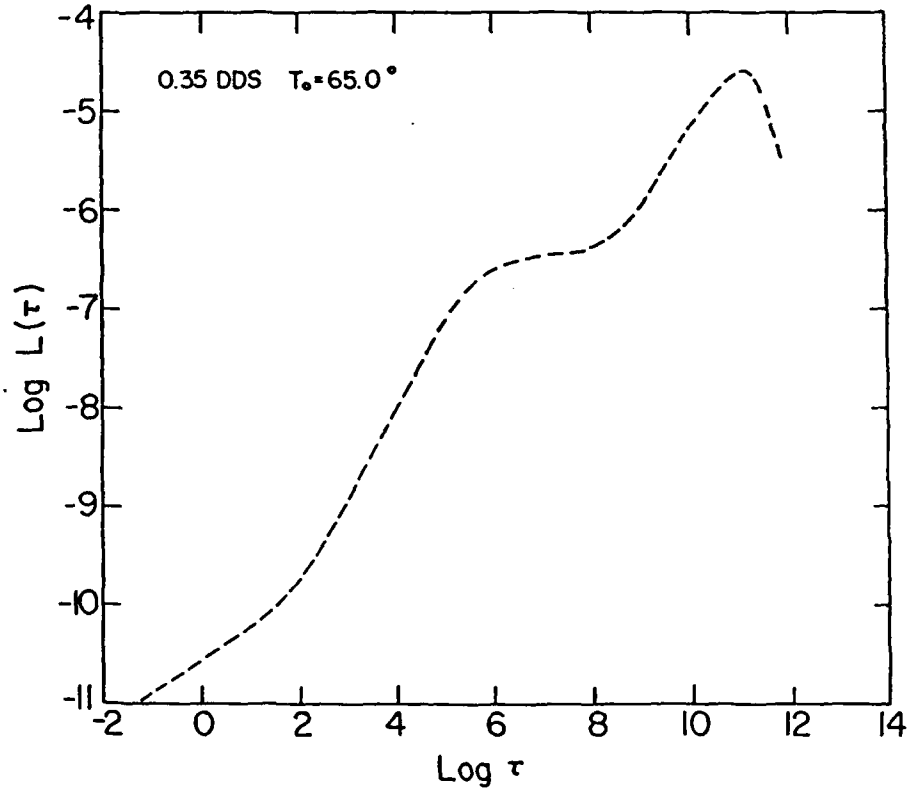

Figure 10

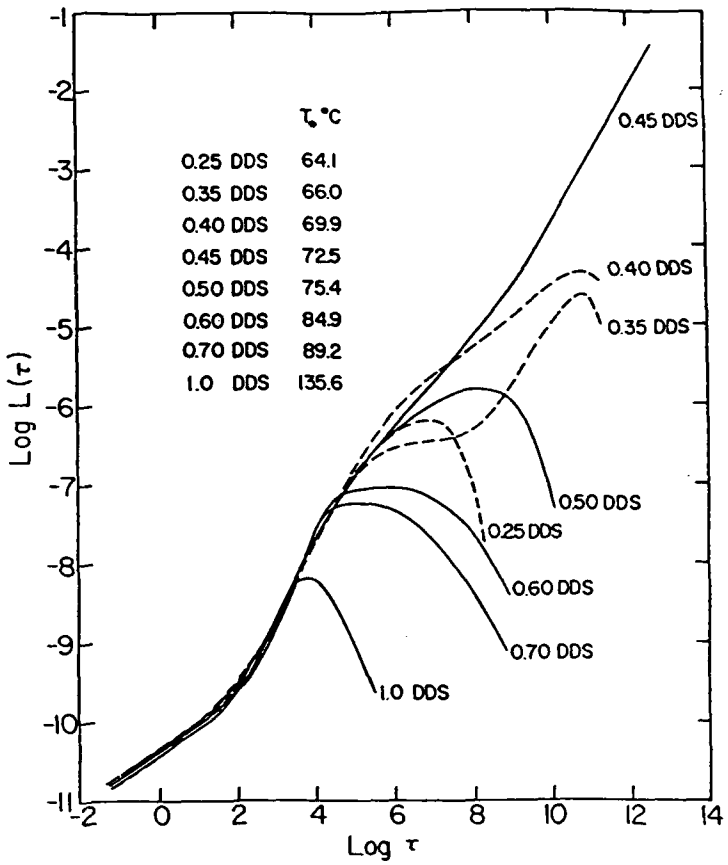

Figure 11

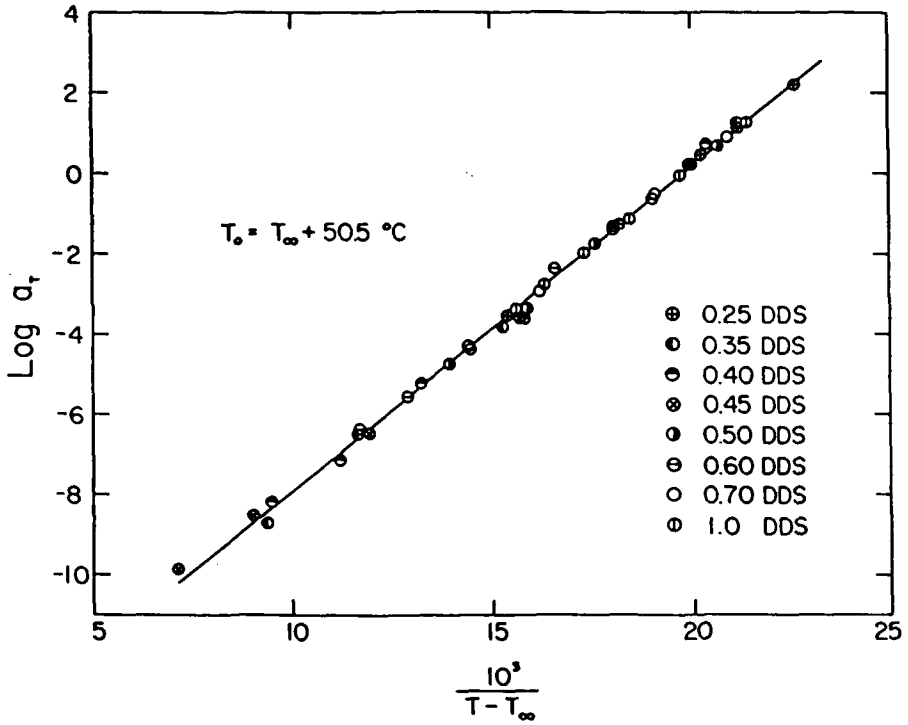

Figure 12

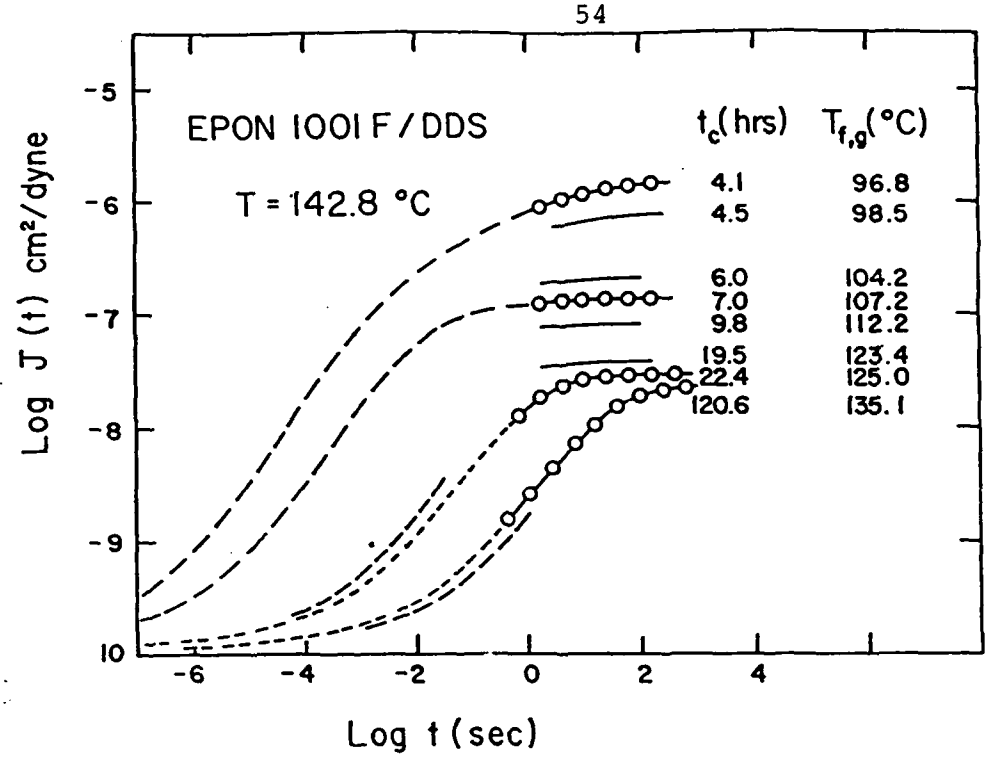

Figure 13

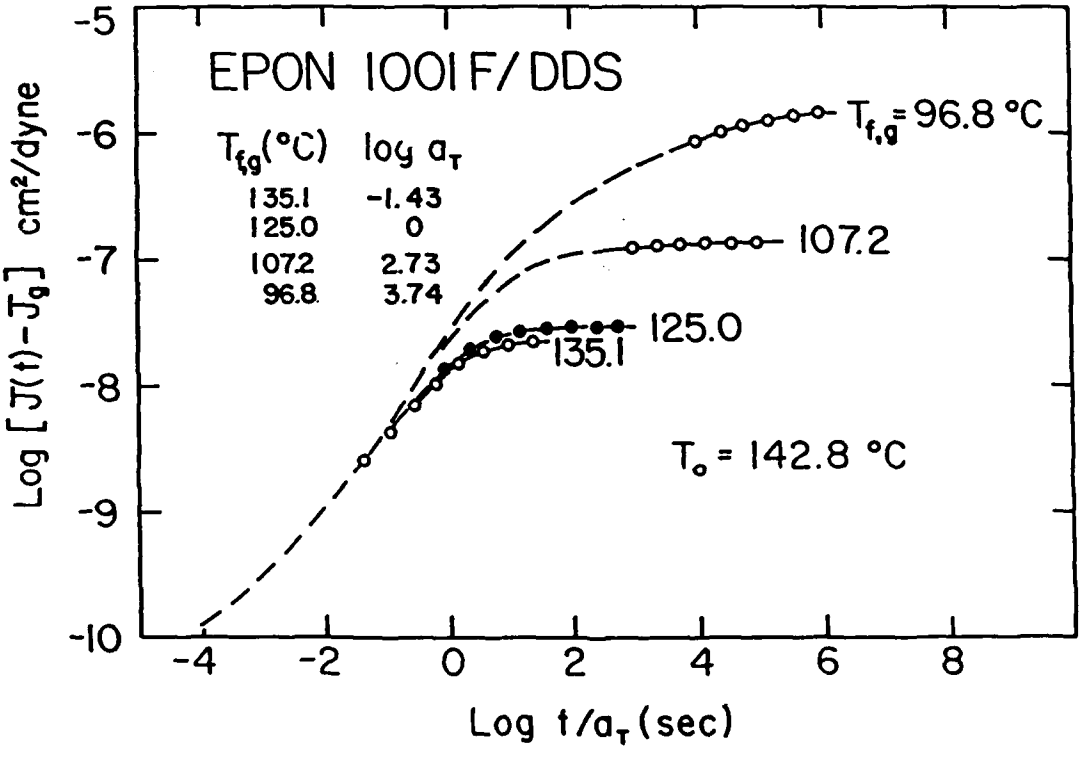

Figure 14

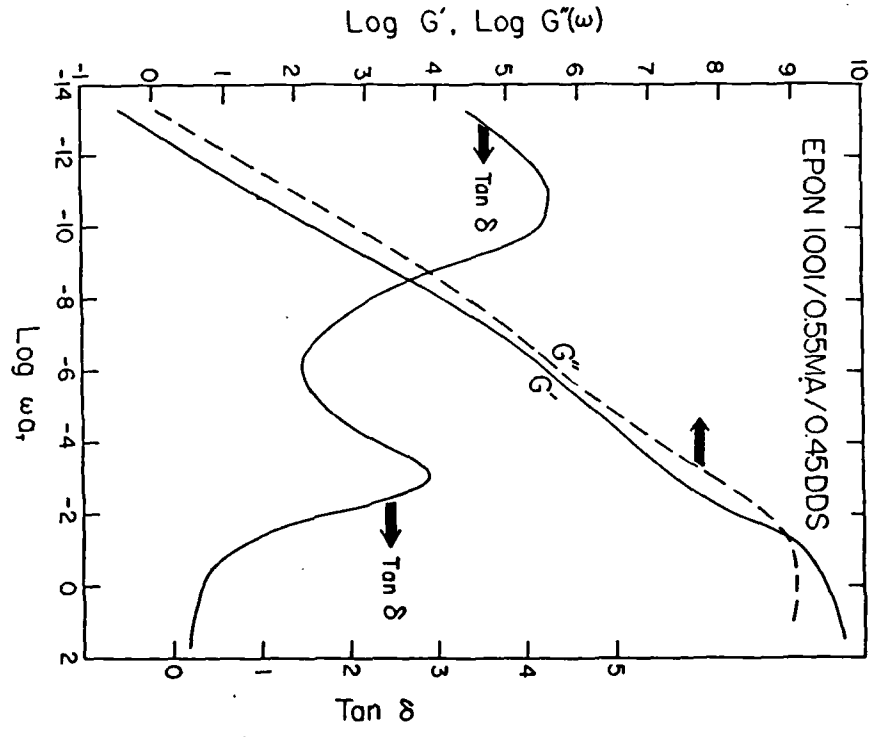

Figure 15

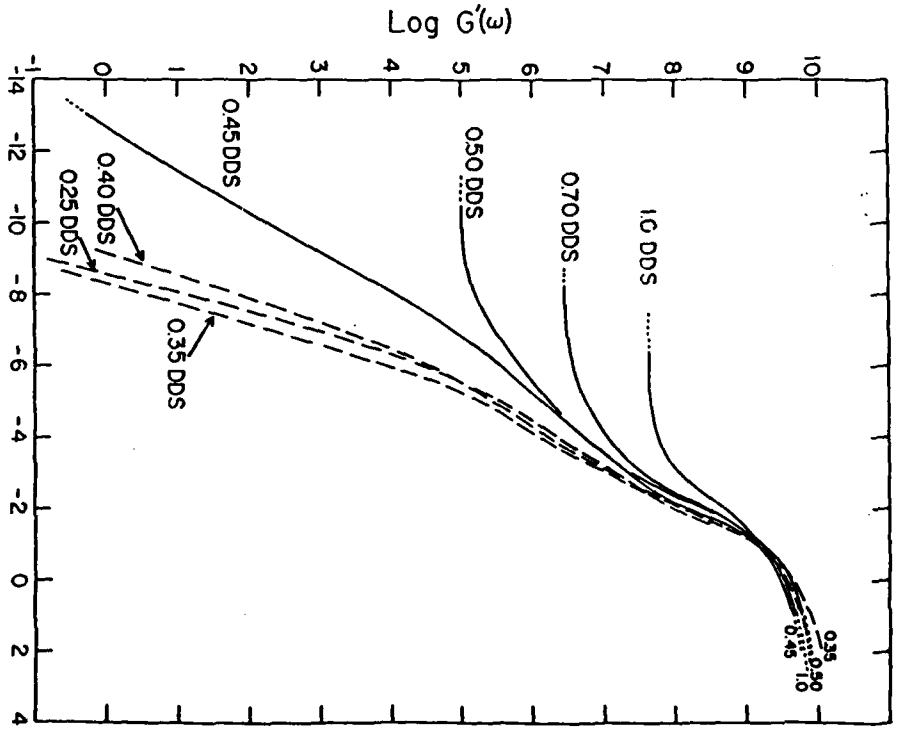

Figure 16

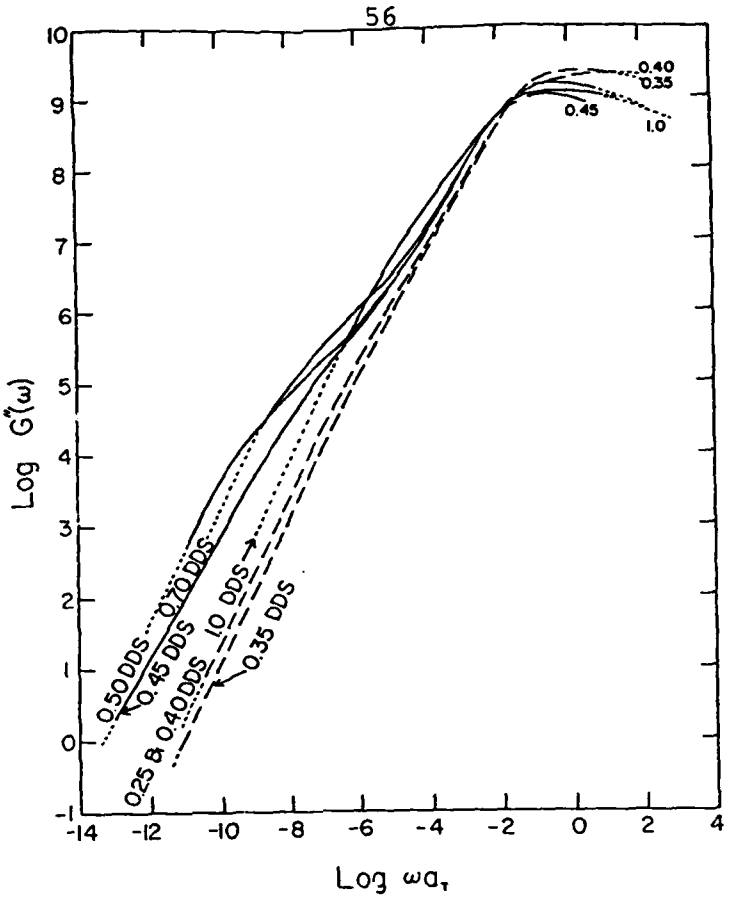

Figure 17

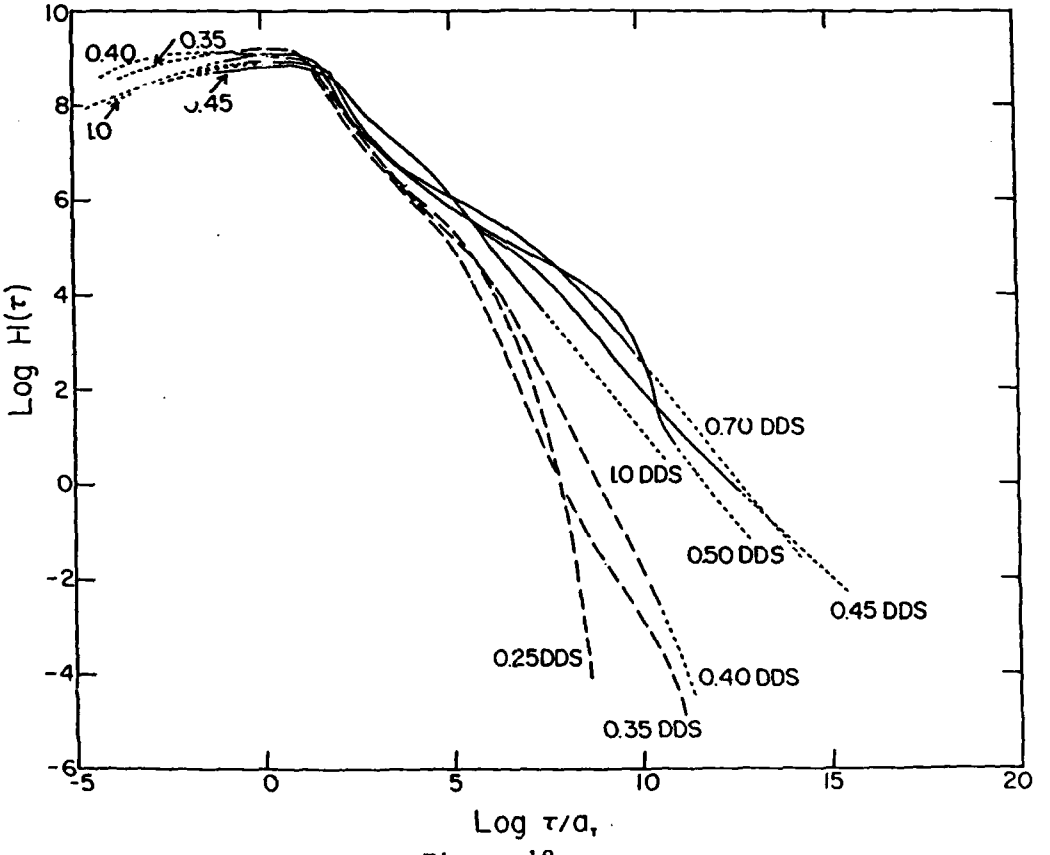

Figure 18

III. EPOXY RESINS (DGEBA), THE CURING AND PHYSICAL AGING PROCESS

By

D. J. Plazek* and Z. N. Frund, Jr.**

ABSTRACT

Differential Scanning Calorimetry (DSC) and Infrared Spectroscopy (IR) were employed to monitor the degree of cure of partially-cured epoxy resin (Epon 828/MDA) samples. The extent of cure, as determined by residual heats of reaction concurred with that determined by monitoring the infrared radiation absorbance of the epoxide group near 916 cm^{-1}. The fictive temperature $T_{f,g}$ was found to increase with the degree of cure, increasing rapidly during cure until reaching a value near the cure temperature T_c of 130°C (approximately 80 percent cure) where the material vitrified. The greatly reduced reaction rate during the final 20 percent of cure was not only a consequence of vitrification but, as revealed by infrared spectroscopy, the result of the depletion in the number of reactive epoxide groups. The endothermic peak areas and peak temperatures evident during the DSC scans were used as a measure of the extent of "physical aging" which took place during the cure of this resin, and after, fully-cured samples were aged 37°C below their ultimate glass temperature for various periods of time. The rate of physical aging slowed down as the temperature increment ($T_{f,g}-T_c$) increased. While an endothermic peak was evident after only one hour of cure ($T_{f,g}$ = 138.3°C), such as a peak did not appear until fully-cured samples were aged for 16 hours or more. Enthalpy data revealed that for partially-cured material, the fictive temperature $T_{f,a}$, reflecting physical aging, increased with curing time. In contrast, the $T_{f,a}$ for fully-cured samples decreased with sub-T_g aging time. The characteristic jump in the heat capacity ΔC_p which occurred at the $T_{f,g}$ decreased as curing progressed. This decrease appears to be dependent upon the rotational and vibrational degrees of freedom of the glass. Finally, a graphical method of determining the fictive temperature $T_{f,a}$ of partially and fully-cured epoxy material from measured endothermic peak areas was developed .

*University of Pittsburgh, Department of Material Science and Engineering, Pittsburgh, PA
**Mine Safety Appliances Company, Pittsburgh, PA

INTRODUCTION

Epoxy resins, traditionally used only as adhesives and coatings have become the most common matrix for aerospace composite materials. The degree of cure of an epoxy is influential in determining its physical properties, i.e., dimensional and thermal stability, compliance, glass temperature, etc. Of particular concern are the consequences of physical aging (densification at a temperature below the glass temperature T_g) (1,2), one of which is the increase in the material's brittleness.

Previous studies (3,4) have been made on the physical properties of epoxy resins during and after curing. During curing the increasing density was monitored in dilatometer. The increasing density was caused by the substitution of shorter primary covalent bonds for secondary, dispersion or van der Waals "bonds" as the chemical reaction proceeded. The higher densities reflect greater molecular crowding; both of which are manifested by the higher glass temperatures T_g.

It was observed that when the T_g of the system became greater than the curing temperature T_c, not only did the reaction deccelerate but endothermic peaks in the heat capacity C_p – temperature curves and maxima in the thermal expansion coefficients α appeared and increased with time. It became clear that these peaks were simply manifestations of what has become known as "physical aging".

When an amorphous material is held at a temperature below its T_g, the density increases spontaneously with the passage of time as an equilibrium liquid structure is approached. In addition, many of its kinetic responses become sluggish. Upon heating, such an aged glass retains the glassy values for the C_p and α to temperatures above T_g. As the material's temperature increases further, acceleration in the enthalpy H and specific volume v_{sp} curves are observed. As higher molecular mobilities are achieved during heating the material can reach an equilibrium structure. This increase in mobility is autocatalytic since the increasing free volume which occurs with thermal expansion is the rate determining parameter.

Once the T_g increases past T_c the material is in the physical aging domain. Network development and physical aging are concurrent. The endothermic peaks found at this stage of curing were so large that it was thought that densification was more efficient during reaction than after full

curing. It was surmised that the mobility of the unattached molecules was possibly greater than that of the molecular segments incorporated into the network. A study of the aging which occurred during the curing reaction and after full cure would have to be performed to study this hypothesis. Such a study was carried out and is reported here.

Differential Scanning Calorimetry (DSC) and Infrared Spectroscopy (IR) were used to monitor the heats of reaction, and infrared absorbance, respectively, of a diglycidyl ether of bisphenol A (DGEBA) epoxy resin cured for different periods of time. Differential Scanning Calorimetry was also used to measure the extent of physical aging which took place during the cure of an epoxy resin at a temperature below T_g (∞) the glass temperature of the fully-cured resin. Fully-cured epoxy samples were also aged at the chosen curing temperature.

BACKGROUND

The Curing Process

Curing of an epoxy resin involves the development of a three-dimensional molecular network from the reactants via branching during polymerization with no volatile by-products. The combination of an epoxide and the primary amine leads to two principal reactions. The first is the expected attack of the epoxide group by the primary amines. When the remaining secondary hydrogens combine with the second epoxy molecule a branch point is formed. As a result of branching, thermosetting resins become set, i.e., infusible and insoluble. Whether branching or linear growth occurs faster depends on the relative reaction rate of the epoxide with the primary or secondary amine (5). Eventually the molecular chains become linked together into networks of effectively infinite molecular weight. The volume contraction which occurs during cure is a result of the exchange of van der Waals "bonds" for shorter covalent bonds. Because of increased molecular crowding, the glass temperature is elevated.

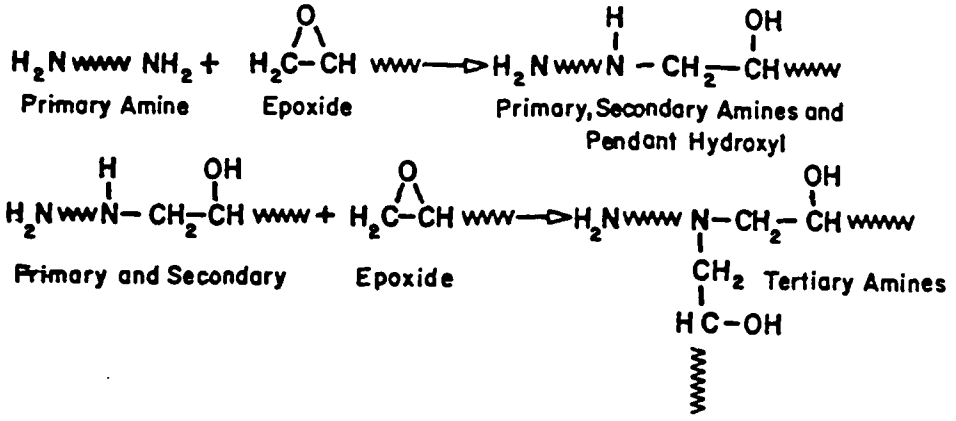

Figure 1. Chemical Reaction of Primary and Secondary Amines with Epoxide Group

The moment of a sudden and irreversible transformation from a viscoelastic liquid to a solid gel is known as the gel point. At this point a covalently bonded molecular network extends throughout and the viscosity becomes infinite. Gelation occurs at a specific point in the course of the chemical reaction and depends on the functionality, reactivity, and stoichiometry of the reactants (6). Gelation typically occurs between 55 and 80 percent conversion (degree of cure p = 0.55 - 0.80).

Distinct from gelation, vitrification may occur at any stage of the reaction. This transformation from a viscous liquid or elastic gel to a glass appears when the glass transition temperature of the material reaches the cure temperature. Further cure in the glassy state is slow and usually diffusion controlled.

Vitrification is a reversible process. Curing can be accelerated by heating the partially-cured thermoset above its glass temperature T_g. Therefore, to assure full cure, thermosets should be cured near or above their ultimate glass temperature.

The Glass Temperature T_g Versus Fictive Temperature T_f

The glass temperature T_g is the temperature below which a material exhibits properties typical of a glass. It is usually defined in terms of the material's specific volume or enthalpy as a function of temperature, obtained at a specified cooling rate. At temperatures above the glass transition the molecular mobility is great enough for the liquid to rearrange rapidly to a structure characteristic for its temperature. Upon cooling, the increase in

molecular crowding decreases the mobility to the point where rearrangements necessary to achieve an equilibrium liquid configuration and density cannot keep up with the rate of cooling. The point of departure from this equilibrium state or break (abrupt decrease in slope) in the specific volume-temperature cooling curve depends on the rate of cooling. The departure or break comes sooner - at a higher temperature with faster cooling. At slower cooling rates the sluggish molecular rearrangements can keep up with cooling until a lower temperature is reached. This break point is identified as a glass transition temperature and is a material characterizing parameter.

According to Toole (7), the fictive temperature is a hypothetical temperature at which the structure of the glass would be at equilibrium. It can be determined from DSC heating curves. The response of any glass upon heating is a function of its thermal history (i.e., time of aging at a constant temperature, rate of cooling, etc.) and the rate of heating. The fictive temperature is a specimen property rather than a characteristic material property. Although Toole's hypothesis may not be correct, the operational definition is useful in characterizing glassy specimens. The fictive temperature can be determined by the intersection point of the measured specific volume-(or enthalpy) temperature line with the equilibrium volume-(or enthalpy) temperature line of the specimen.

The glass transition temperature must be determined from cooling, not heating curves. Unfortunately, because of unavoidable supercooling of calibration standards, accurate T_g values cannot be measured with current differential scanning calorimeters since these instruments cannot be corrected for temperature lags. Even if these lags could be corrected for, partially-cured thermosets cannot be taken to temperatures which are much higher than the curing temperature (to prepare for cooling) without incurring further chemical reaction. This additional reaction changes the value being sought. Consequently, only the fictive temperatures of curing systems can be determined.

In spite of the fact that glass transition temperatures can only be determined from cooling experiments, most reported "glass temperatures" are obtained from heating curves or from measurements of loss moduli or loss tangents. The latter qualitatively correlate with T_g's but are always higher by 15 or 20°C. The chosen frequencies determine the position of the mechanical property maxima. In a material with minimal aging the T_f will not be more than a few degrees below the T_g at the same rates of heating and cooling.

MATERIALS

Epoxy resins are characterized by a chemical structure containing the highly reactive epoxide group or oxirane ring.

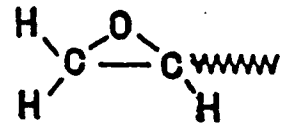

Figure 2. Chemical Structure of Epoxide Group

In the present study, the Epon 828 epoxy resin was cured with methylene dianiline (MDA). Epon 828, principally a diglycidyl ether of bisphenol A, is difunctional. The tetrafunctional methylene dianiline is produced by Uniroyal. The chemical structure and some characteristics of the Shell Epon 828 and Uniroyal Tonox are shown below.

Shell Epon 828 Epoxy (DGEBA) Resin Structure and Characteristics

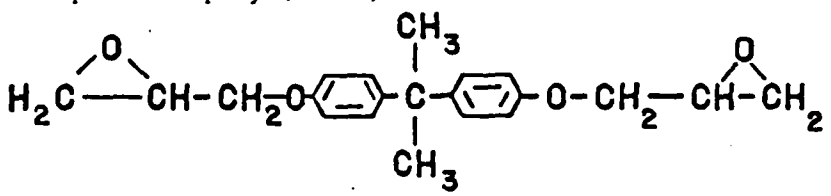

Viscosity (25°C): 110-150 poise
Specific Gravity (20°C): 1.10
Epoxide: 0.52-0.54 eq./110 gms
M_n: 380 gms/mol
T_g: -14°C
Epoxy Equivalent Weight (number of grams of resin containing one chemical equivalent of an epoxy group): 190
Functionality (M_n/epoxy equivalent weight): 2.0

Uniroyal Tonox Methylene Dianiline (MDA)

Specific Gravity (20°C): 1.16
Molecular Weight: 198.3 gms/mol
Melting Point: 90-93°C

EXPERIMENTAL PROCEDURES

Stoichiometric ratios of the Epon 828 and MDA were mixed. The mixture was heated in a Pyrex beaker to 95°C and stirred by hand until a clear homogeneous solution resulted. This beaker, with the mixture, was then partially immersed in ice water for 30 minutes to inhibit further reaction. Heats of reaction and thermal phenomena near the glass temperature T_g were measured with a Perkin-Elmer System 4 Differential Scanning Calorimeter. An Analect AQS-20 Fourier Transform Infrared (FTIR) Spectrophotometer was employed to monitor the changes which occurred within the absorbance band intensities of partially-cured material.

Heats of Reaction and Thermal Phenomena During Cure

Endothermic peaks reflecting the state of densification of aged samples were determined for samples at different stages of cure. This measurement erased the effects of aging and the fictive temperature of the samples were then determined immediately after cooling.

For the DSC investigation, 9-14 milligrams of the uncured mixture were measured into standard aluminum pans and covered with lids. Samples were then placed in 0.625 inch diameter by 0.375 inch deep cavities within a thermostatted metal block. The metal block was preheated and maintained at 130 ± 1°C. Samples were periodically removed from the metal block and placed on a metal surface at 23°C. Within 30 minutes the endothermic peak areas and temperatures, and fictive temperatures were determined at a heating rate of 20°C/minute. The temperature and heat flow calibration of the DSC was performed with indium and synthetic sapphire standards at different heating rates.

To determine the degree of cure samples were removed from the heated metal block and placed in the DSC at 0°C where negligible reaction took place. They were then heated to 169°C at a rate of 100°C/minute. Samples were maintained at 169°C for as long as one hour. The total exotherm during this period was used as a measure of the samples' degree of cure. At 169°C all samples were found to achieve their ultimate fictive temperature of 167°C within one hour or less. A heating rate of 100°C/minute was used to minimize any unrecorded reaction.

Infrared Spectroscopy During Cure

The absorption of infrared radiation due to the molecular vibration of epoxide groups at 916 cm^{-1} was measured as a function of cure time. A microthin-layer of the uncured mixture was evenly spread between two potassium bromide (KBr) windows. Prior to this however, the windows were polished and their spectra obtained and stored in the FTIR spectrophotometer as a background reference. The KBr windows with sample were placed between two metal plates at 130±1°C for discrete periods of time. They were then placed in the spectrophotometer and a spectrum (4000-400 cm^{-1}) from 32 scans obtained.

Thermal Phenomena During Physical Aging With No Reaction

To monitor the physical aging process without a simultaneous chemical reaction, fully-cured DSC samples in which the previous effects of aging had been erased were placed back into the heated metal block at 130±1°C. Fully-cured samples were used so that the aging process was not masked or effected by the curing reaction. Periodically, samples were removed from the metal block and quickly cooled. The endothermic peak temperature and area, and fictive temperature of these samples were then determined.

RESULTS AND DISCUSSION

Thermal Phenomena and Heat of Reaction During Cure

Table I is a listing of the thermal phenomena and degree of cure values determined from DSC studies and infrared spectroscopy for partially-cured samples. After curing for one hour or more the fictive temperatures reached values greater than the cure temperature T_c of 130°C and a dense glass was formed. This was a simple consequence of "physical aging" during cure and is manifested by a large endothermic peak upon first DSC heatings. See Figure 3. Sickfeld and Mielke (8) reported the presence of an endothermic peak when epoxy coatings were cured 22°C below their ultimate T_g.

Figure 3 revealed that the thermograms had similar slopes and that peak areas and temperatures increased with cure time. Such samples were quickly cooled at 80°C/minute from just beyond their endothermic peak. This brief excursion above the glass temperature erased the effects of physical aging yet did not cause appreciable additional cure. A second heating which immediately

followed was necessary to obtain the "normally shaped" curves presented in Figure 4.

Two sets of fictive temperatures are listed as a function of curing time in Table I. The lower values, $T_{f,a}$, were determined from enthalpy values, H, obtained during first DSC heating scans. They reflect the amount of physical aging which occurred during the curing reaction, after the material's T_g became greater than the curing temperature. In Figure 5, the ΔH values for a sample cured for nine hours at $130\pm1^{\circ}C$ are plotted as a function of temperature. The ΔH values were determined from the equation $\Delta H=H(T) - [H(150^{\circ}C) + C_{pg} (T - 150^{\circ}C)]$, where the heat capacity C_{pg} was determined from the slope of the enthalpy H versus temperature curve in the glassy region. A $T_{f,a}$ of $151.0^{\circ}C$ was found by extrapolating back from the linear portion of the curve (above $180^{\circ}C$ in this case) to the portion of the curve having a slope close to zero. Plots of ΔH versus T showed such slight changes in slope that extrapolations were not definitive. The correspondingly higher $T_{f,g}$ values were obtained directly from the second heating curves after aging had been erased by the initial heating to a temperature above T_g.

As illustrated in Figure 4, the fictive temperature $T_{f,g}$ was taken as *the midpoint from the extension* of the pre- and post-transition baselines of the DSC thermogram. The $T_{f,g}$ is the point in the thermogram where the heat capacity changes the most rapidly. All thermograms had similar slopes and their $T_{f,g}$'s increased with cure time. It can be seen in Figure 4 that when there is little or no physical aging, there is no maximum in the heat capacity curve. A sample's $T_{f,g}$ is expected to be close to its glass temperature (normally obtained during cooling) if the heating follows immediately after cooling from above T_g (3).

The total peak areas values listed in Tables I and II were determined by superimposing the second DSC heating scan of a sample over its first. The peak area bounded by these curves was then measured. This is illustrated in Figure 3 for a sample cured for 336 hours at $130^{\circ}C$.

A sample's degree of cure p was calculated from the equation $p = (\Delta H_o - \Delta H_t)/\Delta H_o$ where ΔH_o is the total exotherm for the initially uncured sample and ΔH_t is the exotherm of a partially-cured sample. The Epon 828/MDA was heated to $169^{\circ}C$ immediately after mixing (with no induced cure). Its exotherm yielded a ΔH_o equal to 98.7 calories/gram. Figure 6 presents the isothermal DSC thermograms for an uncured sample and those which had been

partially-cured for 0.166 and 0.250 hours at 130±1°C. It illustrates how the exotherm decreased when a sample was cured for increasing periods of time. After approximately 40 minutes at 169°C, all samples achieved the ultimate $T_{f,g}$ of 167°C.

The fact that perceptible curing proceeds near 130°C, a temperature 37°C below the material's ultimate $T_{f,g}$ where molecular crowding is so great that the equilibrium density cannot be reached in less than a millenium is suprising. Aherne, Enns, Doyle and Gillham (9) have reported similar findings for epoxy when $T_c = T_g - 26°C$.

Infrared Absorbance During Cure

The infrared spectra of this epoxy resin/MDA system exhibited an absorption band due to the vibration of the epoxide groups near 916 cm^{-1}. See Figure 7. This vibration phenomenon was due to the bending of the -C-O-C- triad. According to Antoon, Starkey and Koenig (10) and others (11), an epoxy's extent of reaction can be monitored by measuring the intensity of the 916 cm^{-1} absorption band, $A_{916\ cm^{-1}}$. Figure 7 illustrates how the intensity of the 916 cm^{-1} band decreases with increasing cure time, indicating a reduction in the number of epoxide groups. The $1-A_{916\ cm^{-1}}$ values for partially-cured samples are listed in Table I.

Bands initially at 3340 and 3473 cm^{-1} arose from the stretching of the N-H bonds within the MDA. As curing progressed, the amine hydrogens were depleted and a broad O-H stretch between 3200 and 3600 cm^{-1} became evident. This was due to the hydrogens of the MDA bonding to the oxygens from the reacted epoxide groups. As curing progressed, the quantity of -OH groups increased. The O-H band was very broad because of hydrogen bonding (12).

Kinetics of Curing

Three different measured quantities - the degree of cure obtained from heats of reaction, the fictive temperature $T_{f,g}$ and the infrared absorbance of the 916 cm^{-1} band, listed in Table I were plotted as a function of the logarithmic time of cure. See Figure 8. Within experimental uncertainty, the data points for all three quantities fell on the same sigmoidal curve. It was shown by Choy and Plazek (3) that the $T_{f,g}$ monitored the extent of cure which had been calculated from the volume shrinkage during the cure.

When plotted against log t_{cure}, the fictive temperature $T_{f,g}$ of the Epon

828/MDA rapidly increased until reaching a value near 130°C where it began to vitrify. Subsequently, an abrupt leveling out was observed as the $T_{f,g}$ exceeded the cure temperature T_c. Ultimately, the material achieved a $T_{f,g}$ value near 167°C.

The degree of cure (DSC) and $1-A_{916\ cm^{-1}}$ values rapidly increased until reaching approximately 80 percent of total cure. The greatly reduced rate of reaction during the final 20 percent of cure was not only a consequence of vitrification but, as revealed by infrared spectroscopy, the result of a depletion in the number of reactive epoxide groups. The absorbance reached an asymptotic limit of 0.06. This may reflect isolated epoxide groups which cannot reach amine hydrogens and react in any practical time at any temperature, or reflectance of infrared radiation at the surface of the KBr window.

Physical Aging Phenomenon Without Simultaneous Reaction

The extent of physical aging at 130°C was determined for fully-cured Epon 828/MDA samples aged for as long as 648 hours. As with the curing process, high-density glasses were formed. Such densified glasses responded sluggishly to temperature changes near the fictive temperature. Figure 9 illustrates that upon first heatings, the DSC thermograms had similar slopes and that the endothermic peak temperatures and areas increased with the time of aging. Figures 10 and 11 revealed that both the peak temperatures and areas were linear functions of the log t_{aging}. Kong (13) previously found that a linear relationship existed between the endothermic peak areas and aging time.

Although an endothermic peak was evident after only one hour of cure ($T_{f,g}$=138.3°C), such a peak did not appear until fully-cured samples were aged for 16 hours or more. Physical aging takes place faster when a sample is aged at a temperature nearer to, yet below, its fictive temperature. Therefore, it is not surprising that the effects of physical aging were evident earlier and in greater magnitude in partially-cured samples having a $T_{f,g}$ closer to the aging temperature. Kong (13) demonstrated that the kinetics of aging within epoxy resins slowed down as the increment ($T_g - T_a$) increased.

Sickfeld and Heinze (14) observed endothermic peaks only after an epoxy resin's T_g exceeded its annealing temperature by at least 10°K. As in this investigation, the temperature of the peaks increased with aging time.

Sickfeld surmised that the endothermic peaks were due to a higher degree of order in the glassy state.

Kreibich (15) evaluated the effects of aging in hexahydrophthalic acid glycidyl ester/hexahydrophthalic acid anhydride and found the peak areas to also increase with time. She concluded that by aging the material slightly below its T_g the polymer chains were able to relax in the direction of the thermodynamic state of higher density.

Both series of fictive temperatures listed in Table I increased with time of cure t_{cure} and achieved values greater than T_c. In contrast, the $T_{f,a}$ values listed in Table II for the fully-cured resin decreased with time of aging t_{aging} at 130°C. Figures 12 and 13 can be used to explain these opposing trends.

Events encountered during curing at a temperature $T_c < T_g$ (∞) are depicted in Figure 12. Curve 1 illustrates a hypothetical cooling curve (1°/min.) obtained for the reactants without reaction. If the reaction is chosen to begin at point A, $T_c > T_{g,r}$ (the T_g of the inital reactant mixture). After substantial reaction, the specific volume v_{sp} or enthalpy H of the system decreases from point A to B and the material's T_g becomes greater than T_c. If at this point the reaction is halted, curve 2 would depict the resin's heating curve without accompanying further reaction. Since during part of the curing reaction the material was held below its T_g, densification (physical aging) occurs simultaneously.

During the first heating from point E to C along curve 2 the densified glass responds sluggishly and endothermic peaks in the expansion coefficient and heat capacity C_p are observed. The maxima of these peaks are at the point of inflection in curve 2. The fictive temperature of the aged glass is $T_{f,a}$. If the resin is cooled from point C to D before appreciable reaction occurs, upon immediate reheating at a rate equal to the previous rate of cooling, the $T_{f,g}$ is an approximate measure of the resin's T_g.

As the curing reaction proceeds, not only do the values of $T_{f,g}$ and $T_{f,a}$ increase, but the difference $T_{f,g} - T_{f,a}$ also increases since aging increases. This is manifested by the increasing area of the attendant endothermic peak in the C_p-temperature curve.

The decrease in the $T_{f,a}$ from aging without attendant chemical reaction is illustrated in Figure 13. Upon cooling from temperatures above T_g at 1°/minute curve 3 is generated. If the cooling was halted at point F

isothermal volume contraction ensues. When the specific volume v_{sp} or enthalpy H decreases to point G, the $T_{f,a}$ becomes $T_{f,1}$ and when the volume decreases to point H, a lower $T_{f,2}$ is reached, etc.

The characteristic jump in the heat capacity ΔC_p occurred at the $T_{f,g}$. Although not apparent in Figure 4, the ΔC_p decreased as curing progressed. The ΔC_p values obtained for samples of various cure states are plotted in Figure 14. The uncured and fully-cured Epon 828/MDA having ΔC_p values of approximately 0.200 and 0.115 cal/gm.•°C, respectively. Bair (16) in studying an amine-cured DGEBA epoxy found the ΔC_p of uncured and fully-cured material to decrease from 0.123 to 0.089 cal/gm.•°C.

The measurements of Stevens and Richardson (17) show that the temperature dependence of the C_p of epoxy glasses is greater than that of the liquid of rubber above T_g. As curing progresses, with the concomitant increase in T_g, it appears that the entropy of the glass is approaching that of the liquid/rubber. The decrease in ΔC_p appears therefore to have more dependence upon the greater rotational and vibrational degrees of freedom of the glass, and not the loss of these above T_g.

Graphical Method for Determining the Fictive Temperature $T_{f,a}$

The fictive temperature $T_{f,a}$ of partially and fully-cured material can be approximated graphically from endothermic peak areas. Figure 15 shows the first DSC specific heat scan for an Epon 828/MDA sample cured for nine hours at 130°C. After the endothermic peak area is measured, a parallelogram is constructed to the left of the peak. Sides ① and ② of the parallelogram are parallel to the curve proceeding the peak. Side ③, the right-side boundary of the parallelogram, is located on the onset of the peak. Side ④ will be located such that the area of the parallelogram equals that of the endothermic peak. This left-side boundary is the $T_{f,a}$ of the material.

This procedure was applied to the specific heat scans for several partially and fully-cured Epon 828/MDA samples aged at 130°C and Dylene 8 polystyrene samples aged for 1, 2, 3, 6, and 24 hours at 85°C. In all instances the $T_{f,a}$ values determined by this graphical method were within 1.5°C of those determined from enthalpy values.

CONCLUSION

In summary, the following may be stated:

1. Differential Scanning Calorimetry (DSC) and Infrared Spectrophotometry (IR) were used to monitor the degree of cure within Epon 828 epoxy/MDA samples cured at 130±1°C. Within experimental uncertainty, the data points for the degree of cure obtained from heats of reaction, $T_{f,g}$ and infrared absorbance as a function of time, were within experimental agreement with one another. The greatly reduced reaction rate during the final 20 percent of cure was not only a consequence of vitrification, but also a result of the depletion in the number of reactive epoxide groups.

2. DSC was also used to measure the extent of "physical aging" which took place during the cure of Epon 828/MDA samples at 130±1°C; and after, fully-cured samples were aged at 130°C, 37°C below their ultimate $T_{f,g}$.

3. Spontaneous densification occurred whether or not a reaction took place. After curing for one hour or more the $T_{f,g}$ values exceeded the T_c and a dense glass was formed. The glass responded sluggishly to temperature changes near the fictive temperature and upon first heating an endothermic peak was observed.

4. The fictive temperature is thought to be the hypothetical temperature at which the structure would be in equilibrium and was determined from DSC heating curves. Two sets of fictive temperatures were obtained. The values of $T_{f,a}$ were determined from enthalpy data obtained during first DSC heating scans. They reflect the amount of physical aging which occurred during the curing reaction, after the material's T_g was greater than the T_c. The correspondingly higher $T_{f,g}$ values were obtained directly from the second heatings after aging had been erased. A sample's $T_{f,g}$ is expected to be close to its T_g (normally obtained from cooling) if the heating follows immediately after cooling from above T_g.

5. The endothermic peak temperatures and areas for the epoxy samples increased with curing and aging time. However, enthalpy data revealed that while the $T_{f,a}$ of partially-cured samples increased with curing, the $T_{f,a}$ of fully-cured samples decreased with aging at 130°C.

6. The reported curing and aging studies revealed that although longer periods of time were necessary, fully-cured samples eventually reached a level of aging equivalent to that attained by samples during their cure.

7. The characteristic jump in the heat capacity ΔC_p which occurred at the $T_{f,g}$ decreased as curing progressed. This decrease appears to be dependent upon the rotational and vibrational degrees of freedom of the glass.

8. A graphical method of determining the fictive temperatures $T_{f,a}$ for partially and fully-cured materials from measured endothermic peak areas was developed. Values determined from this method were within 1.5°C of those obtained from enthalpy data.

9. Physical aging is assumed here to be the consequence of the material contracting towards its equilibrium density. The basic idea is that the chain mobility in a closely packed system is primarily determined by the degree of packing within the system. Above T_g the material is in thermodynamic equilibrium. In contrast to chemical aging or degradation, physical aging is a thermo-reversible process. By reheating an aged material above its T_g the original thermodynamic equilibrium state is recovered and the effects of aging erased. The effects of aging can then be repeatedly reproduced.

ACKNOWLEDGEMENT

D. J. Plazek wishes to acknowledge the support of this work by the Air Force Office of Research.

REFERENCES

1. D. J. Plazek and J. H. Magill, J.Chem.Phys., 45, 3038, 1966.

2. L. C. E. Struik, Physical Aging in Amorphous Polymers and Other Material, Elsevier, Amsterdam, 1978.

3. I. C. Choy and D. J. Plazek, Journal of Poly.Sci.: Part B, Poly.Phys., 24, 1303-1320, 1986.

4. D. J. Plazek and I. C. Choy, Journal of Poly.Sci.: Part B, Poly.Phys., in press.

5. K. Dusek, Advances in Poly.Sci., 78, 1-59, 1985.

6. E. F. Oleinik, Advances in Poly.Sci., 80, 49-99, 1985.

7. A. Q. Toole, NBS Journal, 5, 627, 1930.

8. J. Sickfeld and W. Mielke, Prog.Org.Coat., 12, 27-116, 1984.

9. J. P. Aherne, J. B. Enns, M. J. Doyle, and J. K. Gillham, Am.Chem.Soc., Div.Org.Coat., Plast.Chem.Prepr., 46, 574, 1982.

10. M. L. Antoon, K. M. Starkey, and J. L. Koenig, Reinforced Plast./Composites Institute, 33rd Conf., Sec. 15B, 1-6, 1978.

11. M. A. Acitelli, R. B. Prime, and E. Sacher, Polymer, 12, 335-343, 1978.

12. D. H. Lemmon, Westinghouse Corp. R & D Center, personal communication, 1988.

13. E. S. Kong, Advances in Poly.Sci., 80, 125-171, 1985.

14. J. Sickfeld and B. Heinze, Org.Coat., 6, 203-225, 1984.

15. U. T. Kreibich, Angew. Makromol. Chemie, 75, 177, 1979.

16. H. E. Bair, Am.Chem.Soc., Div.Polym.Chem., Poly.Prepr., 26(1), 10-11, 1985.

17. G. C. Stevens and M. J. Richardson, Polymer, 24, 851-858, 1983.

TABLE 1

Differential Scanning Calorimetry and FTIR Data of Partially and Fully-Cured Epon 828/MDA Samples

Time of Cure, log sec.	Peak Temp., ^{o}C	Peak Area, Calories/Gram	Fictive Temp., ^{o}C $T_{f,a}$	Approximate $T_{f,a}$ (Note 1)	Fictive Temp., ^{o}C $T_{f,g}$	Degree of cure (DSC)	1-Absorbance 916 cm^{-1} (FTIR)
1.48	NP	NP					0.788
2.00	NP	NP			-4.8	0.161	
2.48	NP	NP			9.5	0.365	0.826
2.78	NP	NP			36.5	0.479	
2.95	NP	NP			94.4	0.682	0.903
3.25	NP	NP			121.5		
3.56	148.0	0.35			138.3	0.942	
3.86	155.3	0.52	145.7	146.0	152.2	0.980	0.934
4.03	160.6	0.66			156.4	0.988	
4.10	161.7	0.72			156.6	0.988	0.934
4.16	162.7	0.76	147.5	149.0	157.6	0.988	
4.26	164.7	0.80			158.9	0.988	0.933
4.33	165.4	0.91			159.0	0.988	
4.51	166.9	0.97	151.0	151.0	160.2	0.990	0.934
4.76	171.7	1.04			163.1	0.990	
5.24	175.3	1.24	151.7	152.0	164.3	0.992	0.933
5.78	179.7	1.36			167.3	0.996	
6.08	182.1	1.49			167.3		

NP: An endothermic peak was not evident upon first heating.

NOTE 1. Graphical "parallelogram" method used to determine these values.

Table II

Differential Scanning Calorimetry
of Physically Aged Epon 828/MDA Samples

Time of Aging log sec.	Peak Temp., ^{o}C	Peak Area Calories/Gram	Fictive Temp., ^{o}C $T_{f,a}$	Approximate $T_{f,a}$ (Note 1)
4.76	175.5	0.20	166.2	167.5
4.86	176.8	0.26	166.0	
5.54	179.3	0.55	164.3	165.5
5.78	182.0	0.85	163.5	165.0
6.24	184.0	1.15	163.0	163.0
6.37	184.5	1.25	162.4	

Note 1. Graphical "parallelogram" method used to determine these values.

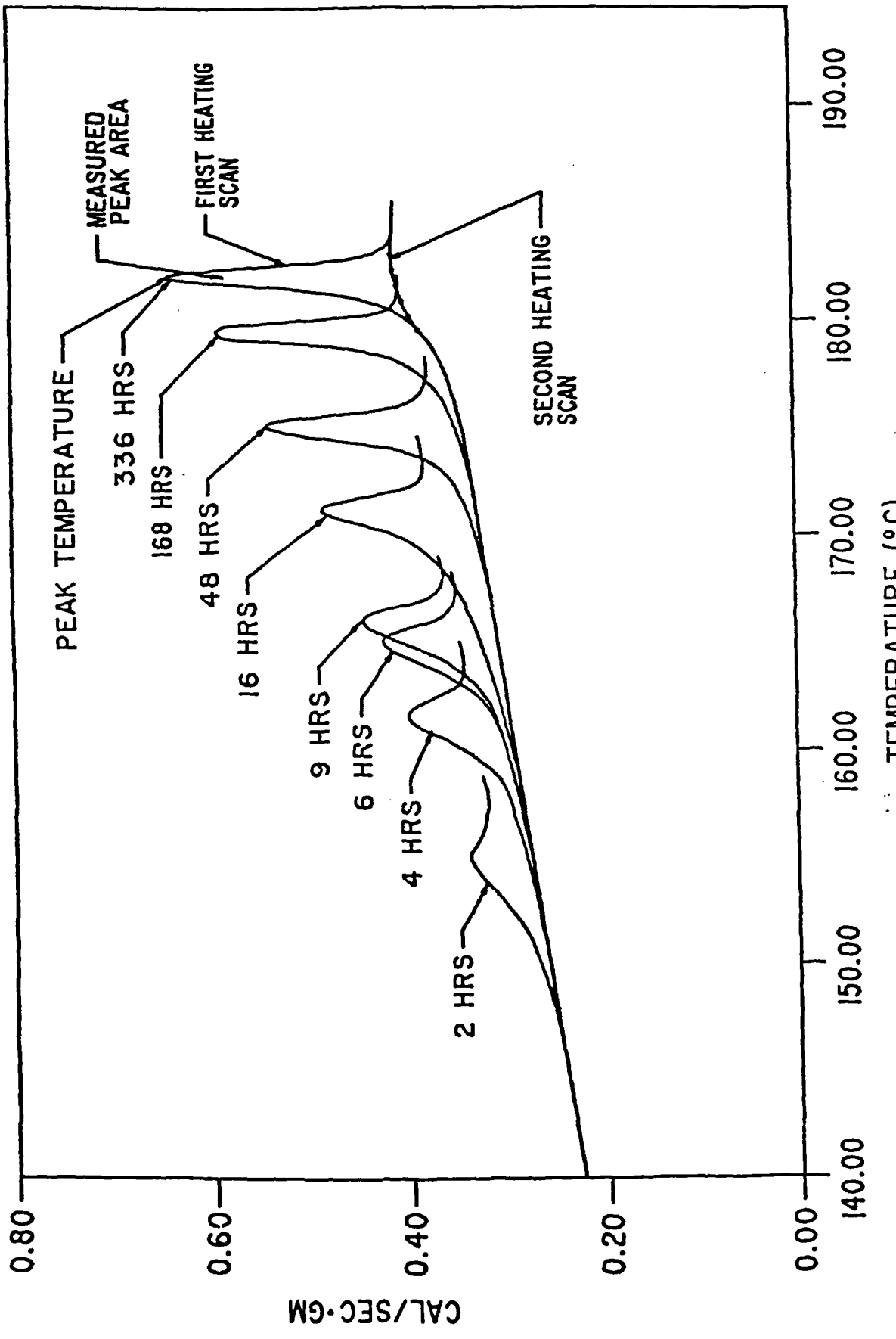

Figure 3: Peak Area and Peak Temperature Determinations for Epon 828/MDA Samples Cured at 130±1°C. First DSC Heating. Heating Rate of 20°C/Min. and Cooling Rate of 80°C/Min. Sensitivity of 0.5 mcal/sec. full scale.

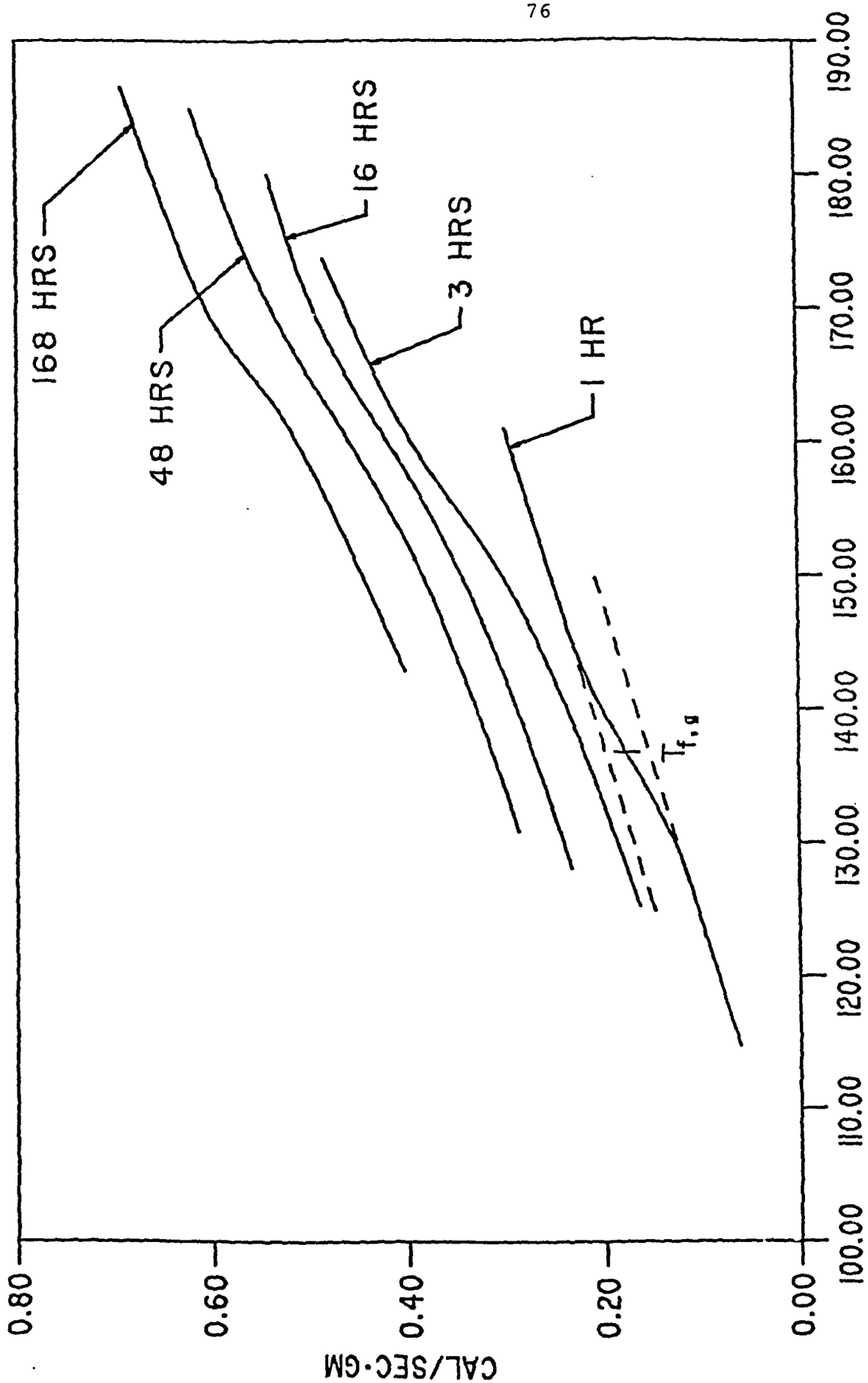

Figure 4: Fictive Temperature Determination for Epon 828/MSA Samples Cured at 130±1°C. Second DSC Heating. Heating Rate of 20°C/Min. and Cooling Rate at 80°C/Min. Sensitivity of 0.5 mCal/sec. full scale. Vertical shift arbitrarily applied.

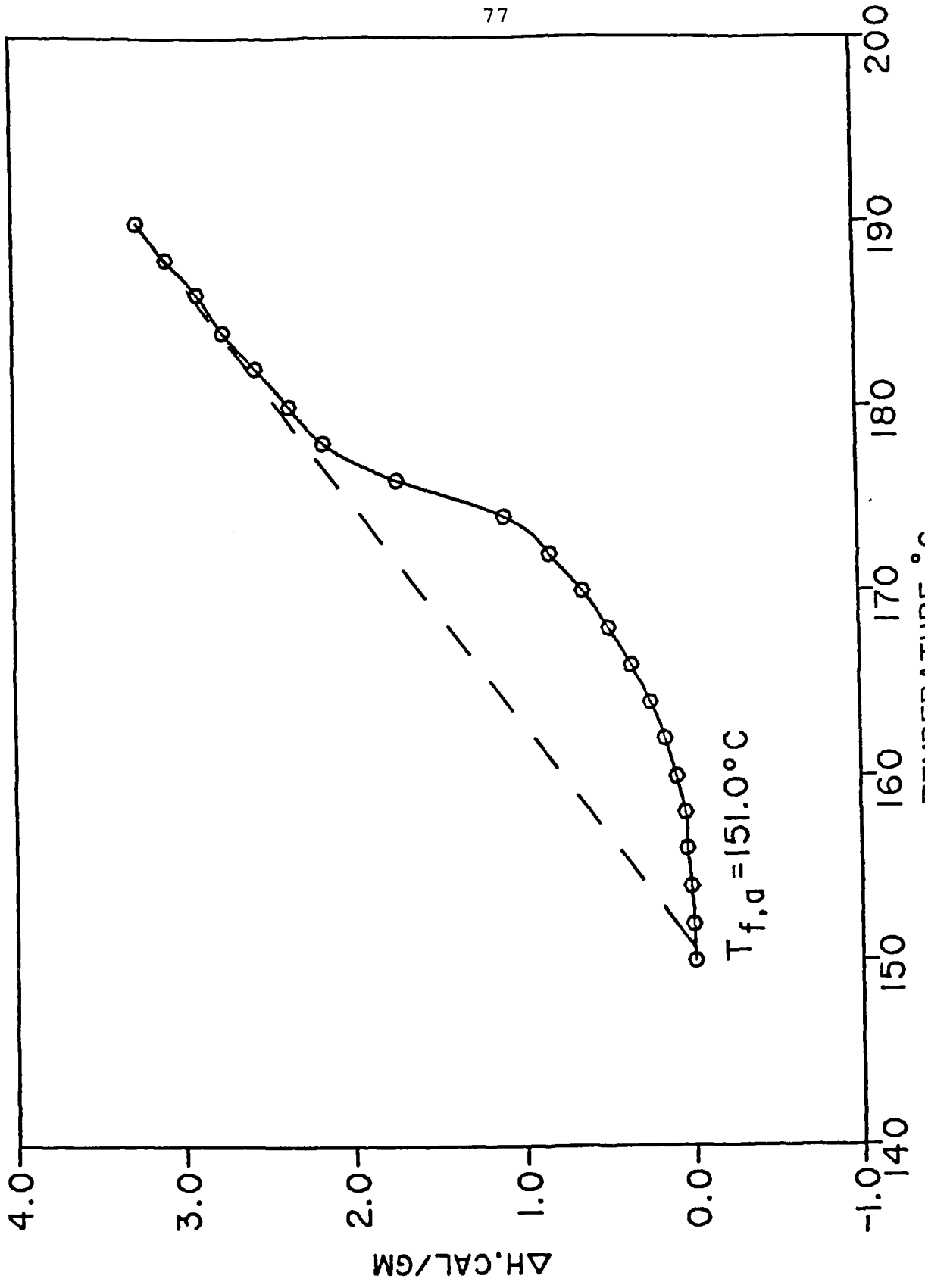

Figure 5. Change in enthalpy ΔH versus temperature for a Epon 828/MDA sample cured for 9 hours at 130°C. First DSC heating.

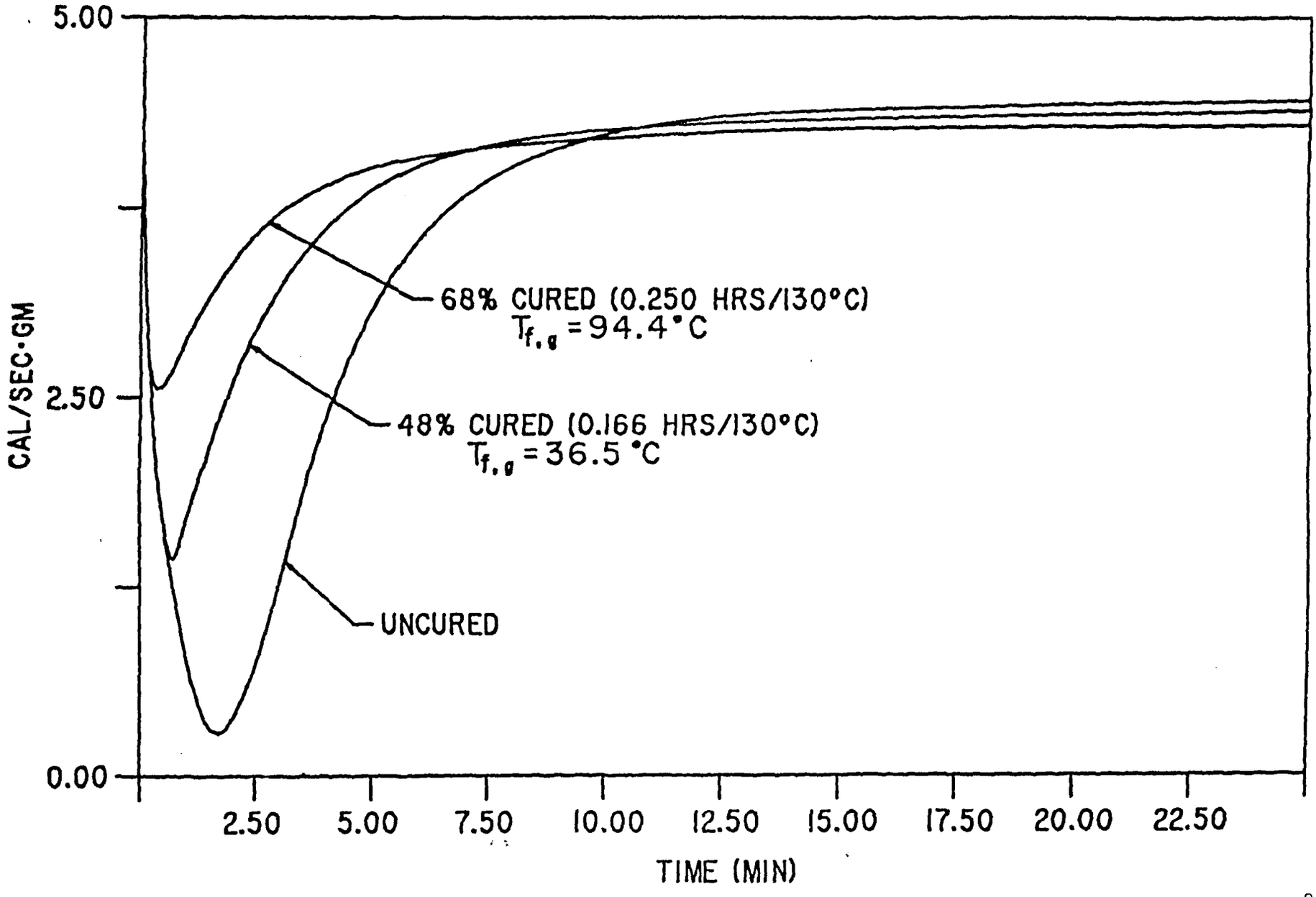

Figure 6: Isothermal DSC Scan of Epon 828/MDA at 169°C on samples partially cured at 130±1°C. Heating rate of 100°C/Min. Sensitivity of 0.5 mcal/sec. full scale.

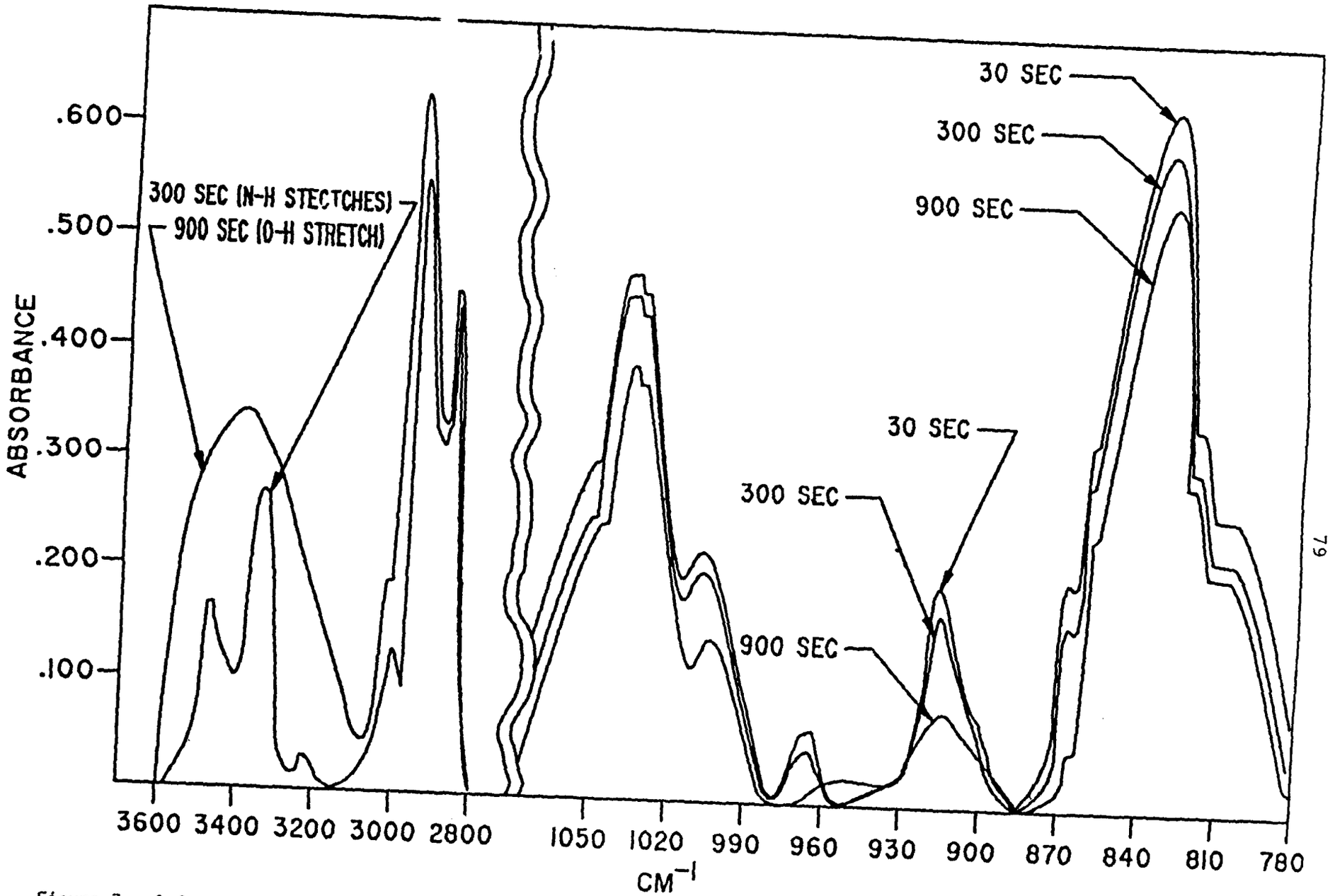

Figure 7. Infrared absorbance spectra of Epon 828/MDA cured for 30, 300 and 900 seconds at 130 °C. With increased curing there is a reduction in the epoxide group absorbance (916 cm-1) and a broadening of the O-H bond stretch (3200-3600 cm-1).

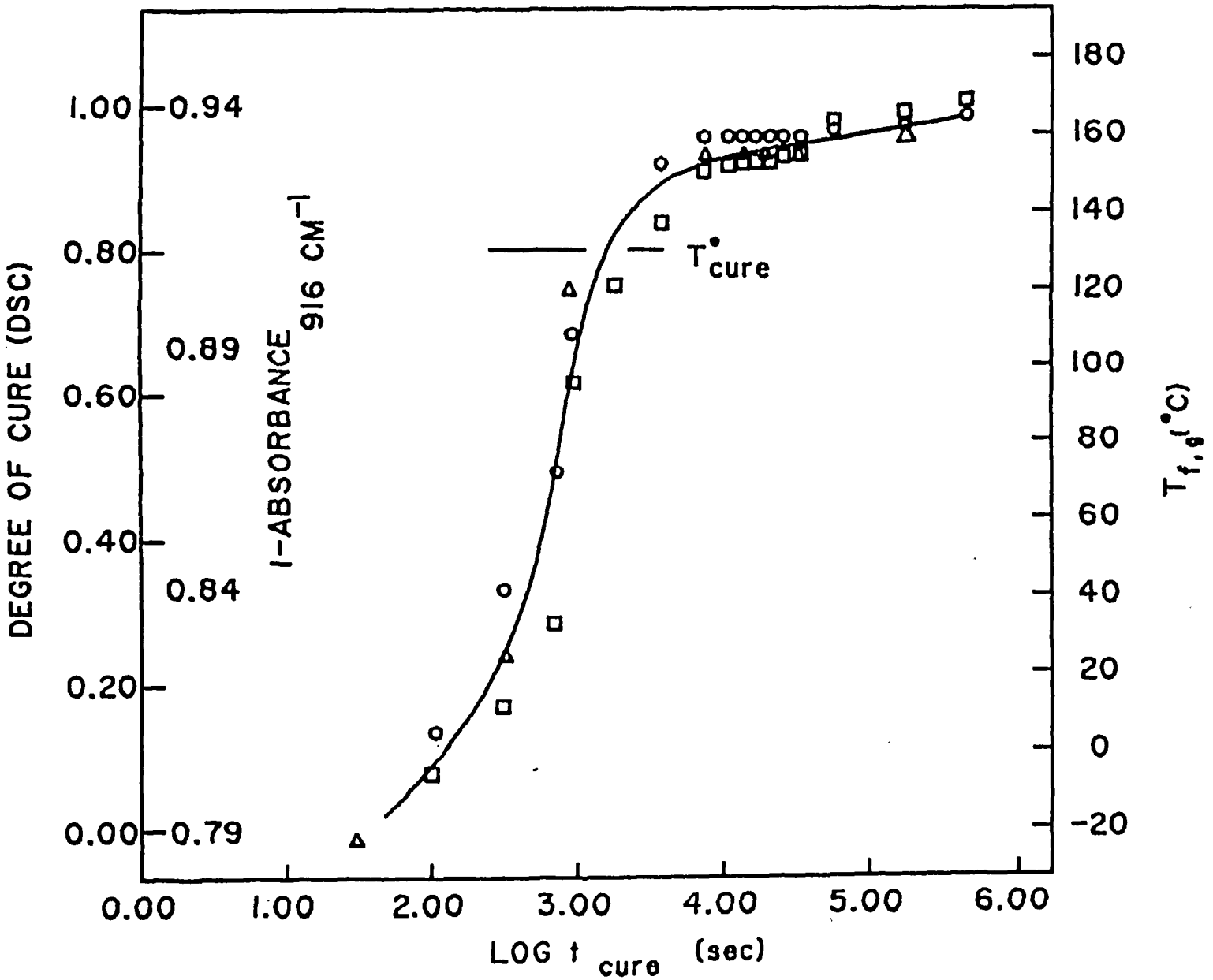

Figure 8. Fictive temperature $T_{f,g}$ □, degree of cure (DSC) ○, and extent of reaction $(1-A_{916\ cm^{-1}})$△of Epon 828/MDA samples cured at 130°C.

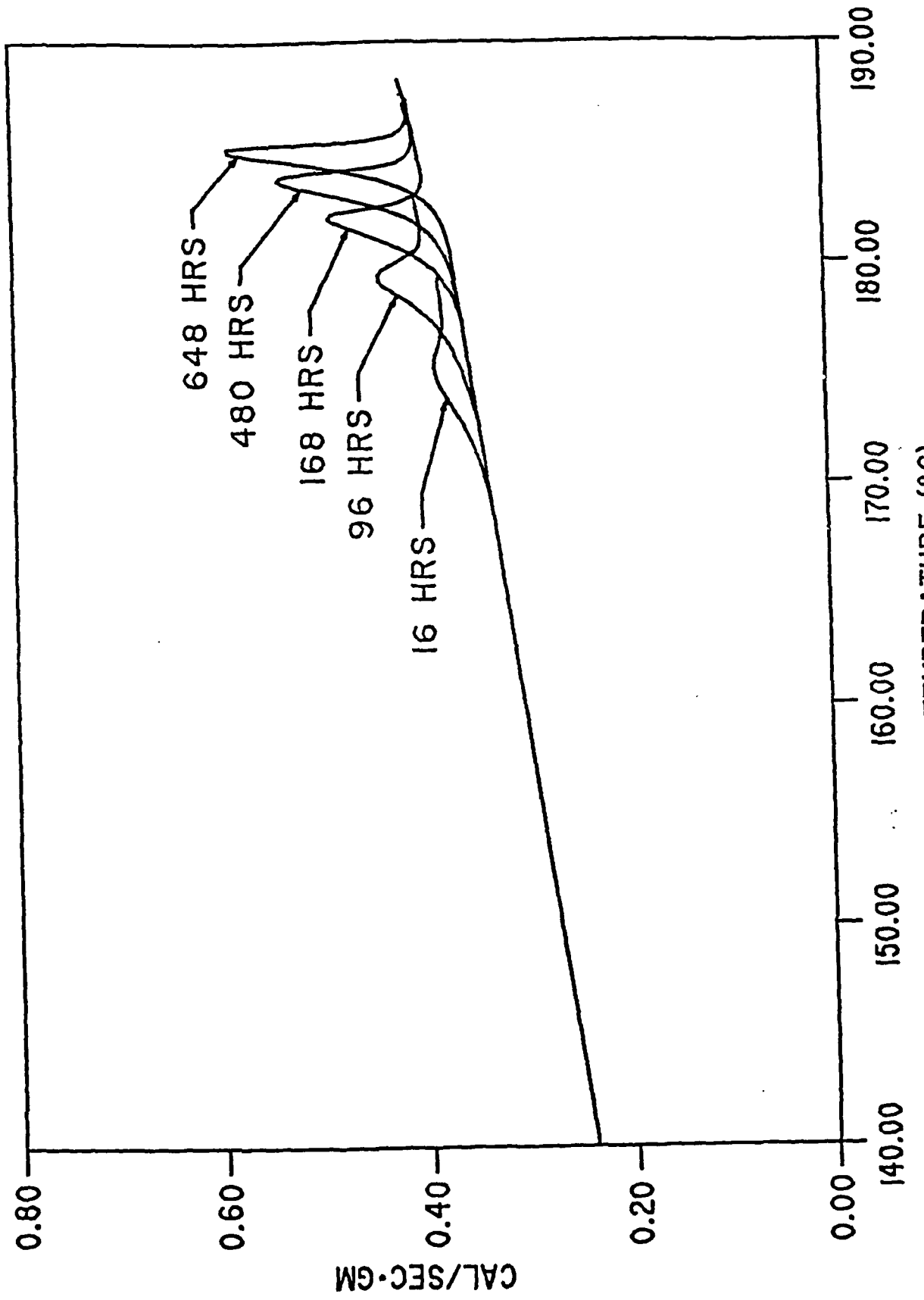

Figure 9. Peak areas and peak temperatures for fully-cured Epon 828/MDA samples physically aged at 130°C. Heating rate of 20°C/min. and cooling rate of 80°C/min. Sensitivity of 0.5 mcal/sec. full scale.

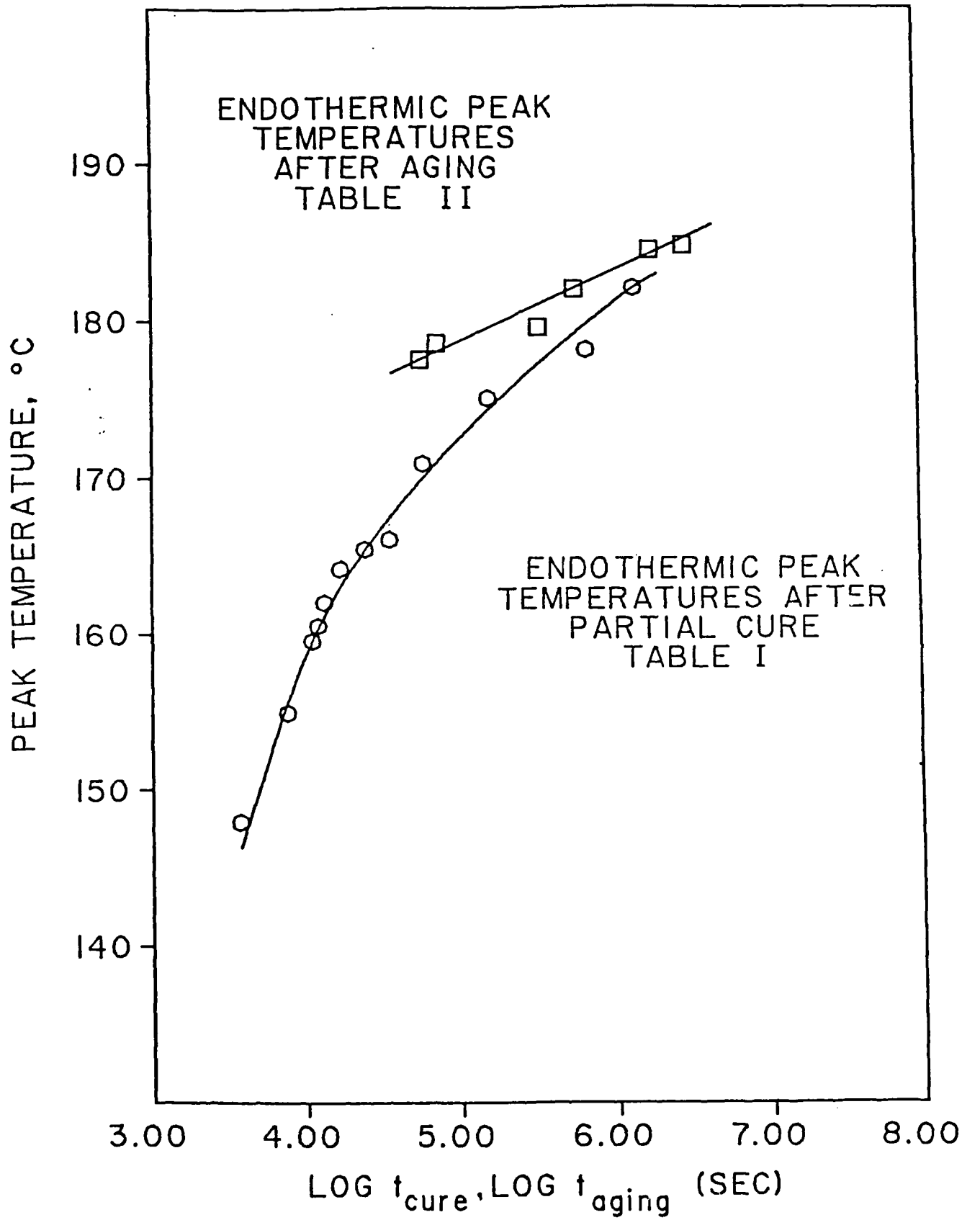

Figure 10. Endothermic peak temperatures of Epon 828/MDA samples after curing O and physical aging □ at 130 °C.

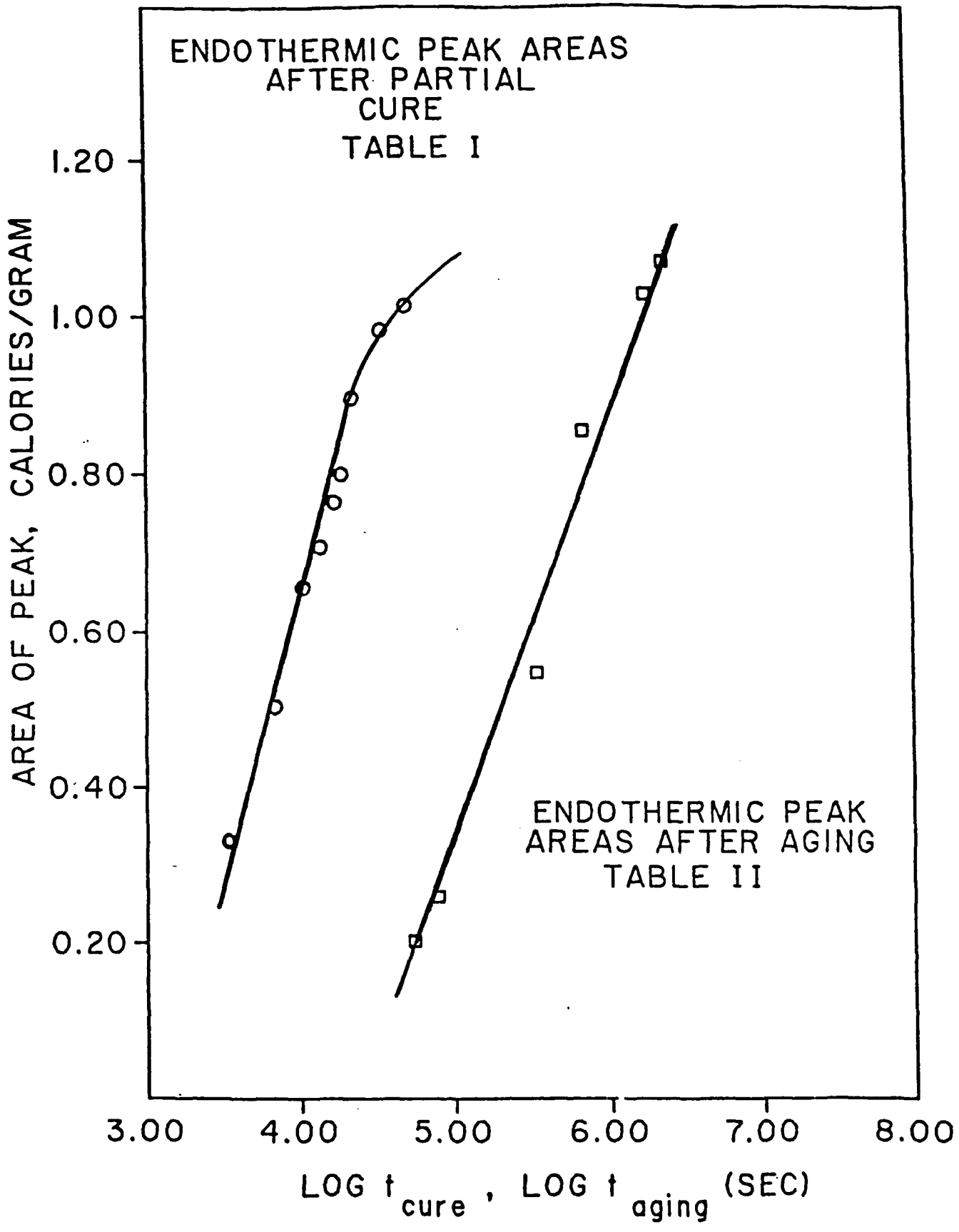

Figure 11. Endothermic peak areas of Epon 828/MDA$_o$ samples after curing ○ and physical aging □ at 130 °C.

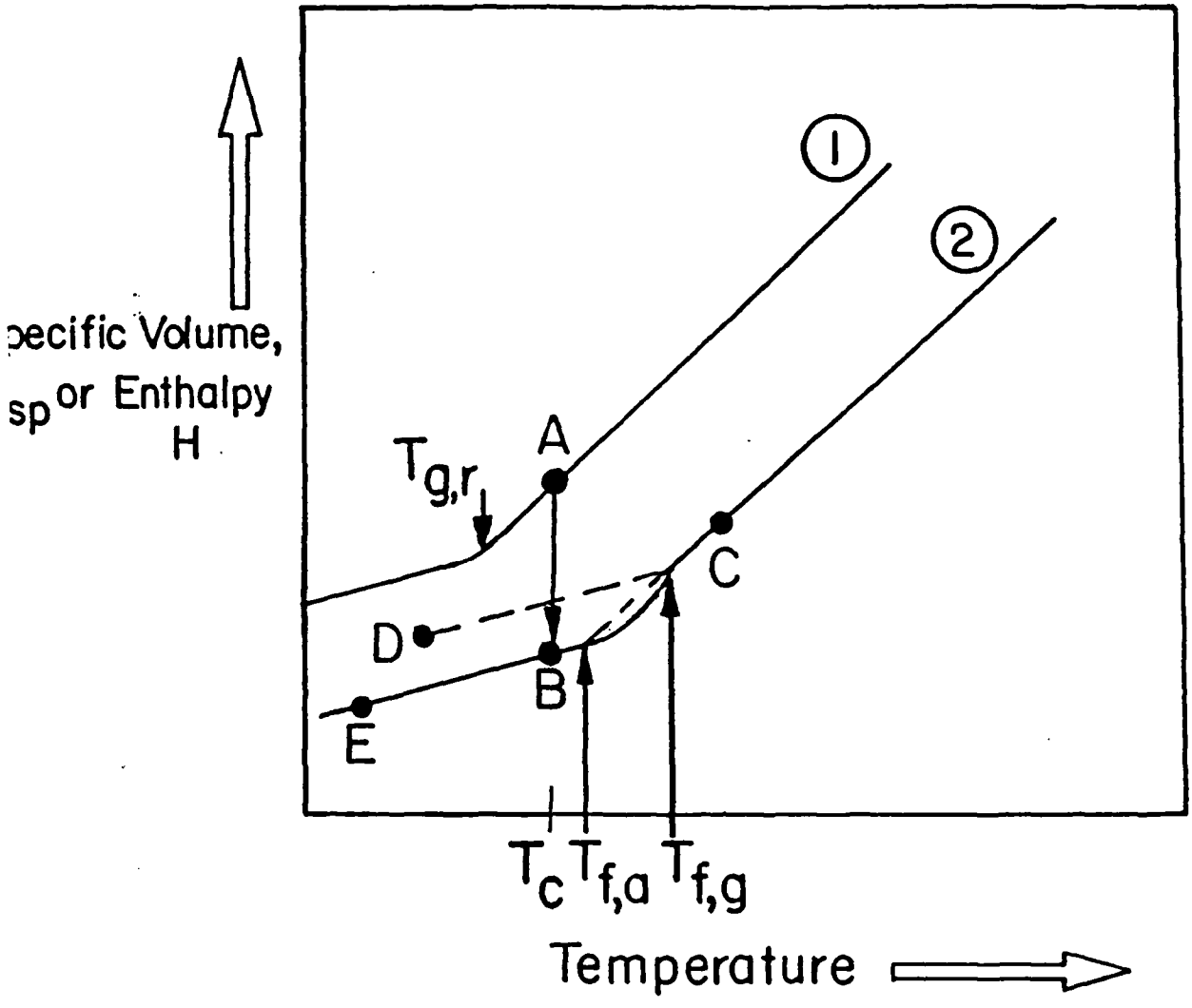

Figure 12. Explanation of the increase in $T_{f,a}$ and $T_{f,g}$ for partially-cured material at T_c.

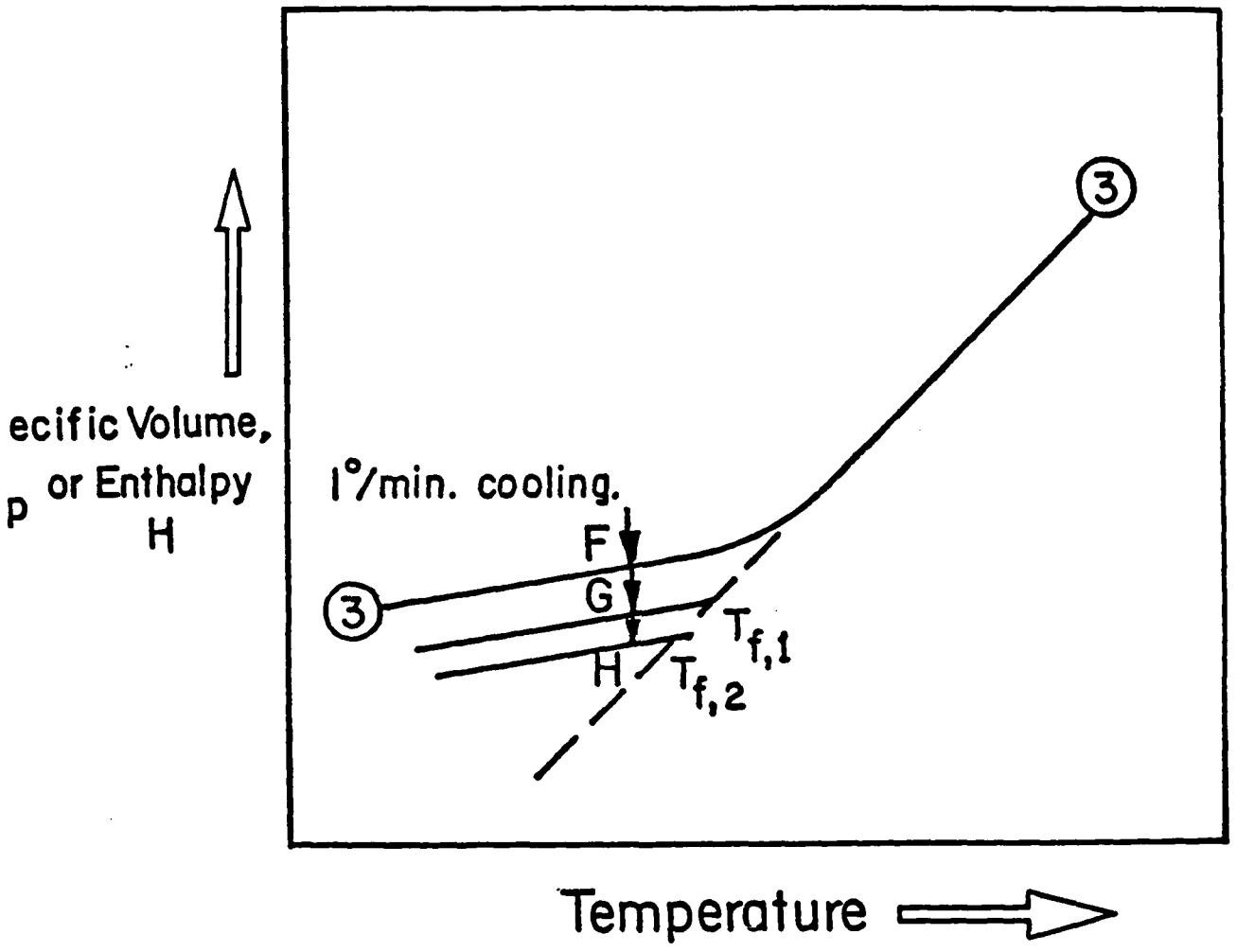

Figure 13. Explanation of the decrease in $T_{f,a}$ for fully-cured material with physical aging at $T_a = T_c$.

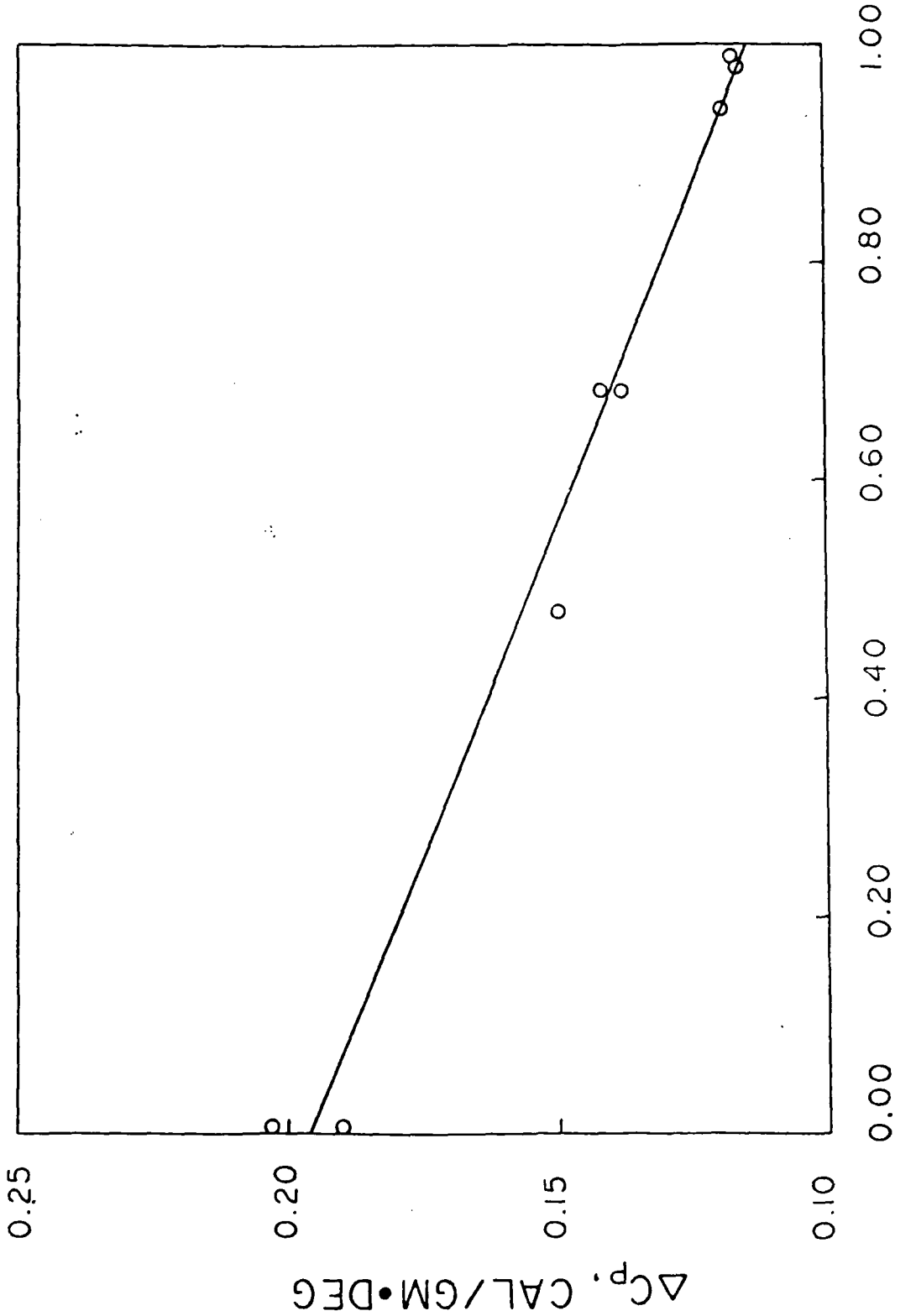

Figure 14. Jump in the heat capacity ΔC_p near $T_{f,g}$ for Epon 828/MDA samples of different states of cure.

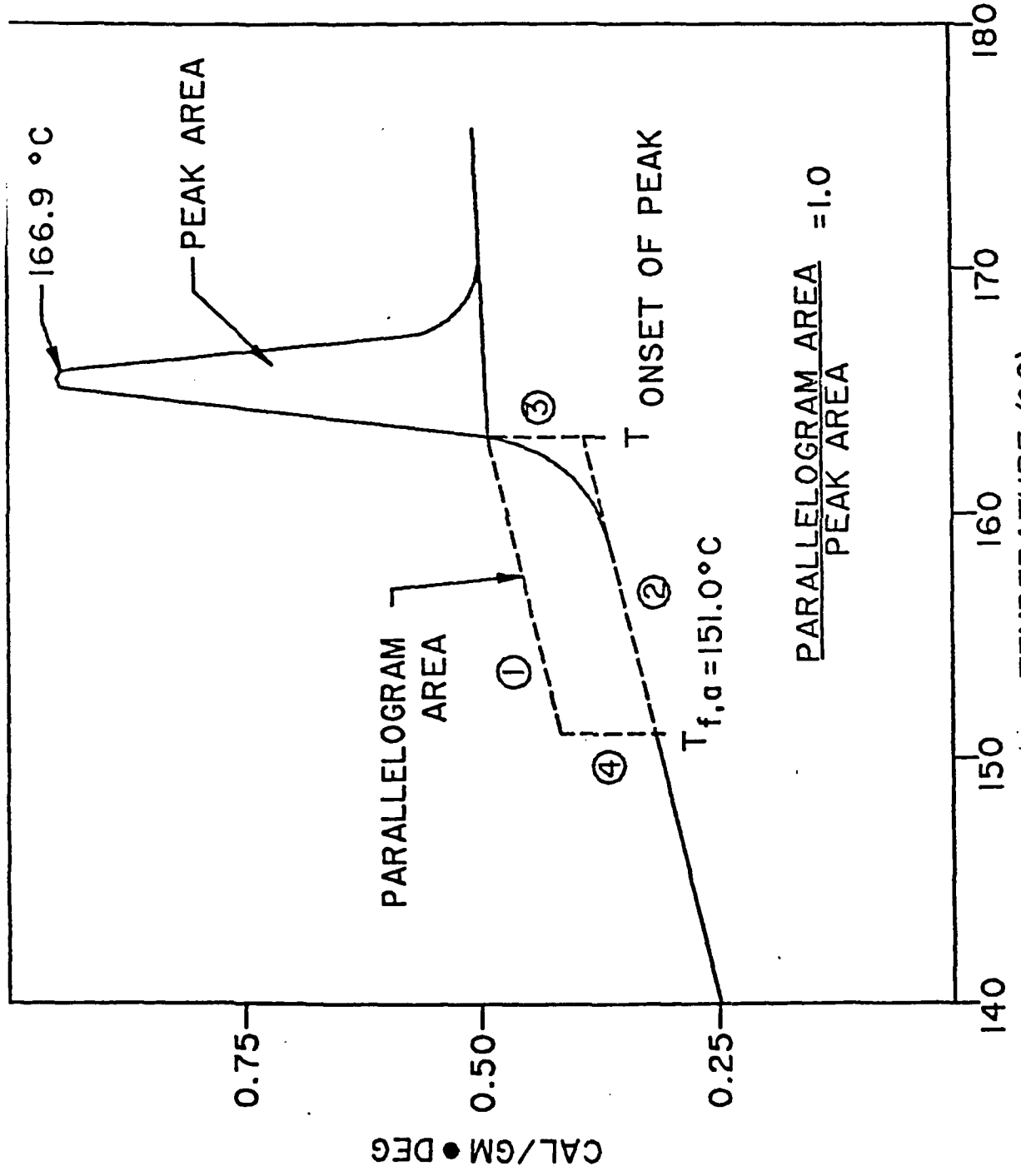

Figure 15. Graphical method of determining the fictive temperature $T_{f,a}$ from endothermic peak area. Epon 828/MDA sample cured for 9 hours at 130°C. First DSC specific heat scan. Heating rate of 20°C/min. Sensitivity of 0.5 mcal/sec. full scale.

IV. VOLUME DEPENDENT RATE PROCESSES IN AN EPOXY RESIN

by

Craig A. Bero
and
Donald J. Plazek

Materials Science and Engineering Department
University of Pittsburgh
Pittsburgh, PA 15261

IV. VOLUME DEPENDENT RATE PROCESSES IN AN EPOXY RESIN

ABSTRACT

Results for four different volume dependent rate processes of an epoxy resin, Epon 1001F, fully cured with a stoichiometric amount of 4,4' diamino diphenyl sulfone are presented: 1) specific volume measurements at constant rates of cooling; 2) time dependent volume measurements after rapid temperature changes; 3) elongational creep compliance measurements; and 4) shear creep compliance measurements. Voluminal and shear retardation spectra are compared as are the temperature time scale shift factors, a_T.

INTRODUCTION

Kinetic processes in amorphous materials are linked to the glass temperature because T_g is a reflection of the local mobility of the molecules or molecular segments. It is properly determined in a cooling experiment because it is close to the first departure from an equilibrium state of the liquid being cooled; that is, at higher temperatures as soon as the cooling is stopped and a uniform temperature is achieved the random fluctuating disposition of the molecules is fixed. Every polymer scientist we know, including ourselves, is aware of the fact that T_g is a function of the rate of cooling, but cannot identify a set of cooling experiments that establishes this fact. This behavior, of course, can be inferred from Kovac's isochronal, 0.02 hr. and 100 hour, glass volume - temperature lines, which were obtained from a series of temperature-jump experiments[1]. The polyvinylacetate studied was quenched from equilibrium above T_g to different temperatures between -20° and 35°C. It is not possible to move directly from point to point along the isochronal glass line.

It was desired in this investigation to obtain a set of cooling curves for a fully cured epoxy resin and to obtain data on the kinetics of isothermal contraction at temperatures where the specimen would be at an equilibrium volume before the rapid change in temperature was made to the temperature where the time-dependent contraction or expansion was to be observed. Since the rate of change in volume observed near T_g is predominantly a function of the volume itself (specifically the relative or fractional free volume), the measurements of such changes are inherently non-linear. This has been made abundantly clear by the classic work of Kovacs[1] and others[2,3]. The non-linearity

was reduced in this study by keeping the temperature change at 2.5°C. The isothermal volume change in all but one experiment was followed until the equilibrium density was reached.

In addition to dilatometric measurements, shear and elongational creep behavior of the same glycidyl ether based epoxy resin were determined over a range of temperatures. Temperature shift factors were obtained for the four different kinds of measurements.

MATERIAL AND INSTRUMENTATION

The shell epoxy resin, EPON 1001F cured with a stoichiometric amount of 4,4' diamino diphenyl sulfone has been characterized at the University of Akron by LeMay, Swetlin and Kelly[4].

Tensile creep and recovery measurements which yielded the recoverable tensile creep compliance, D(t), above and below T_g were carried out with a differential elongational creep apparatus[5].

Torsional creep and recovery measurements which yielded the recoverable torsional creep compliance, $J_r(t)$, above T_g were carried out with a frictionless magnetic bearing torsional creep apparatus (Time-Temperature Instruments, Inc., P.O. Box 40156, Pittsburgh, PA 15201).

Dilatometric measurements were made using a modified version of a mercury dilatometer. The dilatometer consisted of 28 cm of 0.05 cm diameter precision bore capillary tubing connected to a thin walled, stainless steel cylindrical sample chamber (ID = 1.5 cm, height = 4.0 cm, wall thickness = 0.031 cm). The sample chamber is sealed at the top via compression of a teflon O-Ring by a threaded stainless steel cap. Unlike conventional glass or quartz dilatometers, this design allows for easy installation and removal of a sample. The glass capillary is graduated every 0.1 cm allowing for mercury height measurements to $\pm$ 0.01 cm. At the top of the glass capillary there is a ground glass joint for attachment to the mercury distillation apparatus. Mercury is distilled into the dilatometer at a pressure of less than 5 microns of Hg.

Physical aging experiments were performed on the EPON 1001F near its glass transition temperature in which the EPON 1001F sample experienced a "fast" temperature jump of 2.5°C in the temperature range 124.0 - 136.5°C. This was done with two thermostatted, well stirred silicon oil baths differing in temperature by 2.5°C. The dilatometer was placed in one bath allowing the sample to attain its thermal equilibrium volume. The dilatometer was then transferred to the other silicon oil bath and the mercury column height was monitored with time.

When first performing these aging experiments, it was observed that the EPON 1001F took an unusually long period of time to thermally equilibrate to the bath temperature. This was due to the fact that the EPON 1001F sample was a solid cylinder (length = 3.8 cm, Dia = 1.30 cm) with a low thermal diffusivity. EPON 1001F sample was removed from the dilatometer and 1/16" diameter

holes were drilled perpendicular to one another along the entire length of the sample. This allowed mercury to come in contact with the sample interior increasing the heat transfer and thus decreasing the time for the sample to thermally equilibrate. With this "Swiss cheese" sample, it was experimentally determined that the EPON 1001F sample required approximately 100s to thermally equilibrate during a temperature jump of -2.5°C (T-Jump down). The EPON 1001F sample required about 200s to equilibrate during a temperature jump of + 2.5°C (T-Jump Up). This significant increase in time was due to a cooling effect from ambient air that occurred in transferring the dilatometer from the colder bath. During T-Jump Down experiments this cooling from ambient air aided in lowering the sample temperature thus decreasing the time for the sample to become isothermal.

Specific volume of the EPON 1001F as a function of temperature was obtained from cooling experiments over a temperature range of $T_g - 20 \leq T \leq T_g + 10$°C. The sample was heated to T_g + 10°C and allowed to attain thermal equilibrium. Once at equilibrium, the EPON 1001F was cooled at a constant rate to T_g -20°C. Time, temperature, and mercury column height were monitored to assure that the cooling rate remained constant.

Temperature control was achieved by modification of Bailey constant set-point temperature controller. A motor, time relay and gearbox were added to decrease the set point at a constant rate. The gear box (Insco, Main Street, Graton, MA 01450) possessed turn ratios of 1/1 to 1/1000 to achieve cooling at the lower rates. A timing relay was added to turn the motor on for a set percentage of a given amount of time. With these modifications, constant cooling rates covering almost 3 orders of magnitude were achieved.

RESULTS

Cooling at Different Rates

The Epon 1001F epoxy resin, fully cured with DDS, was cooled in a dilatometer over a three-hundred-fold range of rates; from 0.90° to 0.003°C per min. Cooling was initiated in each case after equilibration at ~ 140°C. The specific volume results obtained are shown in Fig. 1. The equilibrium specific volume line is

$$\tilde{V}(cm^3/g) = 0.85446 + 4.28 \times 10^{-4} (T - 130°C) \quad (1)$$

The liquid - like and glassy cubical thermal expansion coefficients at T_g are $\alpha_l (T_g) = 5.01 \times 10^{-4}$ and $\alpha_g (T_g) = 1.93 \times 10^{-4}$/°C. T_g is identified with the intersection of the equilibrium and glassy lines. The specific volumes at the different rates of cooling $Q = 3.0 \times 10^{-3}$, 5.0×10^{-2}, 2.5×10^{-1}, and 9.0×10^{-1}°C/min at $T_g(Q)$ of 126.1°, 129.9°, 130.5°, and 131.7°C are 0.85277, 0.85402, 0.85469 and 0.85523 cm^3/g, respectively. The results of $\tilde{V}(T_g,Q)$ are probably relatively accurate to several parts per 10^5 and absolutely to about one part in 10^4.

The temperature range over which measured specific heat values depart from equilibrium and glassy lines in the absence of physical aging (densification) effects has been called the "glass transformation range". This temperature region corresponds to that where measured specific volume values lie above the equilibrium and glassy lines. This range of departure is a reflection of the breadth of the viscoelastic volumetric retardation function[6,7]. As such it should be a function of the rate of cooling. Careful examination of Fig. 1 shows this to be so. If the departures of the data points from the lines ($\Delta\tilde{V} = \tilde{V}_{meas.} - \tilde{V}_{lines}$) are plotted as a function of temperature, it is eminently clear that the "transformation range" decreases appreciably with a decreasing rate of cooling; see Fig. 2. The half-width decreases by about a factor of two from the highest to the lowest rate. As the rate decreases, mechanisms of contraction with shorter retardation times associated with the changing liquid structure have time to reach their equilibrium state. At the lower temperatures all of the cooling curves reach the glassy lines at about the same time because the temperature shift factors a_T of the mechanisms are growing at a greatly accelerating rate with decreasing temperature because of the rapidly increasing molecular crowding.

Temperature Jump Experiments

When the temperature of an amorphous material is increased or decreased rapidly near or below T_g, after thermal equilibrium is established the volume of the material normally continues to change in the direction of the equilibrium value for the new temperature. Near and below T_g some of the molecular motions involved in attaining the equilibrium structure are very sluggish because of their complexity in the crowded state. These are believed to be the same molecular motions that

are involved in the approach to an equilibrium liquid state following a change in the pressure in the same temperature range. Rehage and Goldbach have shown the similar response of a polystyrene to temperature and pressure jumps[3,8]. The response to temperature changes should be recognized to be a volumetric viscoelastic response.

Kovacs[1] has investigated time dependent volume changes following several different kinds of thermal histories:

1) temperature jumps from equilibrium above T_g at a specific temperature to various temperatures below T_g;

2) temperature jumps from equilibrium at a specific temperature below T_g to several temperatures above T_g;

3) jumps from equilibrium at various temperatures above T_g down to the same temperature below;

4) jumps from equilibrium at several temperatures below T_g up to a specific temperature above T_g;

5) multiple temperature jumps with memory reversals of the volume changes.

The temperature jump experiments that are being reported here are variations on Kovac's histories 1) and 2). In our experiments the Epon 1001F was either cooled or heated by 2.5°C after the fully cured epoxy reached its equilibrium density and the change in volume was observed until equilibrium was achieved before an additional step was taken. The sole exception was the last cooling step, where the time to reach an equilibrium density was excessive.

An example of a pair of curves expanding and contracting toward equilibrium, following 2.5°C temperature steps is shown in Fig. 3. The volume changes following temperature shifts from 129° and 134° to 131.5°C are shown. The ordinate is actually the fractional departure from the equilibrium specific volume curve. Both curves take the better part of a day to reach equilibrium. However, two differences can be seen between the contraction and expansion curves. The asymmetry can be seen which reflects the intrinsic non-linearity of these experiments. The ascending curve is delayed in response because of the great molecular crowding, but reaches greater absolute slopes because of the autocatalytic nature of the expansion. The contraction curve descends at an earlier time toward equilibrium, but decelerates relatively more because a state of greater crowding is being approached. The time of contraction and expansion are corrected for the approximate time to

achieve an equilibrium temperature after the dilatometer is transferred from one thermostatted bath to the other; i.e. t_i is the approximate time for the temperature to become uniform throughout the dilatometer bulb after the transfer. Kovacs was able to assume a $t_i \cong 100$ sec. for both cooling and heating experiments because his transfers of polyvinylacetate dilatometers were made near room temperature. We were required to use a larger thermal equilibration time for the transfers to the higher temperature bath, since at elevated temperatures ~ 130°C, cooling occurred during the several seconds required for the transfer. Thermal equilibration was thus delayed, whereas during the step down transfer the equilibration time was diminished by the extra cooling incurred during the transfer. The t_i values were determined at temperatures somewhat above T_g where the epoxy resin's retardation times were a few seconds or less.

The absolute fractional departures from equilibrium obtained at four temperatures after heating from equilibrium and five temperatures after cooling from equilibrium are presented in Fig. 4. Two and a half degree temperature steps were used in every case.

With 134.0°C chosen as the reference temperatures both sets of data were reduced to common curves which range over an extended logarithmic time-scale. The reduced curves are shown in Fig. 5. The reduced curve obtained following cooling steps is more extended simply because of the long contraction times involved at 124°C. At 126.5°C it took about 3 to 4 days to reach equilibrium. Therefore, a corresponding heating curve starting at 124°C could not be obtained. Only the reduced contractions curve will be further analyzed here. The very same sample and dilatometer were used in both the constant rate of cooling and temperature jump measurements.

Determination of the Bulk Retardation Spectrum

The reduced curve of the fractional volume departure from equilibrium which was obtained following cooling steps $[V(t) - V(\infty)]/V(\infty)$ was normalized with the factor $(V\infty/[V(O^+) - V(\infty)]$ yielding the fraction of the volume change at time t: $[V(t) - V(\infty)]/[V(O^+) - V(\infty)]$. V(t) is the specific volume at t; $V(\infty)$ is the equilibrium specific volume and $V(O^+)$ is the volume obtained following an instantaneous temperature jump. It is related to the equilibrium volume before the jump V(O) by

$$V(O^+) = V(O)(1-\alpha_g \Delta T), \tag{1}$$

where α_g is the thermal expansion coefficient, $\partial(\ln V)/\partial T$, of the glass.

Volume changes can be caused by changes in temperature or pressure. The changes in volume are related to the compressibility by[7]

$$\{[V(O^+) - V(\infty)]/[V(O) - V(\infty)]\}\left[1 - \frac{B(t) - B_g}{B(\infty) - B_g}\right] = \frac{V(t) - V(\infty)}{V(O) - V(\infty)} \tag{2}$$

where B(t) is the time dependent compressibility, $-\partial[\ln V(t)]/\partial P$. $B(\infty)$ and B_g are the equilibrium and glassy compressibilities, respectively. For pressure changes $[V(O^+) - V(\infty)]/[V(O) - V(\infty)] = [B(\infty) - B_g]/B(\infty)$ and for temperature steps $[\alpha(\infty) - \alpha_g]/\alpha(\infty)$.

For our reduced contraction curve.

$$1 - \frac{V(t) - V(\infty)}{V(O^+) - V(\infty)} = \frac{B(t) - B_g}{B(\infty) - B_g} \tag{3}$$

or if we define a normalized volume retardation spectrum $L_v(\tau)^*$ where

$$\int_{-\infty}^{\infty} L_v(\tau)\, d \ln \tau = 1 \tag{4}$$

then

$$\frac{V(O^+) - V(t)}{V(O^+) - V(\infty)} = \int_{-\infty}^{\infty} (L_v(\tau)(1 - e^{-t/\tau})\, d \ln \tau. \tag{5}$$

Using iterative computer calculations[9] $L_v(\tau)$ has been obtained from the normalized reduced data. The resultant bulk spectrum is shown in Fig. 6 where it is compared with the shear spectrum which was deduced from the reduced shear creep compliance J(t) curve[10]. The abscissa for log $L_v(\tau)$ was chosen so that the short time portions of the spectra superpose. The fact that they can be superimposed for at least two decades of time scale suggest that the same molecular motions are involved in both the shear deformation and the densification. The longer time mechanisms which involve larger range coordinated polymer chain backbone motions are reflected in the long-time peak in the shear spectrum. It is no surprise that the long range molecular motions have no measurable effect on the local ordering that determines a material's density.

---

* $L_v(\tau)\, d \ln \tau$ is the normalized distribution function of volume retardation times lying between $\ln \tau$ and $\ln \tau + d \ln \tau$ which contribute to the fraction of the equilibrium bulk (voluminal) compliance, $B(\infty) - B_g$.

Creep Measurements

Elongational creep compliance, D(t), measurements were carried out with a differential instrument[5] in which the lengths of twin samples were monitored. One sample was subjected to the tensile creep loading and fluctuations of length due to thermal variations cancelled out in the differential signal. Reduced Log $D_r(t)$ curves obtained at 10 temperatures between 117.7° and 150.2°C are presented in Fig. 7. The small rubberlike temperature correction was applied to the time dependent contribution above the glassy compliance, D_g;

$$D_p(t) = [D(t) - D_g][T\rho/T_o\rho_o] + D_g. \quad (6)$$

T and T_o are the absolute temperatures of measurement and reference, 130°C, respectively. ρ and ρ_o are the corresponding densities. The corrected curves were reduced by horizontal time-scale shifts onto the curve measured at 130°C. At this chosen reference temperature the material had its equilibrium density. To reach equilibrium a day was required as indicated by the above contraction curves. Excellent superposition of the curve was achieved as can be seen in Fig. 8. The $D_p(t)$ reduced curve is compared with the reduced shear compliance $J_p(t)$ curve shown as a long-dashed line. The torsional creep measurements from which the $J_p(t)$ curve was obtained are new measurements which are in close agreement with previous measurements on fully cured EPON 1001F/DDS.[10] The same mix was used in preparing the specimens for both the torsional and elongational measurements in hope that some information on the bulk compliance B(t) could be obtained from the relation[11]

$$B(t) = 9\,D(t) - 3J(t) \quad (7)$$

at least at relatively short times where D(t) and J(t) are not much larger than B(t). Comparison at long reduced times > 10^4 sec. where the influence of B(t) is not discernible indicated that the $J_p(t)$ curve was at longer times by 0.8 of a decade of time. This obviously reflects a higher glass temperature of the specimen on which the torsional measurements were made. Beyond reduced times of 10^3 sec $J_p(t)$ and $D_p(t)$ are superposable within experimental scatter with

$$J_p(t) \simeq 3D_p(t) \quad (8)$$

indicating a Poisson's ratio of 1/2. Since direct measurements by I. -C. Chay indicate that the equilibrium bulk compliance $B_e \simeq 3 \times 10^{-11}$ cm^2/dyne for this material, no detectible dilation is

expected. The long-dashed line for J(t) has been shifted to shorter times by the required Δlog t of 0.80. The short-dashed line represents log $J_r(t)$ shifted vertically by 0.477, the logarithm of 3. Values for B(t) were estimated in the region where the solid and short dashed-lines diverge. They were found to be substantially greater than the directly measured equilibrium value by about 50%. We believe this is a result of distortions that occur in the time-temperature reduction process. Extrapolating both curves to zero time using a fit to Andrade Creep[10] at short times, a glassy compliance of $D_g = 4.90 \times 10^{-11}$ cm_2/dyne and $J_g = 1.36 \times 10^{-10}$ cm_2/dyne are obtained. These yield a glassy bulk compliance B_g of 3.3×10^{-11} cm^2/dyne and a glassy Poisson's ratio of 0.35 from

$$\nu_g = (J_g/2D_g) - 1 \tag{9}$$

These values are both clearly too large for reasons unknown to us. The differences involved do magnify experimental uncertainties by an order of magnitude.

Discussion

To check the hypothesis that local coordinated molecular motions are the primary contributors to the change in structural arrangements in amorphous materials which is involved in time-dependent dilatation or densification, the kinetic volume changes in the glass transformation range have been measured and the results have been compared with the creep compliance curves which reflects coordinated molecular motions over a very wide range of the time-scale. If the same molecular motions are indeed involved in density changes and various mechanical deformations the temperature dependencies must be the same.

The changes with temperature in the neighborhood of T_g are known to reflect the intrinsic dominating variable, the free volume. Changes in rate under isothermal and isobaric conditions are testing to this fact[12-14]. The comparison of temperature shift factors shown in Fig. 9 does indicate that the changes in volume have the same temperature dependence as the creep compliances. Markovitz has shown[11] that reasoning from Eq. 7 that for the three compliance functions J(t), D(t), and B(t) of a material to be temperature superposable they must all have the same time-scale and magnitude shift factors. The data presented above may be the first such test and are certainly in accord with his conclusions.

In addition the normalized voluminal retardation spectrum $L_v(\tau)$ calculated from the reduced isothermal contraction curve appears to correspond to that obtained from the shear compliance curve $L_s(\tau)$ at short times. The fact that $L_v(\tau)$ does not extend into the realm of long-times supports the expectation that long-range coordinated molecular motions do not play a significant role in determining the liquid structure which determines the density.

Acknowledgement

This work was supported by the Air Force Office of Scientific Research under contract F49620-86-C-0032. The new Torsional creep study reported here was carried out by Timothy Altares. The elongational creep compliance measurements were made by Altares and Kenneth Rumon. Initial dilatometer calibrations and preliminary temperature jump measurements were made by Ling -Yung Hu.

REFERENCES

1) A. J. Kovacs, Adv. Polymer Sci., 3, 394 (1963).

2) R. O. Davies and G. O. Jones, Adv. Physics, 2, 370 (1953).

3) G. Goldbach and G. Rehage, Rheologica Acta, 6, 30 (1967).

4) J. D. LeMay, B. J. Swetlin and F. N. Kelley, ACS Symposium Series No. 243, Characterization of Highly Cross - Linked Polymers, S. S. Labana and R. A. Dickie, Eds. 1984 p. 165.

5) M. -F. Vallat, D. J. Plazek and B. Bhushan, J. Polymer Sci., Part B Polym. Phys. Ed., 24, 1303 (1986).

6) A. J. Kovacs, J. J. Aklonis, J. M. Hutchinson and A. R. Ramos, J. Poly. Sci. Polym. Phys, Ed. 17, 1097 (1979).

7) D. J. Plazek and G. C. Berry, Physical Aging of Polymer Glasses in Glass: Science and Technology Vol. 3, Viscosity and Relaxation, Eds., D. R. Uhlmann and N. J. Kreidl, Academic Press, Inc., New York, Chapt. 7 (1986).

8) G. Rehage and G. Goldbach, Berichte der Bunsengesellschaft, 70, 1144 (1966).

9) Rheological Transforms Software: Time-Temperature Instruments, Inc., P. O. Box 40156, Pittsburgh, PA 15201.

10) D. J. Plazek and I. C. Choy, J. Polymer Sci.: Part B: Polym. Phys., 27, 307 (1989).

11) H. Markovitz, J. Polymer Sci.: Symposium No. 50, 431 (1975)

12) A. J. Kovacs, R. A. Stratton, and J. D. Ferry, J. Phys. Chem., 67, 152 (1963).

13) D. J. Plazek and J. H. Magill, J. Chem. Phys., 45, 3038 (1966).

14) L. C. E. Struik, "Physical Aging in Amorphous Polymers and Other Materials," Elsevier, Amsterdam (1978).

FIGURE LEGENDS

Fig. 1) The specific volume $\bar{V}(cm^3/g)$ of EPON 1001F fully cured with a stoichiometric amount of 4,4/ - diamino diphenyl sulfone, DDS shown as a function of temperature at four different rates of cooling 0.90, 0.25, 0.050, and 0.003 °C/min. Glass temperatures identified by the intersection point of the equilibrium and glass lines are listed.

Fig.2) Deviation of measured specific volume points from the equilibrium and glass lines of Fig. 1 plotted as a function of temperature, showing the extent of the "transformation range" and its change with the rate of cooling.

Fig. 3) Fractional volume deviation from equilibrium as a function of time at 131.0°C after cooling from 134°C and after heating from 129°C plotted versus the logarithm of the corrected aging time $t-t_i$ where t_i is the estimated time for the specimen to reach a uniform temperature.

Fig. 4) Absolute fractional volume deviation from equilibrium as a function of the logarithm of the corrected aging time for five temperatures after cooling 2.5°C from equilibrium and for four temperatures after heating.

Fig. 5) Volume contraction and expansion curves from Fig. 4 reduced by time-scale shifts to the reference temperature T_o = 134°C. The time t is the corrected value.

Fig. 6) Comparison of retardation spectra for voluminal L_v and shear deformation L_s. In this double logarithmic plot of the distribution functions of retardation times τ the ordinate scales have been adjusted to superpose the short time results.

Fig. 7) Double logarithmic presentation of the reduced elongational creep compliance $D_p(t)$ as a function of time for EPON 1001F at 10 temperatures as indicated. The temperature of reduction is 130°C.

Fig. 8) Elongational creep compliance $D_p(t)$ curves from Fig. 7 shifted to superpose at a reference temperature T_o of 130°C. The reduced shear creep compliance $J_p(t)$ curve also shown for comparison (long-dashed line). The latter has been shifted toward shorter times by 0.8 of a decade to match long-time rates. The short-dashed line is the $J_p(t)$ curve diminished by a factor of three.

Fig. 9) Logarithm of time-scale shift factors of EPON 1001F for four different kinds of rate process experiments; 1) volume - constant rate of cooling; 2) volume - temperature jump; 3) shear creep compliance and; 4) elongational creep compliance, presented as a function of temperature.

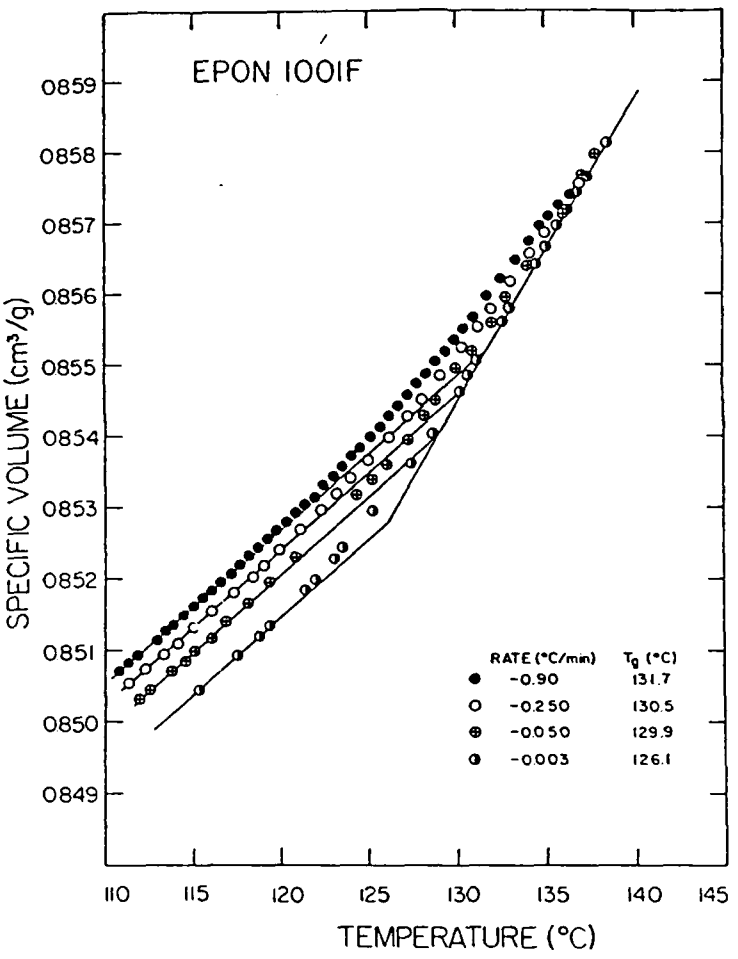

Figure 1

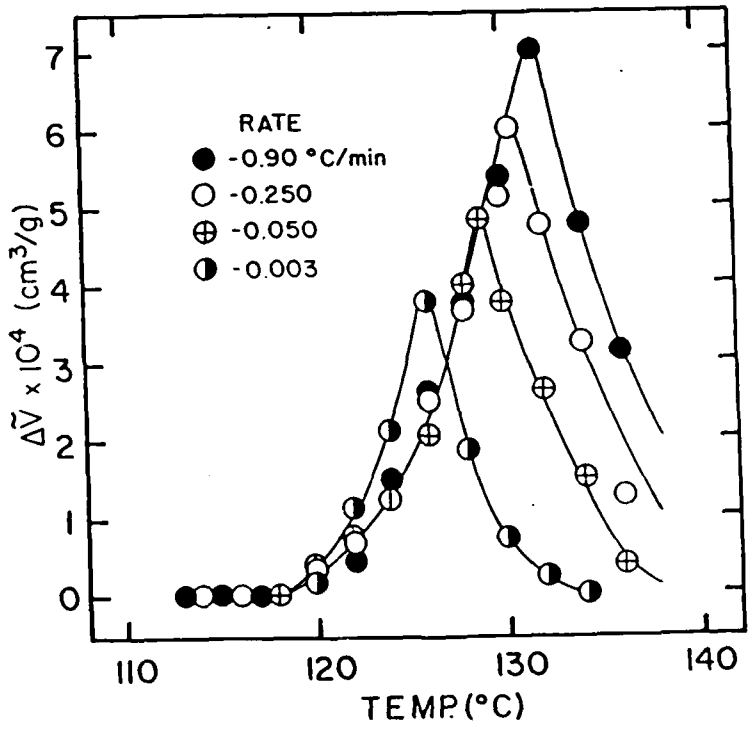

Figure 2

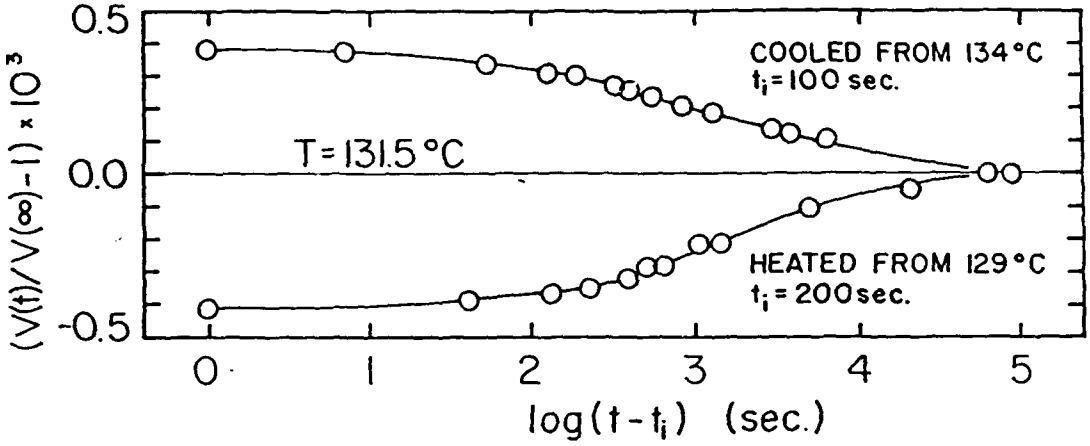

Figure 3

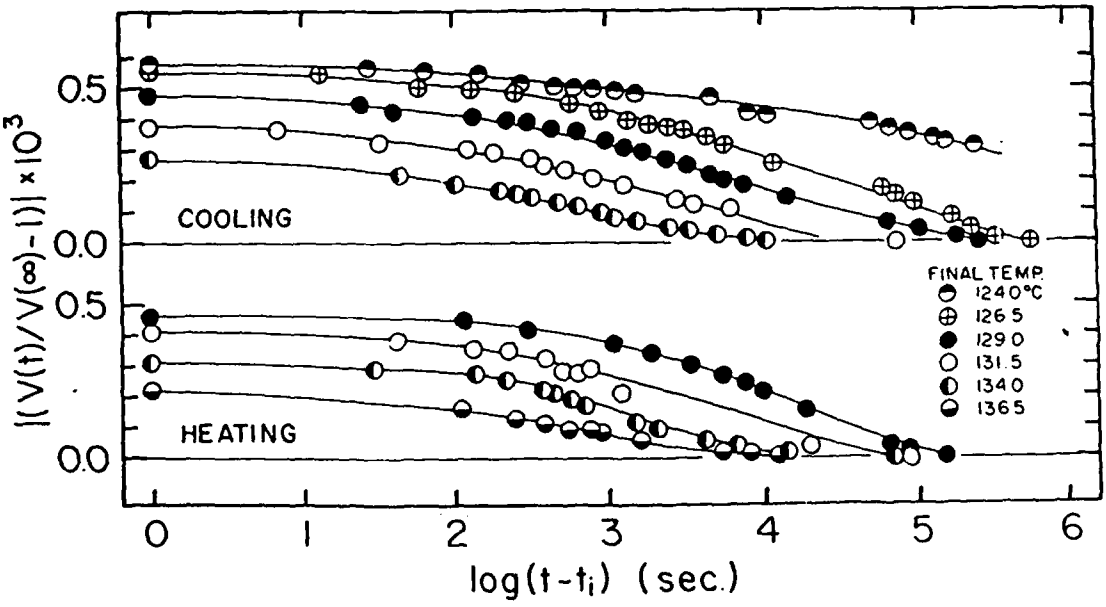

Figure 4

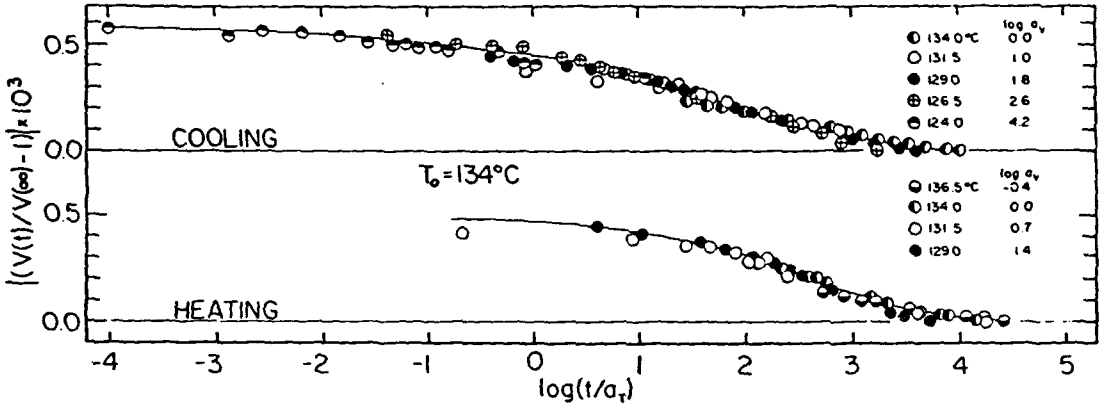

Figure 5

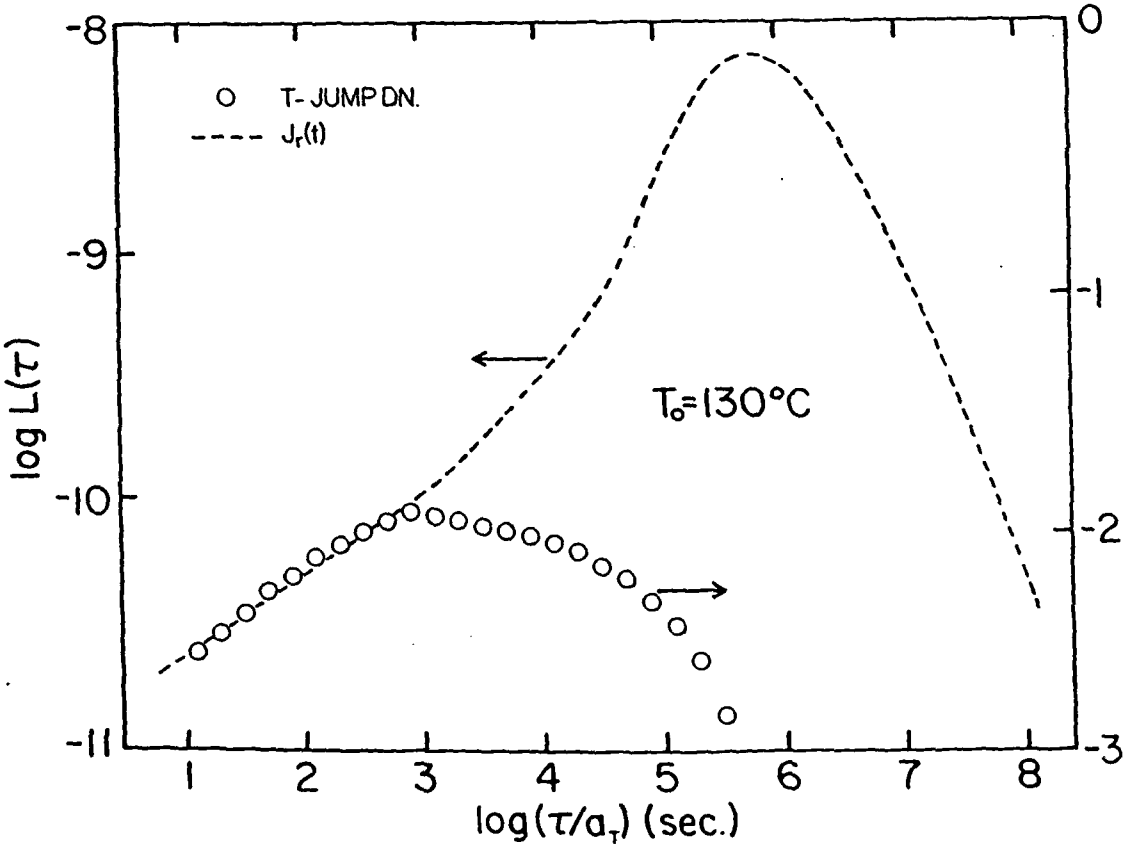

Figure 6

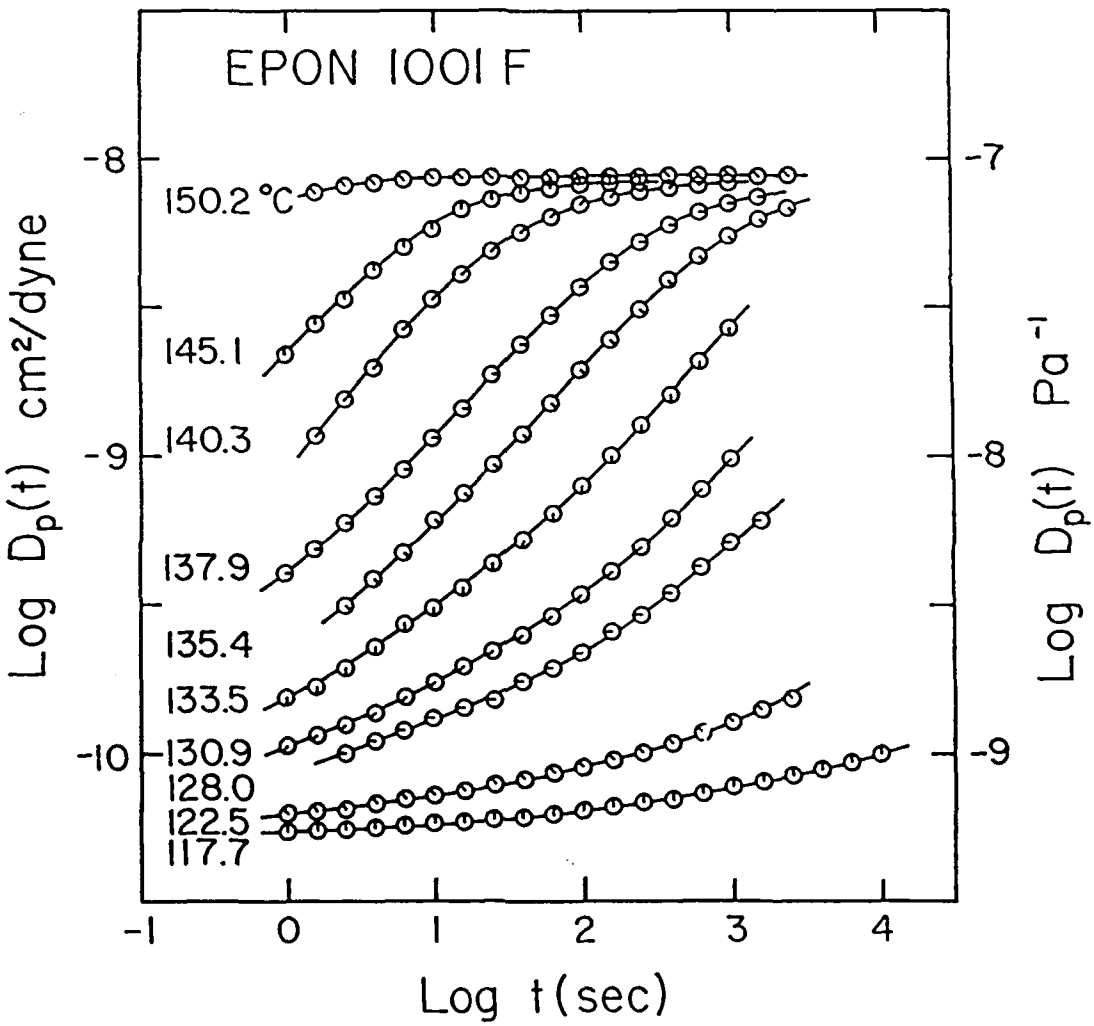
EPON 1001 F
150.2 °C
145.1
140.3
137.9
135.4
133.5
130.9
128.0
122.5
117.7
-8
-9
-10
-7
-8
-9
-1
0
1
2
3
4
Log $D_p(t)$ cm²/dyne
Log $D_p(t)$ Pa^{-1}
Log t(sec)

Figure 7

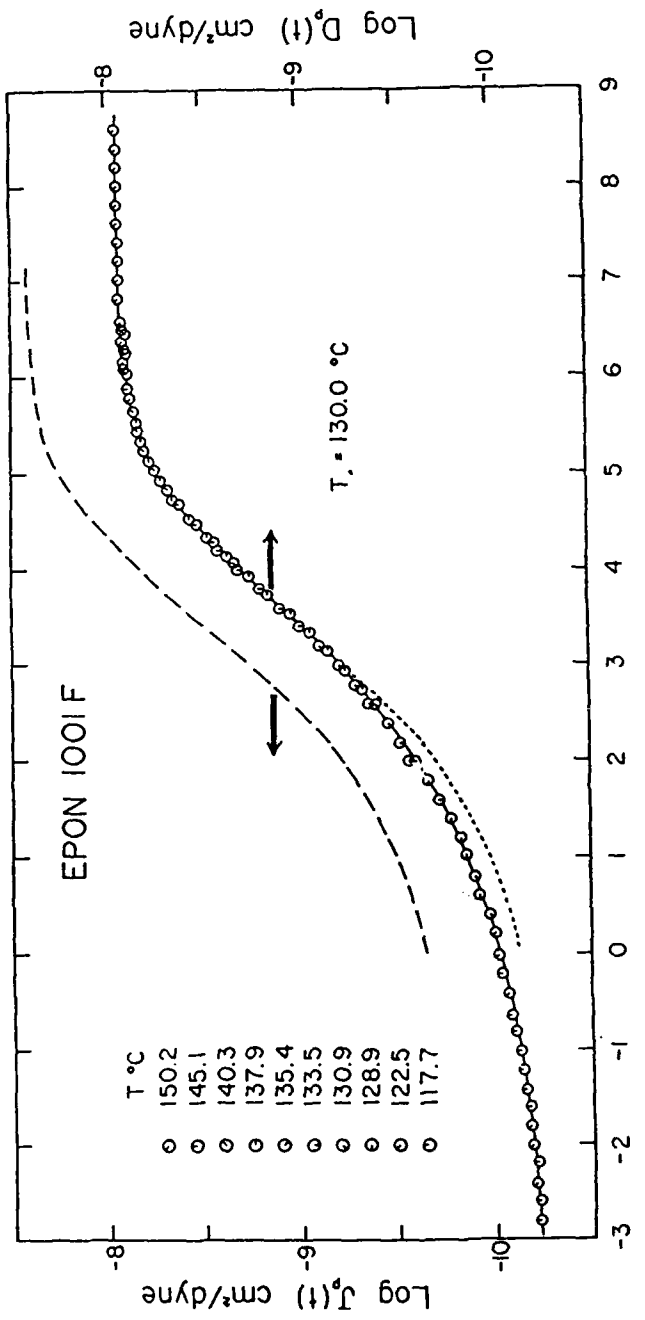
EPON 1001 F
T, = 130.0 °C
T °C
150.2
145.1
140.3
137.9
135.4
133.5
130.9
128.9
122.5
117.7
Log J_p(t) cm²/dyne
Log D_p(t) cm²/dyne
Log t/a_T

Figure 8

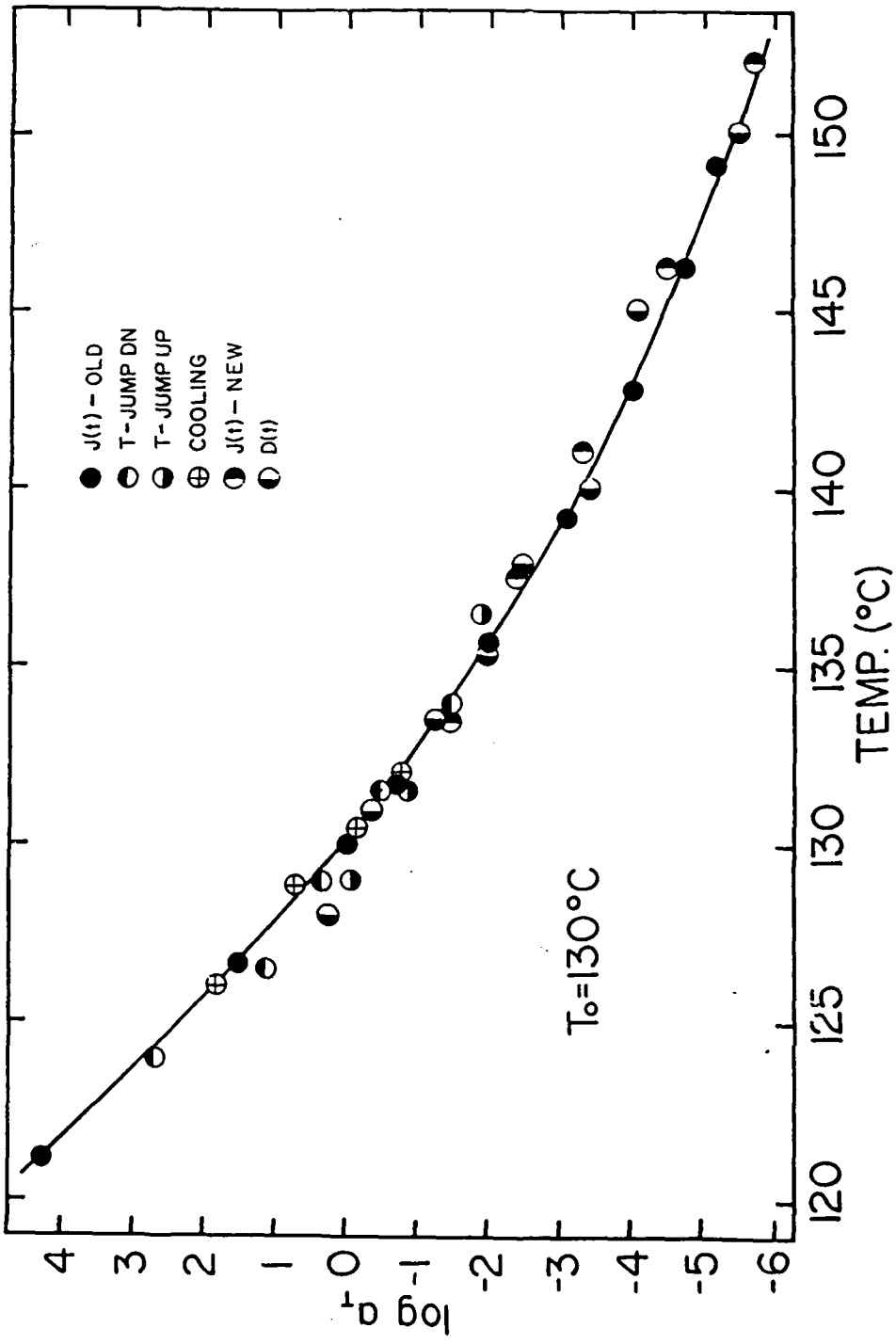
J(t) - OLD
T-JUMP DN
T-JUMP UP
COOLING
J(t) - NEW
D(t)
T₀=130°C
log a_T
TEMP. (°C)
4
3
2
1
0
-1
-2
-3
-4
-5
-6
120
125
130
135
140
145
150

Figure 9

Finite-Element Numerical Simulation of Tearing and Fatigue in Polymers

by

Michael R. Frank

Submitted to The University of Akron
in partial fulfillment of the requirements
of the University Honors Program (B.S.)

Contents

Summary

The behavior of polymer-based material in the vicinity of a crack tip and the subsequent growth of a crack through the material are topics of current research. The model described in this paper is based on a finite element analysis of the region surrounding a crack tip. The parameters used in the model allow for a variety of different materials including those displaying non-Hookian behavior. The model includes a simple mechanism for examining fatigue leading to crack propagation. Further investigation of fatigue crack growth can be done using the results of the present model.

I. Introduction

The fundamental assumptions of classical theoretical analysis of rubber-like elasticity are basically as follows:

1. The distribution of the chain dimensions is describable by the Gaussian statistics of freely-jointed chains.[1]
2. Intermolecular forces are insignificant.
3. Internal energy changes during deformation are non-existent.
4. Network chains deform in proportion to the strain on the sample (affine deformation).

These assumptions lead to an expression for the force per unit unstrained cross-sectional area[2]

$$f = G(\lambda - \lambda^{-2}) \tag{I.1}$$

where

$$G = NKT \tag{I.2}$$

$$\lambda = L/L_0 = 1 + \varepsilon \tag{I.3}$$

In an attempt to treat a wider variety of polymers than the case of ideal rubber, the first assumption can be avoided by using a result of Treloar's for non-Gaussian networks given by[2,4]

$$f = XG(\lambda - \lambda^{-2}) \tag{I.4}$$

The first five terms of X are

$$X = 1 + An^{-1}(3\lambda^2 + 4\lambda^{-1}) + Bn^{-2}(5\lambda^4 + 8\lambda + 8\lambda^{-2}) + Cn^{-3}(35\lambda^6 + 60\lambda + 72 + 64\lambda^{-3}) + Dn^{-4}(630\lambda^8 + 1120\lambda + 1440\lambda + 1536\lambda^{-1} + 1280\lambda^{-4}) \quad (I.5)$$

where $A = 35/25$;

$B = 297/6125$;

$C = 12312/2205000$;

$D = 126117/[(693)(673750)]$; and

n is the number of random links.

It is easy to see that expression (I.4) reduces to the Gaussian case, (I.1), for large n.

The proposed finite element approach enables the use of Equation (I.4) indirectly. That is, using the derivative with respect to extension as an expression for the modulus within each element. This aids in modeling overall non-linearity. To demonstrate simple fatigue behavior, the number of effective crosslinks, N in Equation (I.2), is expressed as a function of the amount of strain and the length of time that the material is subjected to that strain. This is given by

$$N(\delta t, \varepsilon) = N(t-\delta t)\exp(-\alpha\varepsilon\delta t) \quad (I.6)$$

where α is an adjustable parameter which has dimensions of frequency.

The details of the finite element method[3,4] are outlined on the following pages.

II. Finite Element Method

Shown in Figure 1 is a discretized slab representing the material in the vicinity of a crack tip. All of the elements are rectangular for ease in calculation and visualization.

Consider the i^{th} element shown below.

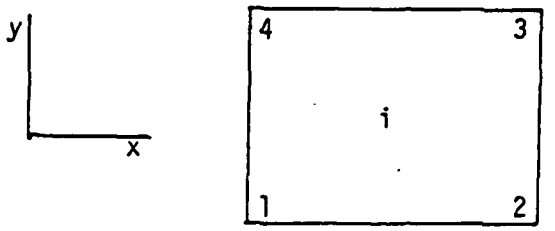

At each corner (node) there are two degrees of freedom, i.e., displacements in the x and y directions. These displacements are described by

$$\begin{aligned} u(x,y) &= A_0 + A_1 x + A_2 y + A_3 xy \\ v(x,y) &= A_4 + A_5 x + A_6 y + A_7 xy \end{aligned} \qquad \text{(II.1)}$$

where u(x,y) is displacement in the x direction and v(x,y) is displacement in the y direction. The form of Equation (II.1) insures continuity across element boundaries. Note that for constant x the displacements vary linearly with y, and similarly for constant y. Equation (II.1) can be written in matrix form as

$$\{\delta\} = \begin{Bmatrix} u \\ v \end{Bmatrix} = [M]\{A\} \qquad \text{(II.2)}$$

where

$$[M] = \begin{bmatrix} 1 & x & y & xy & 0 & 0 & 0 & 0 \\ 0 & 0 & 0 & 0 & 1 & x & y & xy \end{bmatrix}$$

$$\{A\}^t = \{A_0 \quad A_1 \quad A_2 \quad A_3 \quad A_4 \quad A_5 \quad A_6 \quad A_7\}$$

This formulation can be extended to represent all of the nodes in the i^{th} element as shown below.

$$\begin{Bmatrix} u_{i1} \\ v_{i1} \\ u_{i2} \\ v_{i2} \\ u_{i3} \\ v_{i3} \\ u_{i4} \\ v_{i4} \end{Bmatrix} = \begin{bmatrix} 1 & x_1 & y_1 & x_1y_1 & 0 & 0 & 0 & 0 \\ 0 & 0 & 0 & 0 & 1 & x_1 & y_1 & x_1y_1 \\ 1 & x_2 & y_2 & x_2y_2 & 0 & 0 & 0 & 0 \\ 0 & 0 & 0 & 0 & 1 & x_2 & y_2 & x_2y_2 \\ 1 & x_3 & y_3 & x_3y_3 & 0 & 0 & 0 & 0 \\ 0 & 0 & 0 & 0 & 1 & x_3 & y_3 & x_3y_3 \\ 1 & x_4 & y_4 & x_4y_4 & 0 & 0 & 0 & 0 \\ 0 & 0 & 0 & 0 & 1 & x_4 & y_4 & x_4y_4 \end{bmatrix} \begin{Bmatrix} A_0 \\ A_1 \\ A_2 \\ A_3 \\ A_4 \\ A_5 \\ A_6 \\ A_7 \end{Bmatrix}$$

or

$$\{\delta\} = [c]\{A\} \tag{II.3}$$

The vector {A} can then be given by

$$\{A\} = [c]^{-1}\{\delta\} \tag{II.4}$$

The strain within a single element is defined in the usual fashion

$$\{\varepsilon\} = \begin{Bmatrix} \varepsilon_{xx} \\ \varepsilon_{yy} \\ \varepsilon_{xy} \end{Bmatrix} = \begin{Bmatrix} \frac{\partial u}{\partial x} \\ \frac{\partial v}{\partial y} \\ \frac{\partial u}{\partial y} + \frac{\partial v}{\partial x} \end{Bmatrix} \tag{II.4}$$

where

$$\frac{\partial u}{\partial x} = A_1 + A_3 y = 0 + A_1 + 0 + A_3 y$$

$$\frac{\partial u}{\partial y} = A_6 + A_7 x = 0 + 0 + A_6 + A_7 x$$

$$\frac{\partial u}{\partial y} = A_2 + A_3 x = 0 + 0 + A_2 + A_3 x$$

$$\frac{\partial v}{\partial x} = A_5 + A_7 y = 0 + A_5 + 0 + A_7 y$$

Again, this can be expressed in matrix form by

$$\begin{Bmatrix} \varepsilon_{xx} \\ \varepsilon_{yy} \\ \varepsilon_{xy} \end{Bmatrix} = \begin{bmatrix} 0 & 1 & 0 & y & 0 & 0 & 0 & .0 \\ 0 & 0 & 0 & 0 & 0 & 0 & 1 & x \\ 0 & 0 & 1 & x & 0 & 1 & 0 & y \end{bmatrix} \begin{Bmatrix} A_0 \\ A_1 \\ A_2 \\ A_3 \\ A_4 \\ A_5 \\ A_6 \\ A_7 \end{Bmatrix} \qquad \text{(II.5)}$$

or

$$\{\varepsilon\} = [N]\{A\}$$

Finally, substituting Equation (II.4) for {A} into the above equation gives

$$\{\varepsilon\} = [N][c]^{-1}\{\delta\} \qquad \text{(II.6)}$$

The "stiffness" matrix [K] can be obtained by requiring that the potential energy be minimized with respect to the displacements. The potential energy for this case is given by

$$\pi_p = \int_v \frac{1}{2} \varepsilon\sigma dv \tag{II.7}$$

where

$$\{\sigma\} = \begin{Bmatrix} \sigma_{xx} \\ \sigma_{yy} \\ \sigma_{xy} \end{Bmatrix} = [d]\{\varepsilon\} \tag{II.8}$$

and

$$[d] = \frac{1}{(1 - \nu^2)} \begin{bmatrix} 1 & \nu & 0 \\ \nu & 1 & 0 \\ 0 & 0 & \frac{1-\nu}{2} \end{bmatrix} \tag{II.9}$$

Substituting expressions (II.6) and (II.8) for ε and σ into (II.7) gives for the potential energy

$$\pi_p = \frac{1}{2} \int \{\delta\}^t [c^{-1}]^t [N]^t [d][N][c^{-1}]\{\delta\} dv \tag{II.10}$$

By equating the partial derivatives of π_p with respect to the displacements of zero, i.e.,

$$\frac{\partial \pi_p}{\partial \{\delta\}} = 0$$

the following expression for the stiffness matrix is obtained

$$[K]\{\delta\} = 0$$

where

$$[K] = \int_V [c^{-1}]^t [N]^t [d][N][c^{-1}]dv \qquad (II.11)$$

This process is continued for each element in the mesh shown in Figure 1. Finally, the overall stiffness matrix is formed from the individual element stiffness matrices.

Before solving the set of simultaneous equations for the displacements, boundary conditions must be implemented. The boundary conditions used in this model are as follows:

1. The displacement in the vertical direction at the top of the slab is equal to the negative vertical displacement at the bottom of the slab and both displacements are constant in the horizontal direction.
2. The horizontal displacements along the top, bottom and sides is zero, except, of course, in the area representing the crack tip.
3. The vertical displacement along the axis of symmetry is zero.

The first of these conditions is simply that the slab is being stretched by equal amounts in opposite directions at the top and bottom. Since no loads are specified, the displacements are given as boundary conditions.

The second condition amounts to stating that the slab under consideration is far removed from the edges of the material.

The third condition is based on the assumption that the geometric axis of symmetry will remain stationary in the vertical direction due to the

symmetry of the applied strain. This assumption allows the solution of the upper half of the slab to be duplicated for the lower half, thus reducing the number of equations by half.

III. Time Evolution

To model fatigue behavior, the displacement at the top and bottom boundaries is cyclic. In this particular case the displacement is given by

$$d = d_a - d_b \cos(2\pi f n \delta t) \qquad \text{(III.1)}$$

where f is frequency;

$n = 0,1,2,3...n_T$, n_T is the total number of time steps per cycle;

δt is the length of each time step;

d_a, d_b are adjustable parameters for the amplitude of the displacement, $d_a \geq d_b$.

The finite element method, as previously described, is applied at each time step δt. The function for the number of effective crosslinks, Equation (I.6), is updated and the modulus within each element is calculated. Then, as the sample evolves, its characteristics can be examined at any point in time. Measurements could be made of a variety of quantities such as stress in the vicinity of the crack tip, stored elastic energy, or the change in stored energy with respect to the formation of new surfaces.

The criteria for the formation of new surfaces is presently based on the amount of strain at the crack tip. Propagation of the crack is constrained to the axis of symmetry.

Graphics, which are displayed at every time step, allow visualization of the changing sample. Figures 2-5 show a sample at stages just before

and after tearing. Figures 6-9 show the strain contours during the same time period.

IV. Conclusions and Suggestions for Further Work

The model described in this paper can be used to gain valuable information about the behavior of material in the vicinity of a crack tip, particularly material in transition, i.e., changing modulus. By varying the parameters, totally different characteristics can be displayed both visually and quantitatively.

It should be noted, however, that the present model is a starting point or basis for further investigation. It would be interesting, for example, to introduce different fatigue mechanisms such as local heating, or to use more complicated criteria for crack propagation. Ultimately, the description of two-dimensional crack growth should be attainable using this approach.

REFERENCES

1. I. M. Ward, "Mechanical Properties of Solid Polymers," Wiley, New York, (1971).

2. L. R.G. Treloar, "The Physics of Rubber Elasticity," 2nd Ed., Oxford University Press, London, (1958).

3. See for example B. Nath, "Fundamentals of Finite Elements for Engineers," The Athlone Press of the University of London, (1974).

4. J. D. LeMay, Ph. D. Dissertation (Polymer Science), The University of Akron (1985).

FIGURE CAPTIONS

Fig. 1 Discretized slab in the initial state, i.e., no strain. There are 264 total elements. The area which has been removed represents the initial crack tip.

Figs. 2-5 Vertical strain is applied in equal increments for each successive figure. Figures 4 and 5 show the formation of new surfaces.

Figs. 6-9 Hand-drawn regions of strain intensity based on the strain at element boundaries are added to Figures 2-5. The regions are not established by absolute strain but rather the ratio of the strain at a point to the strain at the crack tip on the axis of symmetry, where the maximum strain occurs.

Figures 1-9 follow.

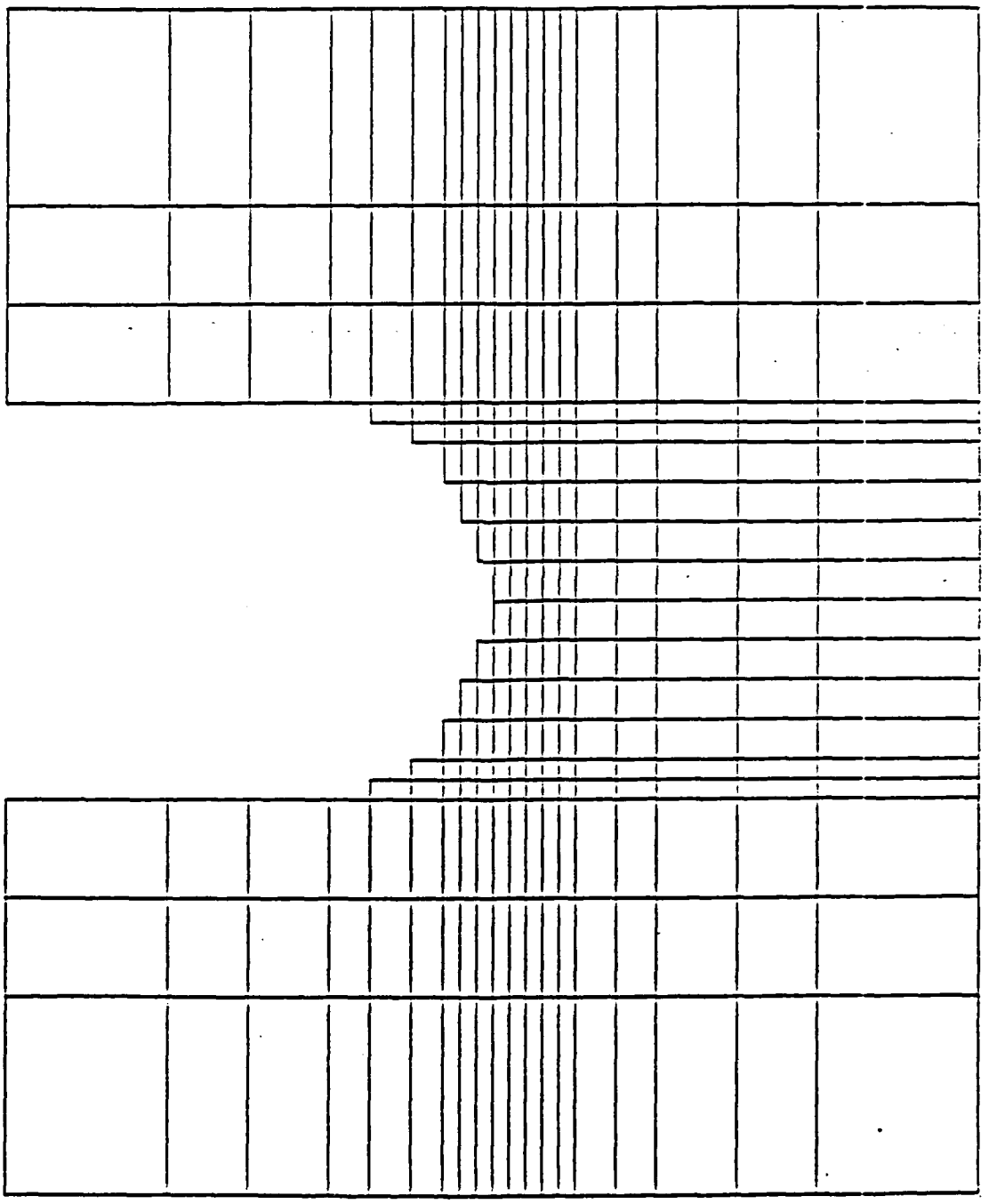

Frank, Fig. 1

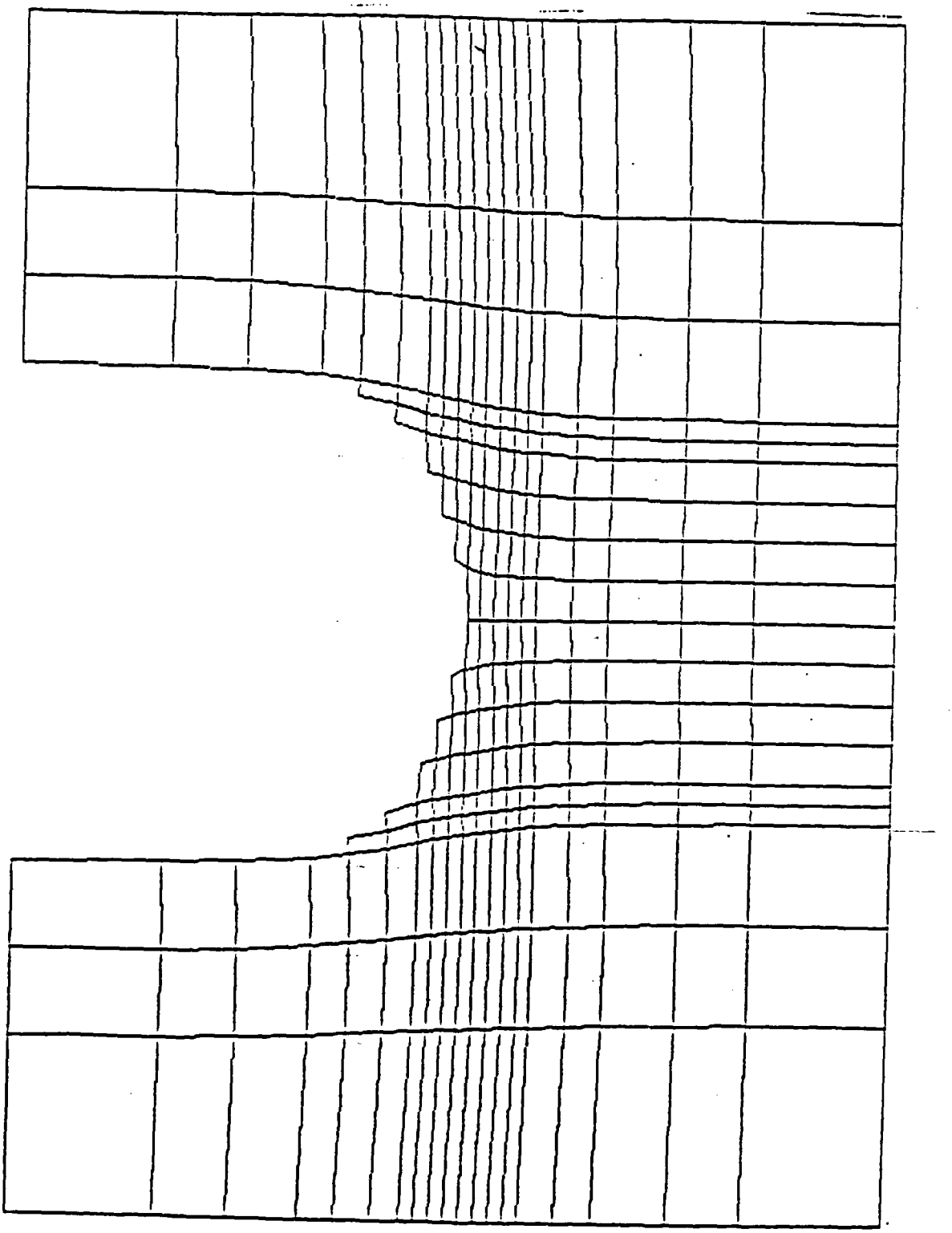

Frank, Fig. 2

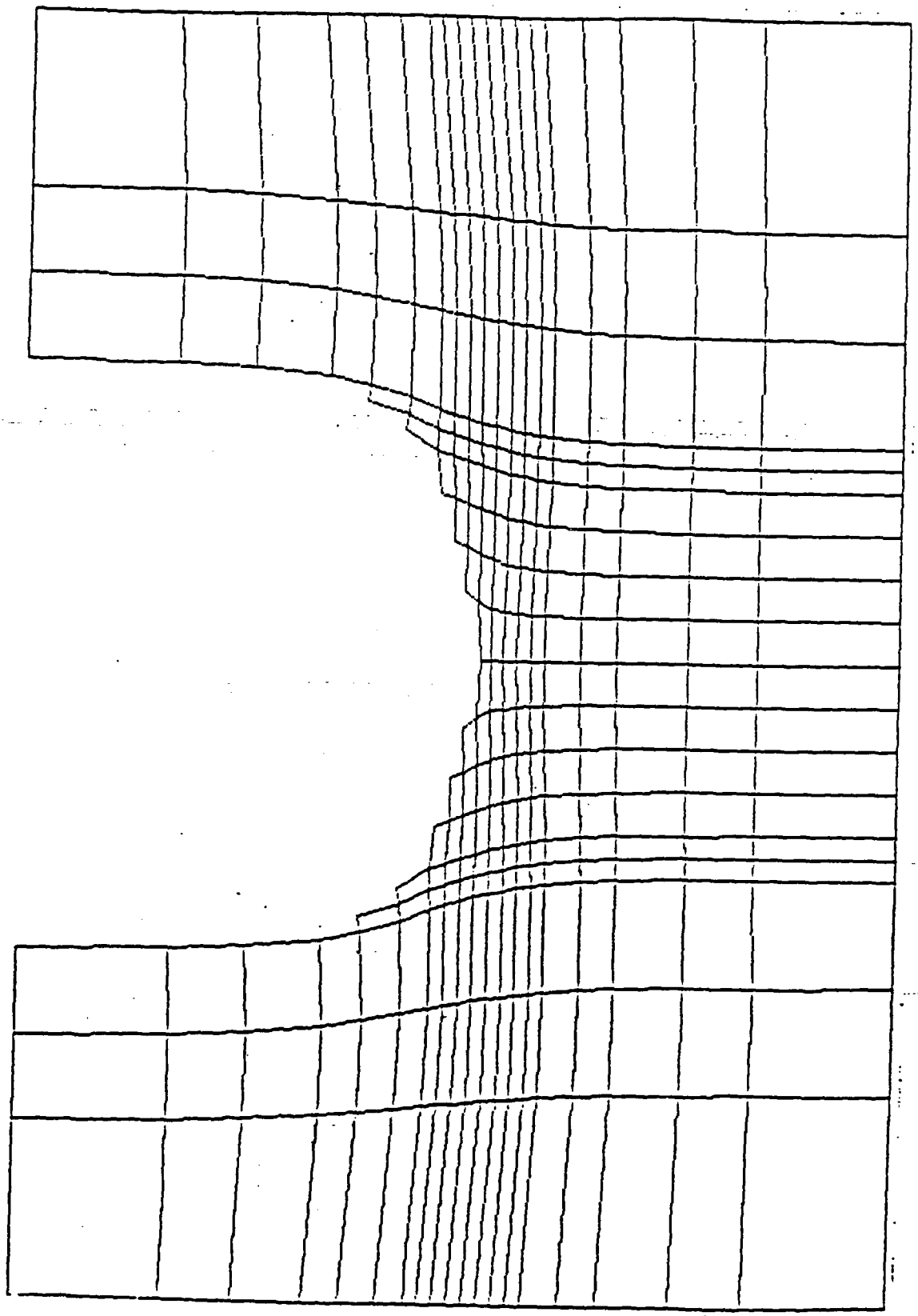

Frank Fig. 3

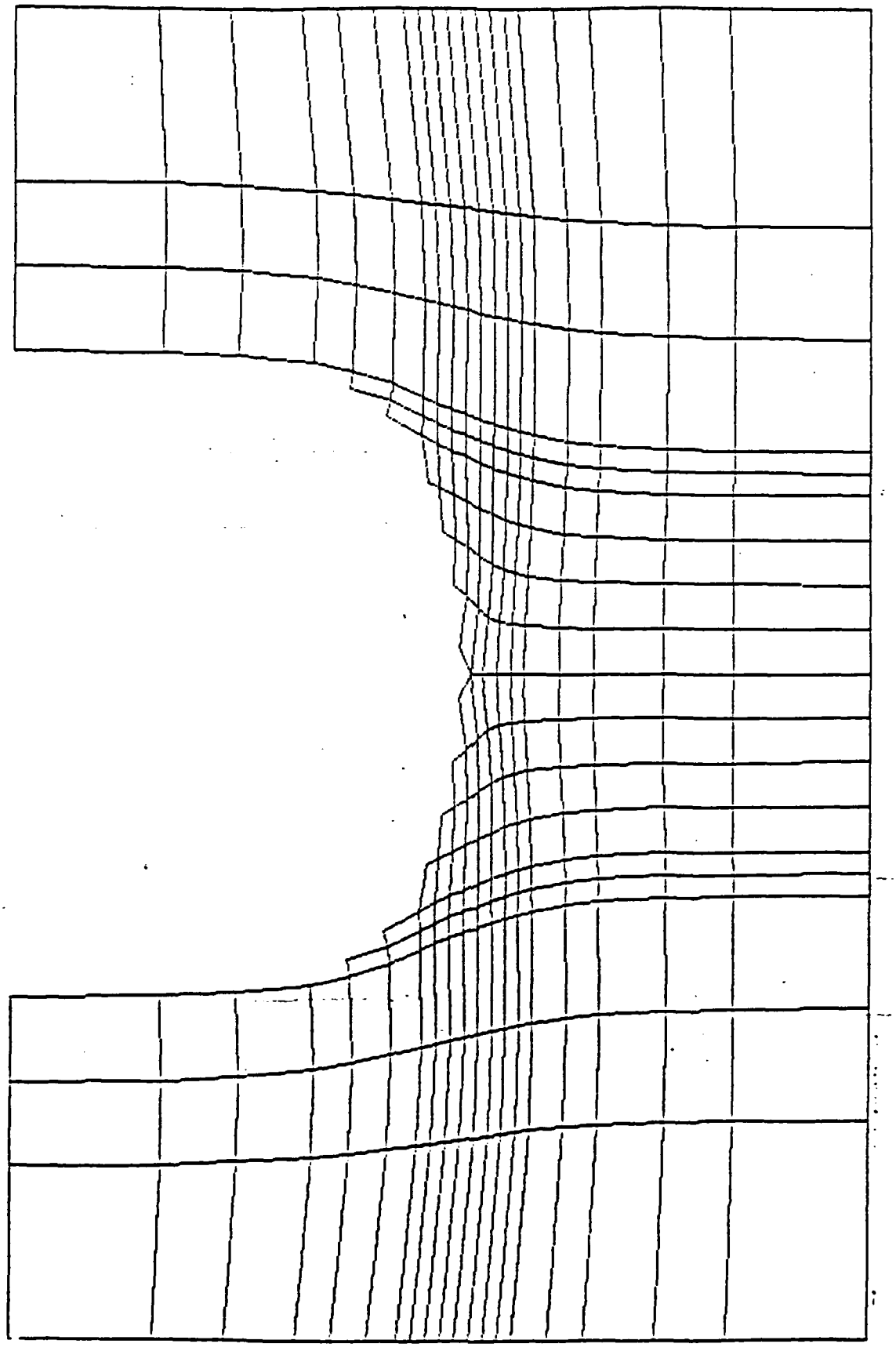

Frank, Fig. 4

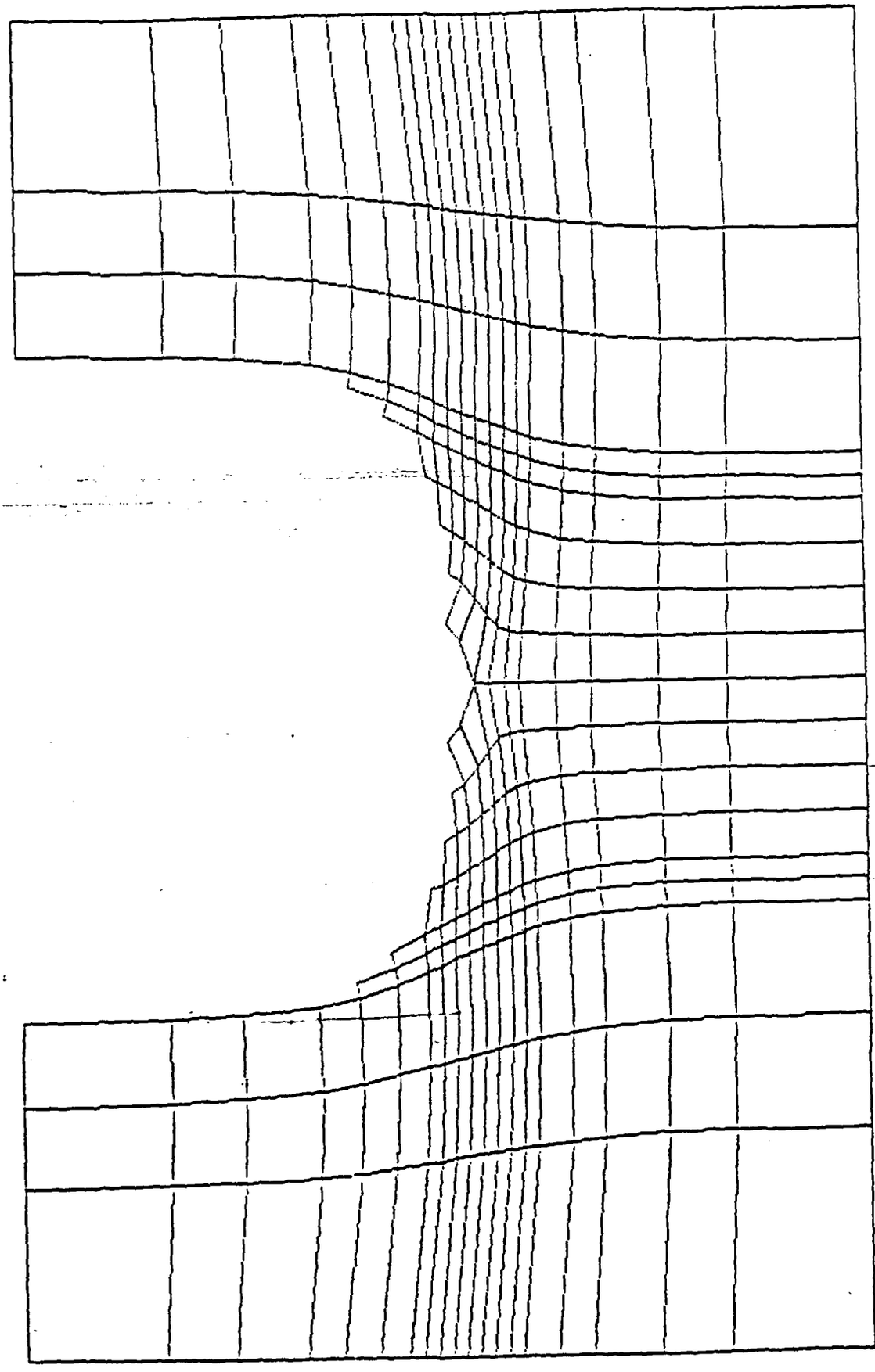

Frank, Fig. 5

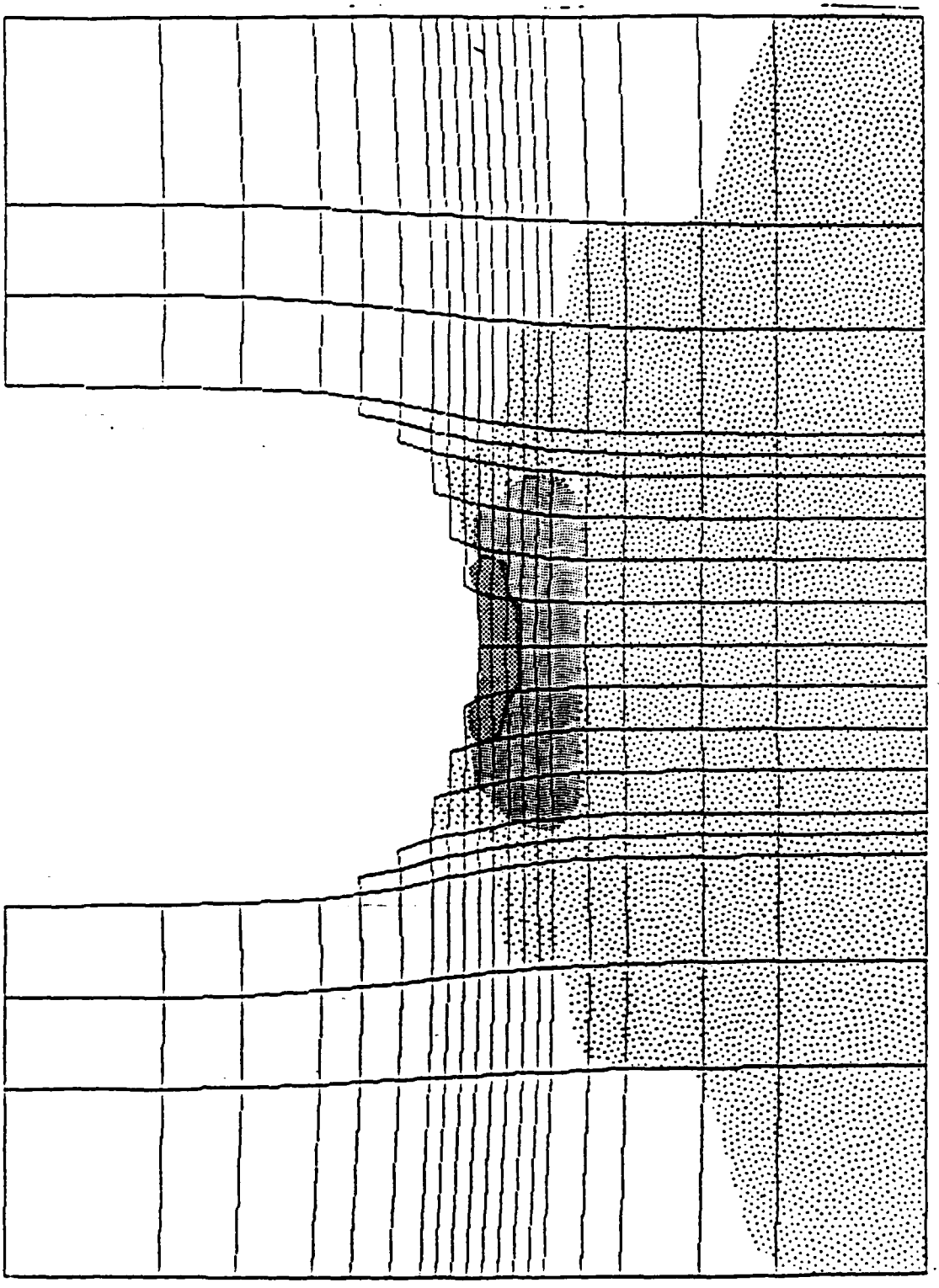

Frank, Fig. 6

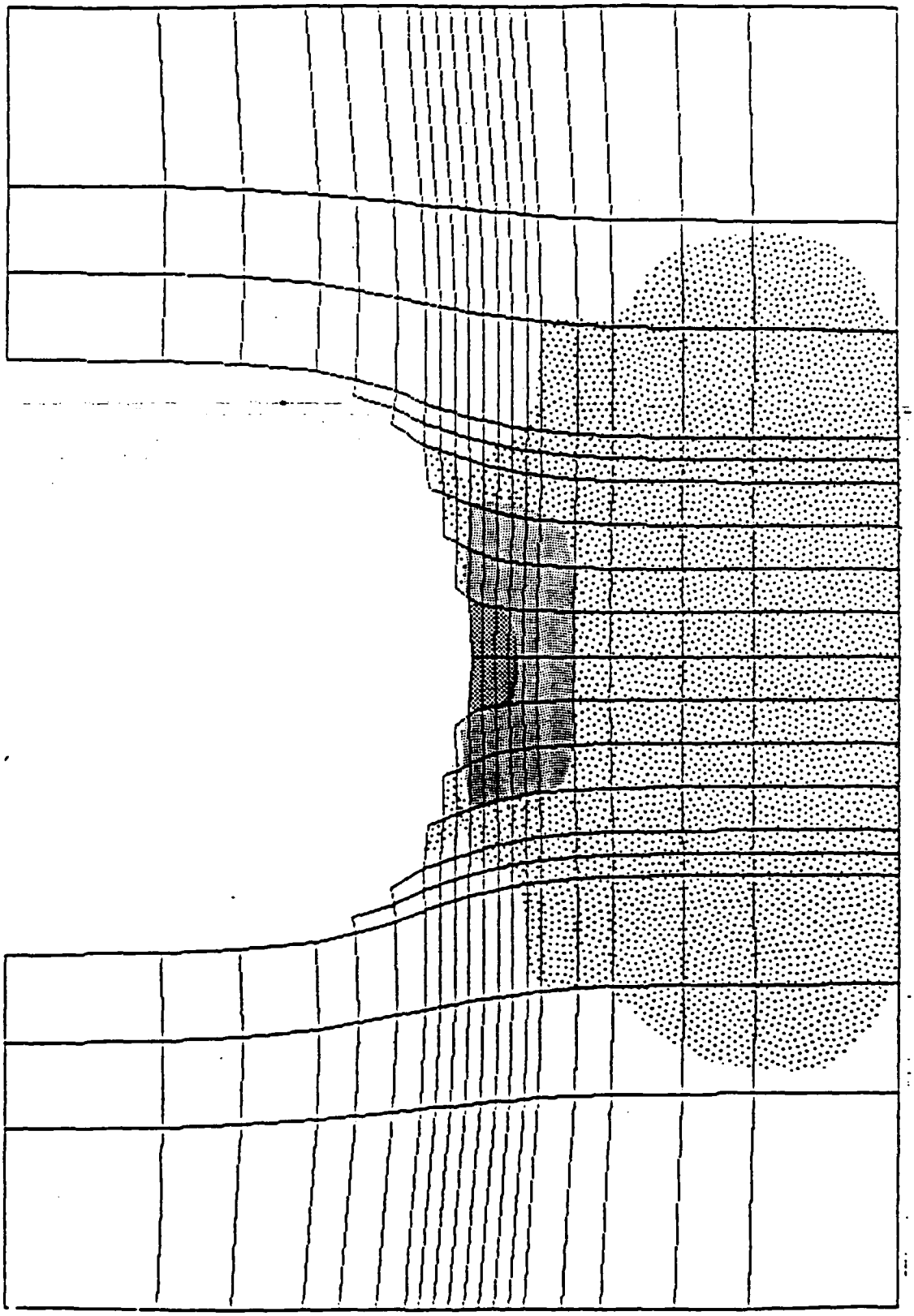

Frank Fig. 7

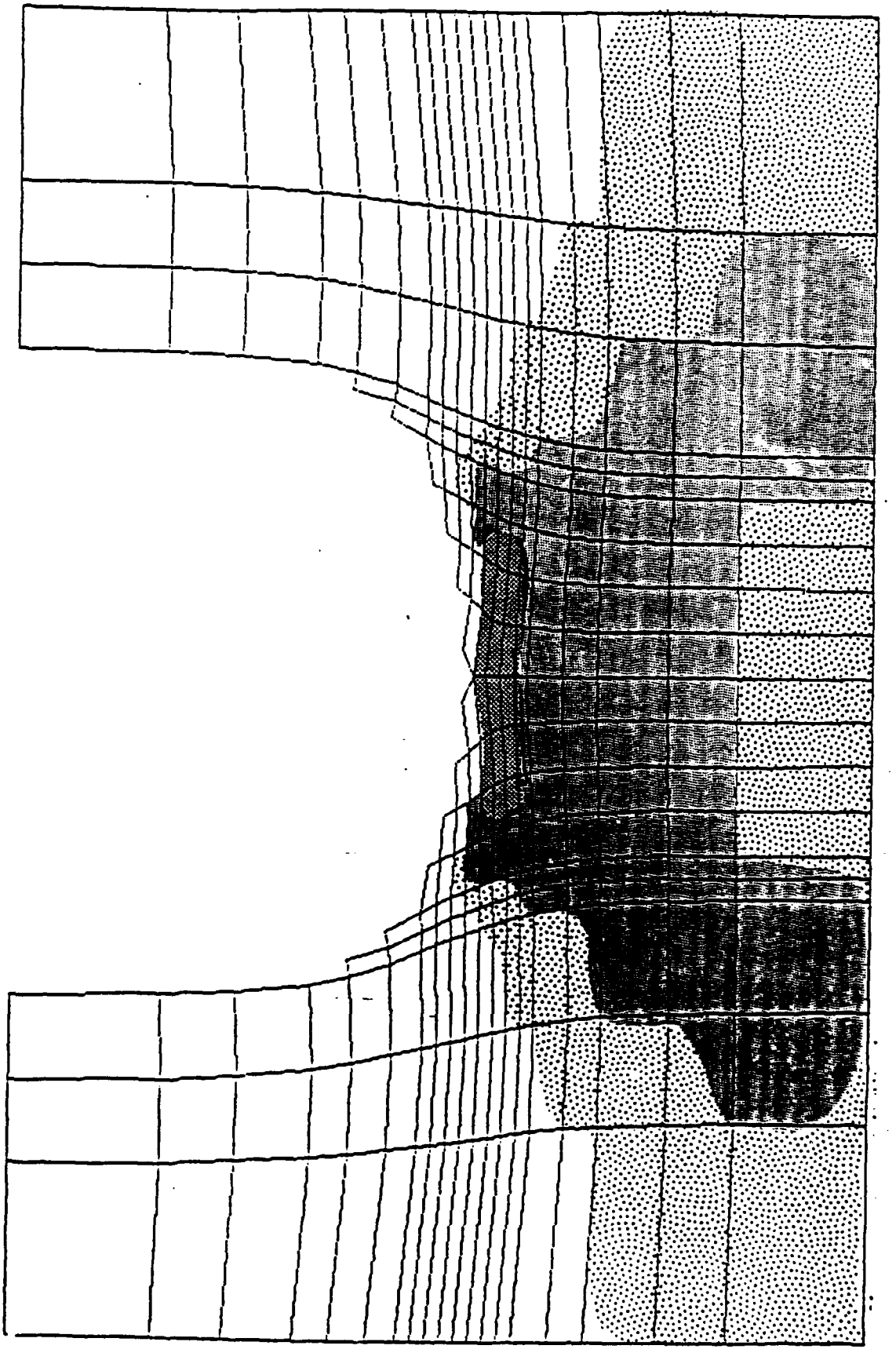

Frank, Fig. 8

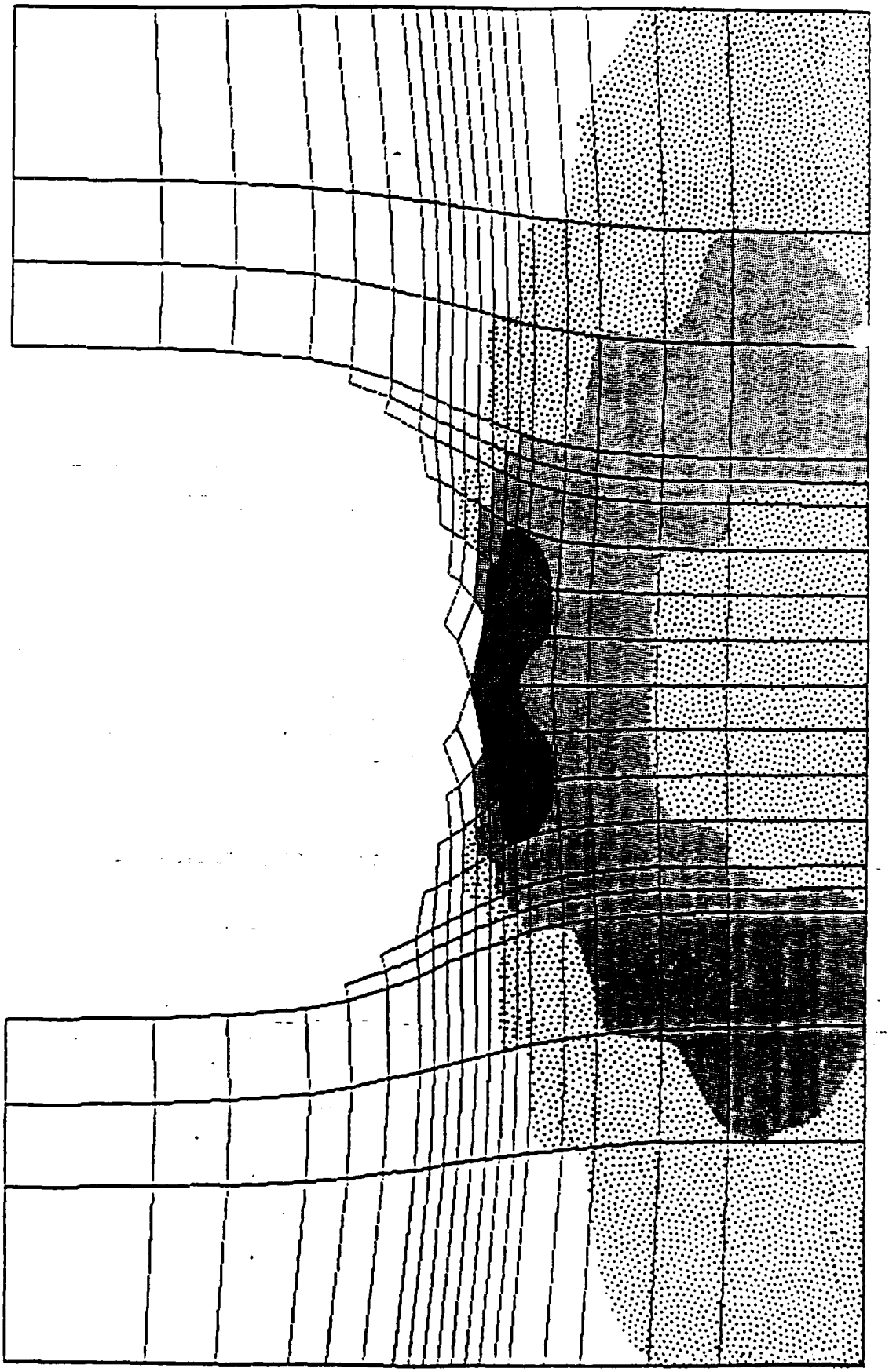

Frank, Fig. 9

APPENDIX

Source Code of FORTRAN Program

```
c     main
      dimension x(200,4),y(200,4),s(200,8,8),c(8,8),ct(8,8),ck(5,8,8)
      dimension p(350),del(350),n1(200,4),n2(4),hh(10),w(20)
      real nu,n(8,8),k(350,350),nec(200)
      integer g,bc(11)
      g=0
      flg=0
      tx=0
      read(*,*)nts,dt,f,nu,h,nel,nei,ndf,dx,da,db,dcrit,g
      call input1(hh,w)
      call gennod(x,y,n1,hh,w)
      do 100 i=1,200
         nec(i)=1.0 e 23
  100 continue
      nen=161
      do 101 i=1,350
  101    del(i)=0
      call main()
      call graphics(x,y,n1,nel,del,tx)
    1 call calcdisp(nts,dt,f,disp,g,da,db)
      do 5 i=1,350
      do 5 j=1,350
    5    k(i,j)=0.
      do 10 it=1,nel
         call calcnec(nec,del,dt,n1,y,it)
         call forme(del,e,nu,n1,y,nec,it)
         call formcinv(c,x,y,ct,it,ck)
         call formn(n,x,y,nu,e,h,it)
         call mmult(ct,n,c,s,it)
         call stifmat(k,s,n1,n2,it,nen,nel,ndf,nei)
   10 continue
      call tstbc(bc,del,y,n1,dcrit)
      call boundcon(k,disp,p,bw,bc)
      call matsolv(k,nen,p,ndf,del)
      call main()
      call graphics(x,y,n1,nel,del,tx)
      g=g+1
      if(g.lt.nts)go to 1
      g=0
      go to 1
      stop
      end
c
c
c
      subroutine calcdisp(nts,dt,f,disp,g,da,db)
      integer g
      pi=3.1415927
      disp=da-db*cos(2*pi*f*dt*g)
      return
      end
c
c
      subroutine tstbc(bc,del,y,n1,dcrit)
      dimension del(350),y(200,4),n1(200,4)
      integer bc(11)
      do 40 i=1,10
         j=51+(i-1)*9
         e1=y(j,4)-y(j,1)
         e2=del(2*n1(j,4))-del(2*n1(j,1))
         ee=e2/e1
         print *,"strain at tip",ee
         if(ee.gt.dcrit)bc(i)=1
   40 continue
      return
      end
```

```
c
c
      subroutine input1(hh,w)
      dimension hh(10),w(20)
      read(*,*)(hh(i),i=1,10)
      read(*,*)(w(i),i=1,20)
      return
      end
c
c
      subroutine gennod(x,y,n1,hh,w)
      dimension x(200,4),y(200,4),n1(200,4),w(20),hh(10)
      integer col
      it=0
      nc=1
      k=3
      do 500 col=1,19
         if(it.ge.12)k=4
         if(it.ge.16)k=5
         if(it.ge.21)k=6
         if(it.ge.27)k=7
         if(it.ge.34)k=8
         if(it.ge.42)k=9
           do 20 i=1,k
              it=it+1
              l=k+1
              x(it,1)=w(col)
              x(it,2)=w(col+1)
              x(it,3)=x(it,2)
              x(it,4)=x(it,1)
              y(it,1)=hh(i+1)
              y(it,2)=y(it,1)
              y(it,3)=hh(i)
              y(it,4)=y(it,3)
              n1(it,1)=nc+i
              n1(it,2)=n1(it,1)+1
              n1(it,3)=n1(it,2)-1
              n1(it,4)=n1(it,1)-1
   20       continue
            nc=nc+1
  500 continue
      return
      end
c
c
      subroutine formn(n,x,y,nu,e,h,it)
      real n,nu
      dimension n(8,8),x(200,4),y(200,4)
      do 5 i=1,8
         n(3,i)=0
         n(1,i)=0
         n(i,3)=0
         n(i,1)=0
    5 continue
      c1=1
      c2=1
      t=e/(1-nu**2)
      w=t*(1-nu)/2
      hx=x(it,2)-x(it,1)
      hy=y(it,4)-y(it,1)
      hx2=x(it,2)**2-x(it,1)**2
      hy2=y(it,4)**2-y(it,1)**2
      hx3=x(it,2)**3-x(it,1)**3
      hy3=y(it,4)**3-y(it,1)**3
      n(2,2)=(t*hx*hy*h)/(c1**2)
      n(2,3)=0
```

```
      n(2,4)=((t/2)*hx*hy2*h)/(c1**2)
      n(2,6)=0
      n(2,7)=(nu*t*hx*hy*h)/(c1*c2)
      n(2,8)=(((nu*t)/2)*hx2*hy*h)/(c1*c2)
      n(3,3)=(w*hx*hy*h)/(c2**2)
      n(3,4)=((w/2)*hx2*hy*h)/(c2**2)
      n(3,6)=(w*hx*hy*h)/(c1*c2)
      n(3,7)=0
      n(3,8)=((w/2)*hx*hy2*h)/(c1*c2)
      n(4,4)=(((t/3)*hx*hy3)/(c1**2)+((w/3)*hy*hx3)/(c2**2))*h
      n(4,6)=((w/2)*hy*hx2*h)/(c1*c2)
      n(4,7)=(((nu*t)/2)*hx*hy2*h)/(c1*c2)
      n(4,8)=((((nu*t)/4)+(w/4))*hx2*hy2*h)/(c1*c2)
      n(6,6)=(w*hx*hy*h)/(c1**2)
      n(6,7)=0
      n(6,8)=((w/2)*hx*hy2*h)/(c1**2)
      n(7,7)=(t*hx*hy*h)/(c2**2)
      n(7,8)=((t/2)*hx2*hy*h)/(c2**2)
      n(8,8)=(((t/3)*hy*hx3)/(c2**2)+((w/3)*hx*hy3)/(c1**2))*h
      do 10 i=2,8
      do 10 l=2,i-1
   10    n(i,l)=n(l,i)
      return
      end
c
c
      subroutine mmult(ct,n,c,s,it)
      dimension ct(8,8),c(8,8),s(200,8,8)
      real n(8,8)
      integer it
      do 20 i=1,8
      do 20 j=1,8
         s(it,i,j)=0
         do 10 k=1,8
         do 10 l=1,8
            s(it,i,j)=s(it,i,j)+ct(i,k)*n(k,l)*c(l,j)
   10    continue
   20 continue
      return
      end
c
c
      subroutine stifmat(k,s,n1,n2,it,nen,nel,ndf,nei)
      dimension s(200,8,8),n1(200,4),n2(4),n3(4)
      real k(350,350)
      integer it,nen,nel
      nn=nen*ndf
      do 5 i=1,4
    5    n3(i)=n1(it,i)
      do 20 i=1,nei
         n2(i)=ndf*(i-1)
         n3(i)=ndf*(n3(i)-1)
   20 continue
      do 50 i=1,nei
         nj=n3(i)
         nl=n2(i)
         do 40 j=1,nei
            nk=n3(j)
            nm=n2(j)
            do 30 l=1,ndf
            do 30 m=1,ndf
               k(nj+l,nk+m)=k(nj+l,nk+m)+s(it,nl+l,nm+m)
   30       continue
   40    continue
   50 continue
      return
```

```
      end
c
c
      subroutine boundcon(k,disp,p,bw,bc)
      dimension p(350)
      real k(350,350)
      integer bc(11)
      z=99 e 8
      do 10 i=1,350
         p(i)=0
   10 continue
      k(1,1)=z
      k(3,3)=z
      k(5,5)=z
      k(7,7)=z
      k(9,9)=z
      k(17,17)=z
      k(25,25)=z
      k(33,33)=z
      k(43,43)=z
      k(55,55)=z
      k(69,69)=z
      k(85,85)=z
      k(103,103)=z
      k(123,123)=z
      k(143,143)=z
      k(163,163)=z
      k(183,183)=z
      k(203,203)=z
      k(223,223)=z
      k(243,243)=z
      k(263,263)=z
      k(283,283)=z
      k(303,303)=z
      k(305,305)=z
      k(307,307)=z
      k(309,309)=z
      k(311,311)=z
      k(313,313)=z
      k(315,315)=z
      k(317,317)=z
      k(319,319)=z
      k(321,321)=z
      p(2)=disp
      call elim(k,2)
      p(10)=disp
      call elim(k,10)
      p(18)=disp
      call elim(k,18)
      p(26)=disp
      call elim(k,26)
      p(34)=disp
      call elim(k,34)
      p(44)=disp
      call elim(k,44)
      p(56)=disp
      call elim(k,56)
      p(70)=disp
      call elim(k,70)
      p(86)=disp
      call elim(k,86)
      p(104)=disp
      call elim(k,104)
      p(124)=disp
      call elim(k,124)
      p(144)=disp
```

```
      call elim(k,144)
      p(164)=disp
      call elim(k,164)
      p(184)=disp
      call elim(k,184)
      p(204)=disp
      call elim(k,204)
      p(224)=disp
      call elim(k,224)
      p(244)=disp
      call elim(k,244)
      p(264)=disp
      call elim(k,264)
      p(284)=disp
      call elim(k,284)
      p(304)=disp
      call elim(k,304)
      do 20 i=61,161,10
         j=int(i/10)-5
         if(bc(j).lt.1)k(2*i,2*i)=z
   20 continue
      return
      end
c
c
      subroutine elim(k,a)
      integer a
      real k(350,350)
      do 10 i=1,350
   10    k(a,i)=0
      k(a,a)=1.0
      return
      end
c
c
      subroutine matsolv(k,nen,p,ndf,del)
      integer nen,ndf
      real k(350,350)
      dimension del(350),p(350),indx(350)
      nn=ndf*nen
      call ludcmp(k,nn,350,indx,q)
      call lubksb(k,nn,350,indx,p)
      do 10 i=1,nn
   10    del(i)=p(i)
      return
      end
c
c
c
      subroutine invert(a,n,np,indx,b,d)
      dimension a(8,8),z(8,8),indx(8)
      do 12 i=1,n
         do 11 j=1,n
            z(i,j)=0
   11    continue
         z(i,i)=1.
   12 continue
      call ludcmp(a,n,np,indx,d)
      do 13 j=1,n
         call lubksb(a,n,np,indx,z(1,j))
   13 continue
      do 14 i=1,n
      do 14 j=1,n
   14    a(i,j)=z(i,j)
      return
      end
```

```
c
c
      subroutine ludcmp(a,n,np,indx,d)
      dimension a(np,np),indx(n),vv(350)
      tiny=1.0 e-10
      d=1.
      do 12 i=1,n
         aamax=0.
         do 11 j=1,n
            if(abs(a(i,j)).gt.aamax) aamax=abs(a(i,j))
   11    continue
         if(aamax.eq.0.)aamax=tiny
         vv(i)=1./aamax
   12 continue
      do 19 j=1,n
         if(j.gt.1)then
            do 14 i=1,j-1
               sum=a(i,j)
               if(i.gt.1)then
                  do 13 k=1,i-1
                     sum=sum-a(i,k)*a(k,j)
   13                continue
                  a(i,j)=sum
               endif
   14       continue
         endif
         aamax=0.
         do 16 i=j,n
            sum=a(i,j)
            if(j.gt.1) then
               do 15 k=1,j-1
                  sum=sum-a(i,k)*a(k,j)
   15          continue
               a(i,j)=sum
            endif
            dum=vv(i)*abs(sum)
            if(dum.ge.aamax)then
               imax=i
               aamax=dum
            endif
   16    continue
         if(j.ne.imax)then
            do 17 k=1,n
               dum=a(imax,k)
               a(imax,k)=a(j,k)
               a(j,k)=dum
   17          continue
               d=-d
               vv(imax)=vv(j)
         endif
         indx(j)=imax
         if(j.ne.n)then
            if(a(j,j).eq.0.)a(j,j)=tiny
            dum=1./a(j,j)
            do 18 i=j+1,n
               a(i,j)=a(i,j)*dum
   18       continue
         endif
   19 continue
      if(a(n,n).eq.0)a(n,n)=tiny
      return
      end
c
c
      subroutine lubksb(a,n,np,indx,b)
      dimension a(np,np),indx(n),b(n)
```

```
      ii=0
      do 12 i=1,n
         ll=indx(i)
         sum=b(ll)
         b(ll)=b(i)
         if(ii.ne.0)then
            do 11 j=ii,i-1
               sum=sum-a(i,j)*b(j)
   11       continue
         else if(sum.ne.0.) then
            ii=i
         endif
         b(i)=sum
   12 continue
      do 14 i=n,1,-1
         sum=b(i)
         if(i.lt.n)then
            do 13 j=i+1,n
               sum=sum-a(i,j)*b(j)
   13       continue
         endif
         b(i)=sum/a(i,i)
   14 continue
      return
      end
c
c
      subroutine formcinv(c,x,y,ct,it,ck)
      dimension c(8,8),x(200,4),y(200,4),ct(8,8)
      dimension temp(8,8),ck(5,8,8),indx(8),b(8)
      do 2 i=1,8
      do 2 j=1,8
   2     temp(i,j)=0
      j=0
      do 5 i=1,8,2
         j=j+1
         temp(i,1)=1
         temp(i,2)=x(it,j)
         temp(i,3)=y(it,j)
         temp(i,4)=x(it,j)*y(it,j)
   5  continue
      j=0
      do 10 i=2,8,2
         j=j+1
         temp(i,5)=1
         temp(i,6)=x(it,j)
         temp(i,7)=y(it,j)
         temp(i,8)=x(it,j)*y(it,j)
   10 continue
      call invert(temp,8,8,indx,b,d)
      do 20 i=1,8
      do 20 j=1,8
   20    c(i,j)=temp(i,j)
      do 50 i=1,8
      do 50 l=1,8
         ct(i,l)=c(l,i)
c         if(it.ge.37)ck(it-36,i,l)=c(i,l)
   50 continue
      return
      end
c
c
c
      subroutine graphics(x,y,n1,nel,del,tx)
      dimension x(200,4),y(200,4),n1(200,4),del(350)
      integer  xo,yo1,yo2,xo2,yo3,yo4
```

```
      do 20 i=1,nel
         do 10 j=1,4
            xo=ix
            yo1=iy1
            yo2=iy2
            xt=0
            yt=0
            xt=x(i,j)+del(2*n1(i,j)-1)
            yt=y(i,j)+del(2*n1(i,j))
            ix=int(xt*50+500)
            iy1=int(400-yt*50)
            iy2=int(400+yt*50)
            call plot(ix,iy1)
            call plot(ix,iy2)
            if(j.eq.1)go to 5
            call draw(xo,yo1,ix,iy1)
            call draw(xo,yo2,ix,iy2)
            if(j.eq.4)go to 7
            go to 10
    5       xo2=ix
            yo3=iy1
            yo4=iy2
            go to 10
    7       call draw(ix,iy1,xo2,yo3)
            call draw(ix,iy2,xo2krn()
      return
      end
c
c
      subroutine forme(del,e,nu,n1,y,nec,it)
      dimension del(350),n1(200,4),y(200,4)
      real lm,l,nu,nec(200),kb
      t=300
      kb=1.38 e-23
      g=nec(it)*kb*t
      l=y(it,4)-y(it,1)
      lm=(l+del(2*n1(it,4))-del(2*n1(it,1)))/l
      f1=func(lm)
      f1=f1*g*(lm-(1/lm)**2)
      lm=((l+del(2*n1(it,4))-del(2*n1(it,1)))/l)+0.2
      f2=func(lm)
      f2=f2*g*(lm-(1/lm)**2)
      e=(f2-f1)*5
      return
      end
c
c
      function func(lm)
      real lm,lm1
      lm1=1/lm
      n=100
      a=1.4
      b=4.84898 e -2
      c=5.58367 e -3
      d=2.70111 e -4
      f1=1+a*(1/n)*(3*lm**2+4*lm1)
      f2=b*((1/n)**2)*(5*lm**4+8*lm+8*lm1**2)
      f3=c*((1/n)**3)*(35*lm**6+60*lm**3+72+64*lm1**3)
      f4=d*((1/n)**4)*(630*lm**8+1120*lm**5+1440*lm**2+1536*lm1
     1   +1280*lm1**4)
      func=f1+f2+f3+f4
      return
```

```
      end
c
c
      subroutine calcnec(nec,del,dt,n1,y,it)
      real nec(200),del(350),dt,y(200,4),l
      integer n1(200,4),it
      l=y(it,4)-y(it,1)
      dl=del(2*n1(it,4))-del(2*n1(it,1))
      stn=dl/l
      alf=1
      nec(it)=nec(it)*exp(-alf*stn*dt)
      return
      end
```

```
#include <stdio.h>
#include <sys/graf.h>
main_()
{
    struct Form screenForm;
        if(g_init(&screenForm))
        { printf(" ERROR: G_init failed\n");
        }
        g_clscreen();
        g_flush();
}
plot_(x,y)
int *x,*y;
{
       g_writepixel(*x,*y,Black);
}
newskrn_( )
{
       g_flush();
}
draw_(x0,y0,x1,y1)
int *x0,*y0,*x1,*y1;
{
       g_drawline(*x0,*y0,*x1,*y1);
}
```

```
10,0.1,1.0,0.5,0.1,132,4,2,0.1,1.0,0.8,0.5,4
6.0,4.0,3.0,2.0,1.8,1.6,1.2,0.8,0.4,0.0
-6.0,-4.0,-3.0,-2.0,-1.5,-1.0,-0.6,-0.4,-0.2
0.0,0.2,0.4,0.6,0.8,1.0,1.5,2.0,3.0,4.0,6.0
```